REPURPOSING SMALL MOLECULE TO TARGET CGG REPEAT RNA AND POLYG AGGREGATES IN FRAGILE X-ASSOCIATED TREMOR/ATAXIA SYNDROME (FXTAS)

M.Sc. Thesis

By SHUBHI KHANDELWAL



DEPARTMENT OF BIOSCIENCES AND BIOMEDICAL ENGINEERING INDIAN INSTITUTE OF TECHNOLOGY INDORE

MAY, 202

REPURPOSING SMALL MOLECULE TO TARGET CGG REPEAT RNA AND POLYG AGGREGATES IN FRAGILE X-ASSOCIATED TREMOR/ATAXIA SYNDROME (FXTAS)

A THESIS

Submitted in partial fulfillment of the requirements for the award of the degree of

Master of Science

SHUBHI KHANDELWAL



DEPARTMENT OF BIOSCIENCES AND BIOMEDICAL ENGINEERING INDIAN INSTITUTE OF TECHNOLOGY INDORE

MAY, 2025



INDIAN INSTITUTE OF TECHNOLOGY INDORE

CANDIDATE'S DECLARATION

I hereby certify that the work which is being presented in the thesis entitled REPURPOSING SMALL MOLECULE TO TARGET CGG REPEAT RNA AND POLYG AGGREGATES IN FRAGILE X-ASSOCIATED TREMOR/ATAXIA SYNDROME (FXTAS) in the partial fulfillment of the requirements for the award of the degree of MASTER OF SCIENCE IN BIOTECHNOLOGY and submitted in the DEPARTMENT OF BIOSCIENCES AND BIOMEDICAL ENGINEERING, Indian Institute of Technology Indore, is an authentic record of my own work carried out during the time period from June 2024 to May 2025 under the supervision of Prof. Amit Kumar, BSBE, IIT Indore.

The matter presented in this thesis has not been submitted by me for the award of any other degree of this or any other institute.

Signature of the student with date (SHUBHI KHANDELWAL)

This is to certify that the above statement made by the candidate is correct to the best of my knowledge.

21.05.25

Signature of the Supervisor of M.Sc. thesis (with date)

(PROF. AMIT KUMAR)

SHUBHI KHANDELWAL has successfully given his/her M.Sc. Oral Examination held on 6th May, 2025.

Signature of Supervisor of MSc thesis

Date: 21.05.20215

Convener, DPGC

Date: 21/05/2025

ACKNOWLEDGEMENTS

First and foremost, I express my heartfelt gratitude to my supervisor, **Prof. Amit Kumar**, whose exceptional guidance, patience, and encouragement have been instrumental throughout my M.Sc. thesis journey. His profound knowledge, constructive feedback, and engaging discussions have shaped this work and enriched my academic experience, for which I am deeply thankful. I am also sincerely grateful to the Department of Biotechnology, Government of India, for awarding me the fellowship that supported my studies, enabling me to focus on my research.

My sincere thanks extend to the head, faculty, and staff of the Department of Biosciences and Biomedical Engineering (BSBE) for their constant support and for creating an enriching academic environment. My lab members have been a constant source of help and encouragement. I would like to express my appreciation to **Mr. Krishna Singh Solanki**. His readiness to troubleshoot obstacles, coupled with our engaging scientific discussions and light-hearted conversations, made my time at IIT Indore memorable.

A special thank you to **Ms. Sakshi Shukla** for her generous support, both professionally and personally. Her invaluable guidance in the lab, thoughtful advice, and willingness to assist at every step have made a significant impact on my journey. Our shared moments and meaningful conversations, provided much-needed encouragement and camaraderie, making this experience truly memorable. I would also like to express my gratitude to **Ms. Masnsee Patel**, **Ms. Aditi Kumari Pramod**, **Mr. Ashmad Nayak**, and **Mr. Aritra Chakraborty** for their constant support, both inside and outside the lab, engaging in scientific and non-scientific discussion. I am extremely thankful to my batch mates and dear friends, **Soumalya Das** and **Ritika Rawat**, whose constant support, both academically and emotionally, has been invaluable throughout this journey. Their willingness to help, thoughtful advice, and dependable

presence made even the most challenging moments more manageable. Their friendship brought balance, laughter, and strength to my M.Sc. journey, and I am truly grateful for having them by my side. I am thankful to **Ms. Pronomika Chetia**, **Ms. Priya Gupta**, and **Ms. Aakriti Singh**. I am grateful to Dr. Ravinder, Mr. Ghanshyam Bhavsar, and Mr. Kinny Pandey from SIC, IIT Indore, for their help with high-end techniques. My sincere gratitude goes to the Director of IIT Indore, and I also thank all the non-teaching staff, housekeeping staff, and security staff at IIT Indore.

I would also like to extend my heartfelt thanks to my wonderful group of friends—Yashi Singh, Rigzin Yangdol, Ayushi, Chaitali Vora, Sanjana, Milan Khanda, and Mahesh Sahu—whose unwavering support, constant encouragement, and countless joyful moments we shared, made my journey even more meaningful. Their presence brought laughter, strength, and a sense of balance to my M.Sc. experience, and I am forever grateful for their companionship. I am thankful to Mr. Khandu Wadhonkar for his personal support throughout this journey. His kindness and encouragement have been deeply appreciated.

Finally, I am truly indebted to my loving parents, Mrs. Rani Khandelwal and Mr. Virendra Khandelwal, and my brother, Vasu Khandelwal, for their unwavering love, support, and motivation. Their sacrifices, guidance, and endless patience have been the foundation of my journey, and this achievement would not have been possible without them.

While it is impossible to mention every individual who has contributed to my journey, I want to extend my deepest thanks to all those—named and unnamed—who have directly or indirectly supported me along the way. I also wish to express my deepest gratitude to God, the ultimate source of strength, wisdom, and guidance.

Shubhi

Dedicated to my Parents-

Rani Khandelwal

Virendra Khandelwal

ABSTRACT

Fragile X-associated tremor/ataxia syndrome (FXTAS) arises from the expansion of CGG repeats within the 5' untranslated region (5'-UTR) of the FMR1 (Fragile X messenger ribonucleoprotein gene 1). These expanded repeat transcripts, r(CGG)_{exp}, can accumulate as RNA foci or undergo Repeat-Associated Non-AUG (RAN) translation, leading to the production of neurotoxic homopolymeric proteins in neurons. Identifying small molecules that selectively and tightly bind to these pathogenic repeat RNAs holds significant promise as a therapeutic strategy for treating repeat expansion-related neurodegenerative disorders. This study investigates the therapeutic potential of FDAapproved small molecules capable of binding to expanded CGG repeat sequences implicated in FXTAS pathology and mitigate its associated toxicity. Through biophysical analyses, compound P2 was identified as a selective binder of CGG repeat-containing RNA motifs. Subsequent cellular assays demonstrated that P2 effectively reduced the accumulation of toxic polyglycine (FMRPolyG) proteins. Moreover, treatment with P2 led to measurable improvements in neurological and behavioral responses in in vivo models. These findings highlight P2 as a promising candidate for the treatment of FXTAS resulting from CGG repeat expansions and support the broader application of this strategy in addressing other trinucleotide repeat-associated neurodegenerative disorders.

Keywords- CGG, Repeat Expansion Disorders, FXTAS, Drug Repurposing, Small molecules.

LIST OF PUBLICATIONS

- (a) Publication from Thesis
- Shubhi Khandelwal, Aditi Pramod Kumari, Soumalya Das, Krishna Singh, Sakshi Shukla, Amit Kumar*. Exploring the Neuroprotective Role of P2 in the treatment of FXTAS. (Manuscript to be communicated)
- (b) Publications apart from Thesis
- Shubhi Khandelwal[#], Soumalya Das[#], Sakshi Shukla, Amit Kumar^{*}. Exploring the Pleiotropic Effects of IncRNA in different Repeat Expansion Disorders. (Submitted to-Molecular Basis of Disease; Manuscript Id: BBADIS-25-1420) (# equal contribution) (Under review)
- Soumalya Das, Mansee Patel, Shubhi Khandelwal, Ritika Rawat, Sakshi Shukla, Aditi Kumari Pramod, Krishna Singh, Amit Kumar*. From Mutations to Microbes: Investigating the Impact of the Gut Microbiome on Repeat Expansion Disorders. (Submitted to- Journal of Neurochemistry; Manuscript ID: JNC-2025-0291) (Under review)
- Soumalya Das; Aditi Kumari; Krishna Singh; Sakshi Shukla;
 Shubhi Khandelwal; Amit Kumar*. Molecular Repositioning
 of Celecoxib as a Neurotherapeutic Agent in Fragile X-associated Tremor Ataxia Syndrome (FXTAS) (Submitted to-ACS Pharmacology & Translational Science, Manuscript ID: pt-2025-003265) (Submitted)

TABLE OF CONTENTS

	Page no.
List of figures	XIII
List of tables	XVII
Nomenclature	XIX
Acronyms	XXI
Chapter 1 Introduction	1
1.1 Repeat Expansion Disorder	2
1.2 FXTAS (Fragile X-associated Tremor	r/Ataxia 3
Syndrome)	
1.3 Pathogenic Mechanisms	5
1.4 Therapeutic Approaches against Repeat Ex	pansion 7
Disorders	
1.5 Drug Repurposing	9
1.6 Drosophila as a model organism	m for 10
Neurodegenerative Disorders	
1.7 Drosophila life cycle	11
1.8 Identification of male and female Dro	osophila 13
melanogaster	
1.9 Organization of the thesis	15
Chapter 2 Literature Review and P	roblem 17
Formulation	
Chapter 3 Materials and Methods	21
3.1 Materials	21
3.2 Synthesis of RNA oligo synthesis using T	77-RNA 21
Polymerase (In-vitro transcription)	
3.2.1 Expression and Purification of T7-RNA Poly	ymerase 21
3.2.2 <i>In-vitro</i> Transcription	22
3.3 Fluorescence Titration Assay	23
3.4 Circular Dichroism Spectroscopy	24
3.5 Electrophoretic Mobility Shift Assay	25
3.6 PCR Stop Assay	25

3.7	RNA Thermal Denaturation Profile	26
3.8	Molecular Docking of P2 with CGG RNA	26
3.9	Nuclear Magnetic Resonance (NMR) Spectroscopy	27
3.10	Quantification of PolyG proteins by Western blot	27
3.11	Reversal of pre-mRNA splicing defect in the cellular	28
mode	el	
3.12	Drosophila stocks, dietary conditions, and drug	28
treatr	ment	
3.13	Assessment of rough eye phenotype, pigment loss,	29
and F	FMR1PolyG inclusion bodies using Nikon SMZ745T	
Micro	oscope and Fluorescence Confocal Microscopy	
3.14	Scanning Electron Microscopy Analysis of	30
Dros	ophila External Eye	
3.15	Negative Geotaxis Assay (Drosophila Climbing	30
Assa	y)	
3.16	Larval Crawling Assay	30
3.17	Western blot analysis from Drosophila	31
3.18	Assessment of ROS levels	31
3.19	Histological Analysis of Larval Brain Tissue	32
3.20	Lifespan Analysis	32
3.21	Statistical Methods	33
Chap	oter 4 Results and Discussion	35
4.1	P2 shows specific binding affinity and selectivity	35
towa	rds r(CGG) _{exp} RNA, elucidated by Fluorescence	
Titrat	tion Assay.	
4.2	Confirmation of specific topological effects of P2	41
bindi	ng to target RNA by Circular Dichroism	
Spect	troscopy and Thermal Profile.	
4.3	Validation of thermal stabilization of CGG repeat	43
RNA	s by small molecule P2.	

4.4 Changes in band patterns in Electrophoretic Mobility	45
Shift Assay and Polymerase Chain Reaction Stop Assay	
upon the interaction of P2 and r(CGG) _{exp} .	
4.5 Structural evaluation of the r(CGG) ₆ repeat RNA-	47
drug complex using NMR spectroscopy and Molecular	
Docking.	
4.6 Evaluation of functional inhibition of RAN	50
Translation by P2 in cellular FXTAS model.	
4.7 Improvement in pre-mRNA alternative splicing	53
defects in FXTAS cell line models.	
4.8 P2 reduces neurodegeneration, alleviates rough eye	56
phenotype, and prevents pigment loss in fly model of	
FXTAS induced by PolyG toxicity.	
4.9 P2 rescues eye morphology disrupted by FMR1PolyG	59
repeats, demonstrating dose-dependent effectiveness in a	
Drosophila FXTAS model.	
4.10 P2 effectively reduces PolyG protein levels in	60
FXTAS model flies.	
4.11 P2 improves locomotor defects induced by PolyG	62
accumulation in the Drosophila FXTAS model.	
4.12 Quantitative analysis of ROS generation.	66
4.13 Assessment of P2's impact on mitochondrial	67
oxidative stress and membrane potential.	
4.14 Detection of neuronal cell death via Propidium	71
iodide (PI) staining.	
4.15 Dosage-dependent lifespan profiling of P2.	73
4.16 Expression analysis of neuroinflammatory,	74
neuroprotective, and autophagy-related genes via RT-	
qPCR.	
Chapter 5 Conclusion and Future Perspectives	79
Appendix	81

References

83

LIST OF FIGURES

	Page no.
Figure 1.1. Representing hallmarks of	1
neurodegenerative diseases.	
Figure 1.2. Representing different types of Repeat	3
Expansion Disorders.	
Figure 1.3. Depicting the premutation and full	4
mutation condition in FXTAS.	
Figure 1.4. Representing the molecular pathological	5
mechanisms underlying the Repeat Expansion	
Disorders.	
Figure 1.5. Schematic representation of key	7
pathophysiological mechanisms involved in FXTAS.	
Figure 1.6. Schematic representation of the life cycle	12
of Drosophila melanogaster.	
Figure 1.7. Showing Adult <i>Drosophila</i> Fly, Male and	13
female adult flies.	
Figure 2.1. Pie chart representing the chance of	18
developing FXTAS symptoms by age in case of male	
carriers.	
Figure 2.2. Schematic representation of the mode of	20
action of small molecules in inhibition of RAN	
translation and reduction in sequestration of RNA	
binding proteins involved in splicing.	
Figure 3.1. Jablonski diagram depicting fluorescence	24
phenomenon where the molecule is excited to a higher	
energy state followed by the release of energy.	
Figure 3.2. Schematic representation of Electrophoretic	25
shift mobility.	
Figure 4.1. Primary screening showing binding	36
affinities of 14 FDA-approved drugs towards r(CGG) ₆	
as screened by Fluorescence Binding Assay.	

Figure 4.2. Secondary structures of different RNA	37
sequences with internal loops comprise one nucleotide	
each.	
Figure 4.3. P2 shows specific binding affinity and	40
selectivity towards r(CGG) _{exp} RNAs as demonstrated	
by Fluorescence Titration Assays.	
Figure 4.4. CD spectroscopy titration of P2 with	42
r(CGG) _{exp} , r(AU) ₆ duplex RNA, r(CCG) ₆ , r(CAG) ₆ , and	
r(CUG) ₆ RNA.	
Figure 4.5. Thermal Denaturation Profile. Normalized	44
CD melting plots of r(CGG) _{exp} with increasing D/N	
ratio.	
Figure 4.6. Gel retardation images show that with an	46
increasing concentration of P2, the mobility of CGG	
repeat RNAs significantly increases over AU duplex	
RNA.	
Figure 4.7. Gel images show the decreased intensity of	47
the PCR product with increasing concentration of P2	
compared with the AU-paired template.	
Figure 4.8. Molecular Docking study for molecular	48
interactions between CGG repeat RNA and molecule	
P2.	
Figure 4.9. Proton spectrum 1D-1H NMR peak	49
broadening of P2 with (CGGx6) RNA.	
Figure 4.10. Validation of P2's efficiency to reduce the	51
intracellular FMR1PolyG aggregation.	
Figure 4.11. Assessment of P2's potency to inhibit RAN	52
translation.	0.2
Figure 4.12. Evaluation of in-vitro potency of P2 to	55
improve the splicing defects in developed FXTAS	33
cellular models.	
Contain models.	

Figure 4.13. P2 reduces rough eye phenotype and	58
pigment loss induced by PolyG toxicity in the	
Drosophila model of FXTAS.	
Figure 4.14. P2 helps to mitigate the PolyG aggregates	61
in the FXTAS <i>Drosophila</i> model.	
Figure 4.15. P2 improves locomotor dysfunctions	62
(Larval crawling assay).	
Figure 4.16. P2 improves locomotor dysfunctions	64
(Climbing assay).	
Figure 4.17. P2 improves locomotor dysfunctions	65
(Flight assay).	
Figure 4.18. Assessment of ROS levels in Elav-	67
GAL4>UAS-(CGG)90-EGFP and Elav-GAL4>UAS-	
\textit{EGFP} fed with different concentrations (25.0 μM and	
50.0 μM) of P2.	
Figure 4.19. Assessment of mitochondrial ROS	68
production.	
Figure 4.20. Assessment of the membrane potential	70
upon treatment with P2.	
Figure 4.21. P2 treatment reduces cell death in the	72
FXTAS <i>Drosophila</i> model.	
Figure 4.22. <i>In-vivo</i> efficacy of P2 in enhancing	73
lifespan in FXTAS Drosophila model.	
Figure 4.23. Effect of P2 on the expression levels of	75
Autophagy genes in FXTAS Drosophila using RT-	
qPCR.	
Figure 4.24. Effect of P2 on the expression levels of	77
neuroprotective and neuroinflammatory genes in	
FXTAS Drosophila using RT-qPCR.	

LIST OF TABLES

	Page no.
Table 4.1. Binding constants for 14 FDA-approved	36
small molecules towards r(CGG) ₆ as screened by	
Fluorescence Binding Assay.	
Table 4.2 Table aboveing the aboves in the malting	45
Table 4.2. Table showing the changes in the melting	43
temperature upon titration with P2 to D/N 1.	

NOMENCLATURE

Λ Wavelength

ε Extinction coefficient

°C Degree Centigrade

Δ Delta

μL Microliter

mL Milliliter

nm Nanometer

nM Nano molar

μM Micro molar

M Molar

s Seconds

min Minutes

hr Hour

ACRONYMS

CD Circular Dichroism

FBA Fluorescence Binding Assay

D/N Drug/ Nucleic Acid

DMSO Dimethyl sulfoxide

EDTA Ethylenediaminetetraacetic acid

EMSA Electrophoretic Mobility Shift Assay

LB Luria Broth

PAGE Polyacrylamide gel electrophoresis

PCR Polymerase Chain Reaction

PDB Protein Data Bank

RNA Ribonucleic acid

K_d Dissociation constant

DTT Dithiothreitol

SDS Sodium dodecyl-sulfate

Ni-NTA Nickel-Nitrilotriacetic Acid

IPTG Isopropylthio-β-galactoside

DCF-DA 2,7-dichlorofluorescein diacetate

TMRM Tetramethylrhodamine methyl ester

OD Optical Density

Chapter 1

Introduction

Neurodegenerative Disorders (NDDs) constitute a diverse group of debilitating neurological conditions characterized by progressive degeneration and neuron loss in the central nervous system (CNS) and peripheral nervous system (PNS) (Liguori et al., 2023), (Wilson et al., 2023). A distinct set of pathological features of NDD involves- abnormal protein aggregation, disruption of neuronal network integrity and synaptic function, dysregulated energy metabolism, impaired proteostasis, cytoskeletal disorganization, DNA and RNA instability, neuroinflammation, and progressive neuronal loss (Wilson et al., 2023; Jellinger, 2010), The global burden of these disorders is rising rapidly with aging populations, and current therapies primarily focus on symptom management rather than halting or reversing disease progression.

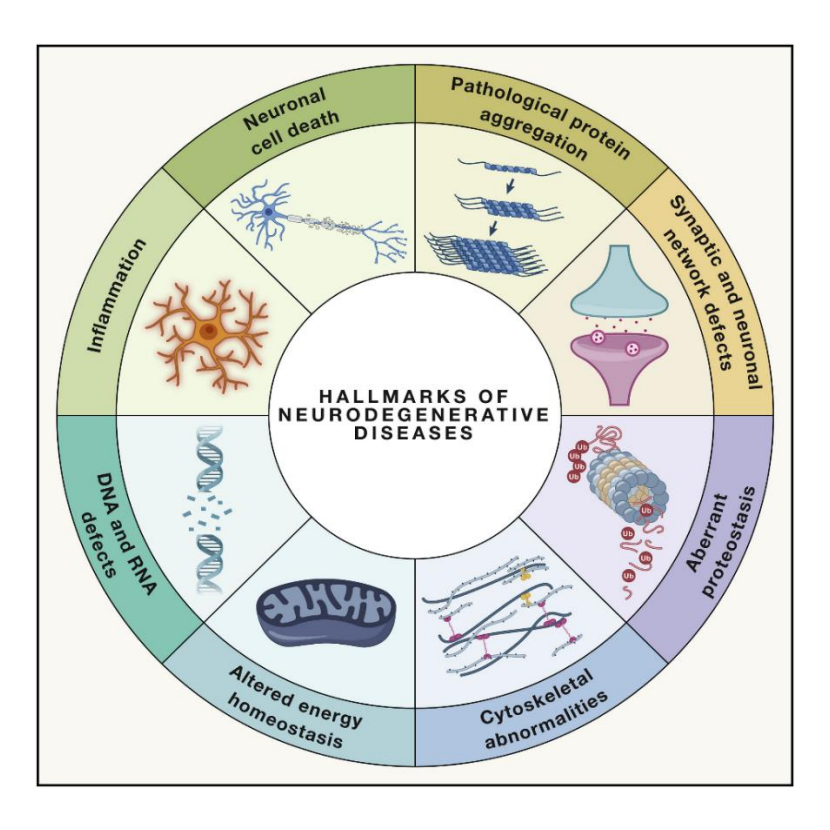


Figure 1.1: Representing hallmarks of neurodegenerative diseases. (Wilson et al., 2023)

A deeper understanding of molecular and cellular mechanisms underlying NDDs is critical to developing effective disease-modifying treatments (Erkkinen et al., 2018). These disorders include Alzheimer's disease (AD), Parkinson's disease (PD), Huntington's disease (HD), Amyotrophic Lateral Sclerosis (ALS), and Fragile X-associated Tremor/Ataxia Syndrome (FXTAS), among others. While each condition exhibits distinct clinical manifestations—such as memory loss in AD, motor impairment in PD and ALS, or cognitive and behavioral disturbances in FXTAS—they share several overlapping pathological features. Certain neurodegenerative disorders, such as FXTAS, myotonic dystrophy, and spinocerebellar ataxias, are caused by nucleotide repeat expansions that induce RNA toxicity and protein dysregulation (Todd & Paulson, 2010). These insights have driven the development of targeted approaches, including antisense oligonucleotides (ASOs), RNA interference, CRISPR gene editing, and small molecule modulators. Advancing our understanding of these mechanisms is crucial for creating disease-modifying therapies.

1.1 Repeat Expansion Disorders

The human genome consists of more than a million short tandem repeat (STR) sequences, and the abnormal expansion of specific repeat tracts is implicated in the pathogenesis of over fifty genetic disorders (Malik et al., 2021). Minor variations in the number of STRs can influence gene regulation by affecting processes such as DNA methylation, transcriptional activity, and alternative splicing (Quilez et al., 2016). However, this inherent instability may also have detrimental consequences. Repeat expansion disorders arise due to the expansion of DNA sequences that can be of variable length (Ellerby, 2019). These expansions can occur in both coding and non-coding regions of many genes, causing a diverse range of clinical symptoms (Paulson, 2018). These can occur in 5' UTR or intronic region or 3' UTR. Repeat expansions present in the promoter or 5'UTR or other regulatory genes are generally rich in GC such as CGG triplet repeat expansion in FMR1

and hexanucleotide (GGGCC) expansion in C9ORF72 (Renton et al., 2011).

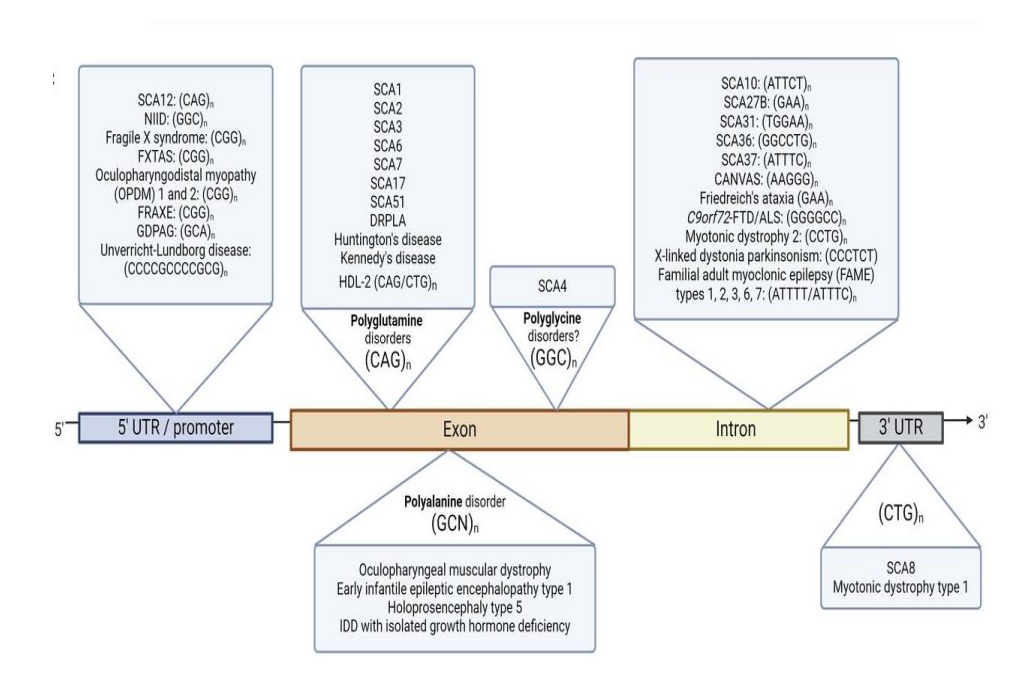


Figure 1.2: Representing different types of Repeat Expansion Disorders. (Chen et al., 2024)

1.2 FXTAS (Fragile X-associated Tremor/Ataxia Syndrome)

FXTAS is a neurodegenerative condition that develops later in life and predominantly affects individuals who carry premutation alleles (55–200 CGG repeats) in the *FMR1* (Fragile X messenger ribonucleoprotein 1) gene on the X chromosome. First described in 2001, FXTAS is marked by a gradual onset of clinical features, including intention tremor, gait ataxia, cognitive impairment, parkinsonian symptoms, and autonomic disturbances, typically manifesting after the age of 50 (Jacquemont et al., 2003). Due to the X-linked inheritance pattern, the disorder is more frequently observed and more severe in males, although heterozygous females may also present with a spectrum of symptoms, generally milder in nature (Tassone et al., 2000).

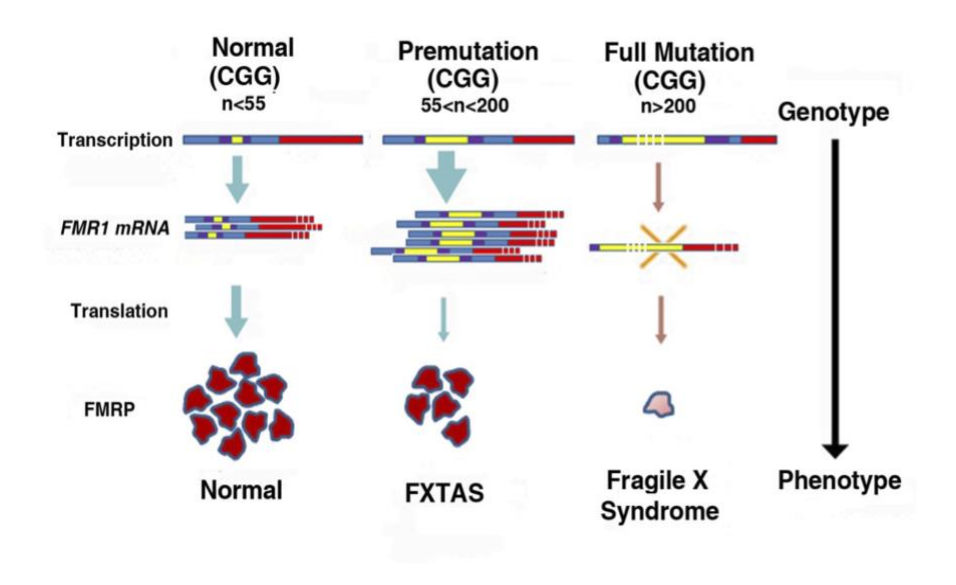


Figure 1.3: Depicting the premutation and full mutation condition in FXTAS. (Willemsen et al., 2011)

This syndrome is one of several conditions linked with expansions in the FMR1 gene, collectively termed Fragile X-associated disorders. These include Fragile X syndrome (FXS), caused by a full mutation (greater than 200 CGG repeats), and Fragile X-associated primary ovarian insufficiency (FXPOI), which affects reproductive function in females. In contrast, FXTAS is linked specifically to the premutation range, which results in a distinct clinical and molecular phenotype (Oostra & Willemsen, 2009). The risk of developing FXTAS increases with age, with studies estimating that 30-45% of male premutation carriers over 50 years will develop clinical symptoms, whereas the penetrance in females remains comparatively lower (Leehey, 2009). Magnetic resonance imaging (MRI) findings frequently reveal white matter hyperintensities, particularly in the middle cerebellar peduncles (MCP sign), which serve as a supportive diagnostic marker (Brunberg et al., 2002). FXTAS is becoming more recognized as a major public health concern due to its high frequency in the elderly and the possibility of intergenerational transmission of FMR1 permutations. Genetic screening of Fragile X Syndrome families has identified numerous asymptomatic premutation carriers who may develop FXTAS later in

life (Oostra & Willemsen, 2009). Despite rising awareness, clinical identification of FXTAS remains difficult due to symptom overlap with other neurodegenerative disorders and varying presentation across carriers.

1.3 Pathogenic Mechanisms

The Repeat expansions can affect gene function via a number of molecular processes, including RNA toxicity, repeat-associated non-AUG (RAN) translation, RNA foci formation, and epigenetic changes, resulting in cellular malfunction and neurodegeneration (Paulson, 2018).

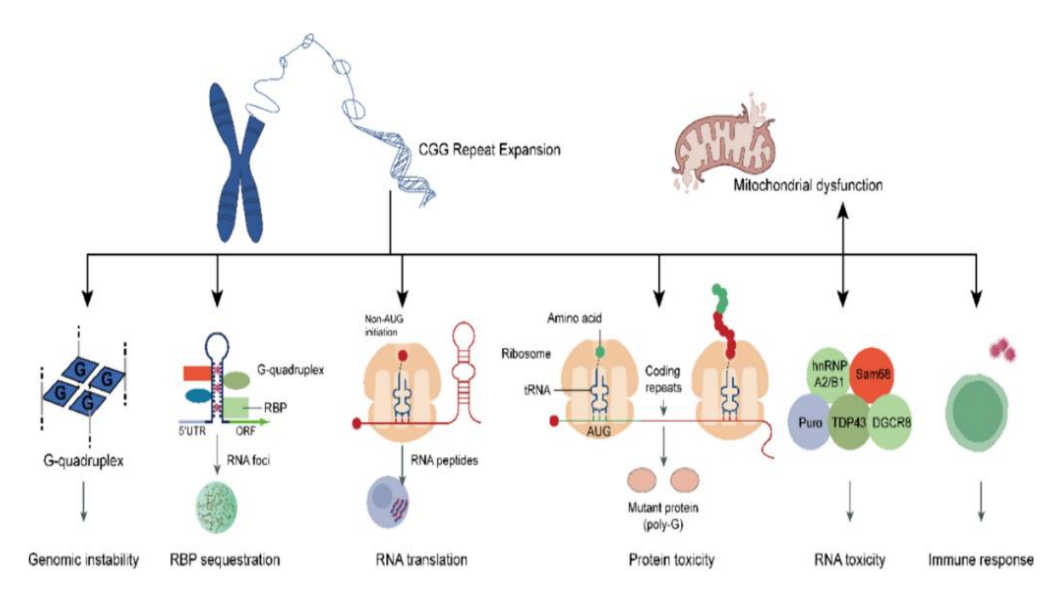


Figure 1.4: Representing the molecular pathological mechanisms underlying the Repeat Expansion Disorders (Zhang et al., 2024)

Individuals with FXTAS have increased FMR1 mRNA expression due to a premutation allele of the FMR1 gene, which is defined by 55 to 200 CGG trinucleotide repeats in its 5' UTR, as opposed to gene silencing FXS. This overexpression of mRNA is linked to a harmful gain-of-function mechanism. The key RNA-centric mechanisms driving the FXTAS RNAopathy (Belzil et al., 2013) condition are toxic RNA and protein gain-of-function. The stable hairpin structure of the CGG repeat harboring mRNA can sequester the essential RNA binding proteins

(RBPs) participating in various cellular mechanisms like microRNA processing (DGCR8 and Drosha), mRNA transportation out in the cytoplasm (hnRNP A2/B1, Pur-α), and splicing (hnRNP A2/B1) (Glineburg et al., 2018; Sellier et al., 2013). This pathology is characterized by the formation of intranuclear RNA foci (Greco et al., 2006) and splicing anomalies which arise as the critical RBPs get sequestered disrupting their regulatory roles in RNA metabolism and contributing to cellular dysfunction. In other mechanism of Repeatassociated non- AUG (RAN) translation which occurs out of frame of the FMR1 gene, causing the translation to start non-canonically from the extended CGG repeats rather than the AUG start codon. This results in the formation of toxic protein aggregates - FMR1PolyG (polyglycine stretch) or FMR1PolyA (polyalanine stretch) in the neuronal cells (Todd et al., 2013). Ubiquitin-positive inclusions harboring FMR1 mRNA are formed in the cerebrum and brainstem in the FXTAS pathology (Tassone et al., 2004). Additionally, mitochondrial dysfunction, oxidative stress, and poor proteostasis have been linked to FXTAS development. Cells expressing the CGG-expanded FMR1 premutation exhibit altered mitochondrial dynamics and increased generation of reactive oxygen species (ROS), potentially exacerbating neuronal susceptibility (Gohel et al., 2020).

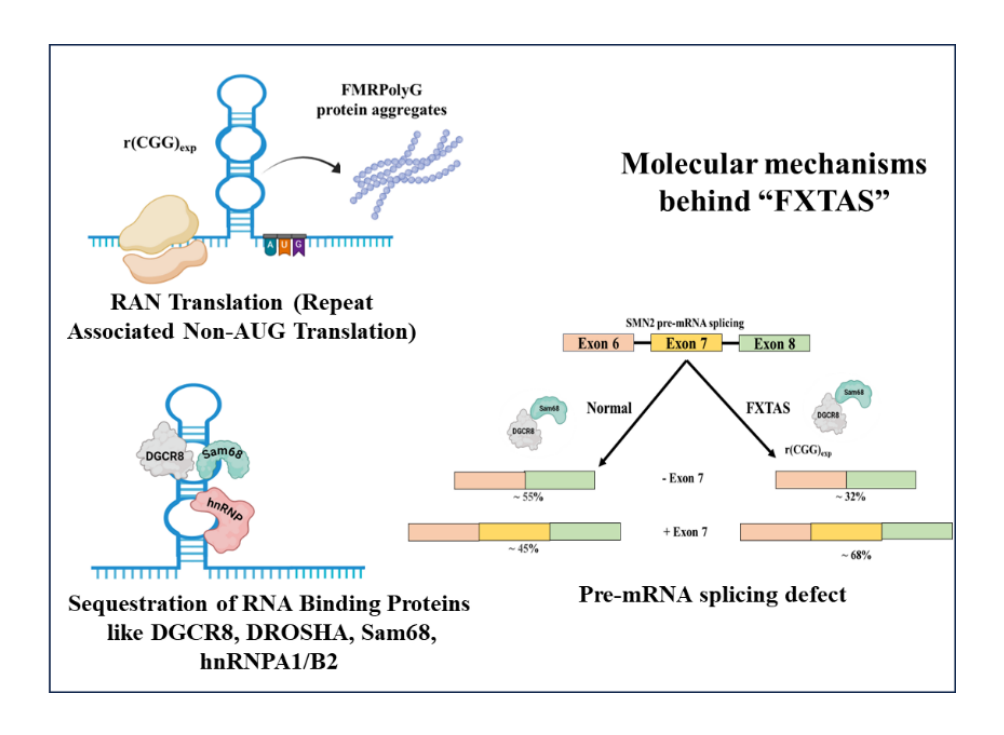


Figure 1.5: Schematic representation of key pathophysiological mechanisms involved in FXTAS.

Together, these molecular changes degrade neuronal function and viability, contributing to the neurodegenerative phenotype seen in FXTAS. Understanding these pathways not only sheds light on FXTAS pathogenesis, but also has broader implications for therapeutic efforts across the range of repeat expansion disorders.

1.4 Therapeutic Approaches against Repeat Expansion Disorders

Currently, there are no curative treatments available for CGG repeat expansion disorders, and existing clinical interventions are limited to symptomatic relief. A significant barrier to the development of effective therapies remains the incomplete understanding of disease mechanisms. As mutant RNA harboring expanded CGG repeats contributes to pathogenesis through sequestration of RNA-binding proteins and the production of toxic peptides via aberrant translation, several promising therapeutic strategies are under investigation. These include interventions aimed at reducing the synthesis or enhancing the degradation of repeat-containing RNAs, disrupting harmful RNA-

protein interactions, and minimizing toxic protein aggregation. Targeting these processes at the DNA, RNA, or protein level holds potential for the development of disease-modifying treatments (Xu et al., 2021).

Targeted approaches such as antisense oligonucleotides (ASOs) have shown promise by selectively degrading the mutant RNA, thereby reducing RNA foci and rescuing cellular dysfunction (Smith & Zain, 2019). In ALS, antisense oligonucleotides (ASOs) targeting GGGGCC repeat-containing RNA have been shown to reduce RNA foci, rescue glutamate-induced toxicity, and correct gene expression abnormalities in patient-derived cells (Sareen et al., 2013). In mouse models, ASO treatment decreased toxic RNA and protein accumulation, leading to improvements in behavioral and cognitive symptoms (McCampbell et al., 2018).

RNA interference (RNAi) has demonstrated promise as a treatment method for repetitive expansion disorders. This method employs double-stranded RNA molecules that attach to certain target mRNAs, causing their degradation and a concomitant decrease in the production of the relevant proteins (Castanotto & Rossi, 2009). The use of RNAtargeting CRISPR/Cas9 systems has demonstrated effective clearance of toxic repeat expansion RNAs—such as CUG, CAG, CCUG, and GGGGCC—in human cell models, alongside the correction of associated molecular abnormalities, including the reduction of polyglutamine-containing proteins. These findings suggest its potential applicability to CGG repeat-associated disorders like FXTAS; however, additional studies are required to validate its efficacy in this specific context (Xu et al., 2021). Certain small molecules can reduce CGG repeat toxicity by binding to CGG RNA hairpins and preventing RBP sequestration. Their small size and better blood-brain barrier permeability make them advantageous over ASOs for neurological disorders (Disney et al., 2012). Drug repurposing has emerged as a valuable approach for accelerating treatment development, particularly for rare neurodegenerative diseases like FXTAS. Though still largely at

preclinical or early clinical stages, these strategies collectively represent a multifaceted therapeutic landscape aimed at addressing both the molecular pathology and clinical manifestations of FXTAS.

1.5 Drug Repurposing

The development of a new drug typically requires an investment of several billion dollars and spans approximately 9 to 12 years. Drug repurposing has emerged as an efficient alternative strategy (Y. Wang et al., 2022). This approach involves identifying new therapeutic applications for existing drugs and has gained momentum as a costeffective and time-efficient pathway in pharmaceutical development (Y. Wang et al., 2022; Oprea & Mestres, 2012). Drug reprofiling involves the use of medications that have already received approval from regulatory bodies such as the FDA (Food and Drug Administration), EMA (European Medicines Agency), MHRA (Medicines and Healthcare Products Regulatory Agency), and others (Parvathaneni et al., 2019). Many pharmaceutical firms are undertaking a drug repurposing approach for some of the FDA-approved drugs and the previously failed compounds to offer pharmacotherapy for different medical conditions (Aubé, 2012; Parvathaneni et al., 2019). Additionally, compounds with broad pharmacological activity, antiinflammatory effects, or prior regulatory approval can be effectively redirected to treat various diseases. The promising therapeutic molecules can be used for the treatment of both common and rare diseases. There are over 10,000 rare diseases, and less than 5% of them have an approved therapy Homepage - Global Genes. Off-label use of drug molecules presents an accessible treatment method for such rare diseases. Interestingly, Kinase inhibitors designed for oncology treatment purposes have been shown remarkable neuroprotective effects (Kakoti et al., 2022). Small molecules have the potential to be repurposed for neurodegenerative diseases (Liu et al., 2022). Regardless of their complementary sequences, small molecules can readily identify secondary and tertiary RNA structures (Verma, Khan, Bhagwat, et al., 2020). Therapeutic potential of various small molecules such as

myricetin and other synthetic molecules have been reported for $r(CAG)_{exp}$ RNA causing HD (Huntington's disease) and SCA (spinocerebellar ataxia) (Khan et al., 2018, 2019).

1.6 *Drosophila* as a model organism for Neurodegenerative Disorders

Drosophila melanogaster, commonly known as the fruit fly, has emerged as a powerful model organism for studying human neurodegenerative diseases. Its utility lies in its genetic tractability, short life cycle, low maintenance cost, and the high degree of conservation of disease-related genes and cellular pathways with humans.

- Genetic Similarity to Humans- About 75% of human disease-related genes have homologs in *Drosophila*. Many key cellular pathways (autophagy, oxidative stress, mitochondrial function) are conserved (Reiter et al., 2001).
- Advanced genetic toolkit- The GAL4/UAS binary expression system allows spatial and temporal control of gene expression in specific tissues, including the nervous system (Brand & Perrimon, 1993). In addition, genome-wide RNAi lines, CRISPR/Cas9 technology, and Pelement-mediated mutagenesis have enabled the rapid generation of disease models (Perkins et al., 2015; Port et al., 2014). These tools make it possible to manipulate gene expression, introduce disease-associated mutations, and conduct large-scale genetic screens with remarkable precision.
- Neuroanatomical and Functional Relevance- Though simpler,
 Drosophila shares key neuronal properties with humans (Bilen &
 Bonini, 2005). Behaviors like climbing, locomotion, and lifespan serve
 as readouts for neurodegeneration and disease progression.
- Established models for various neurogenerative diseases- Several repeat
 expansion disorders, including Huntington's disease (HD), and various
 subtypes of Spinocerebellar ataxias (SCA), are marked by progressive
 neurodegeneration. *Drosophila melanogaster* models of these
 conditions effectively replicate critical pathological hallmarks such as

neuronal degeneration, aberrant protein aggregation, and impaired motor function. The use of these models enables the elucidation of underlying molecular mechanisms and facilitates the identification of potential therapeutic targets for intervention (Lu & Vogel, 2009). *Drosophila* can be employed to study rare human disease (Verheyen, 2022).

Drosophila melanogaster has been a pivotal model for studying transmission genetics and developmental biology due to its experimental tractability. Genetic analyses have revealed that many developmental genes and pathways are evolutionarily conserved, with numerous human developmental genes having orthologs first identified in *Drosophila*. It offers numerous experimental advantages that make it ideal for disease modeling, including:

- Small body size, allowing easy maintenance and handling in the laboratory.
- Low chromosome number (four pairs), simplifying genetic analysis and mapping.
- Compact genome (~165 Mb), fully sequenced and wellannotated.
- Polytene chromosomes in salivary glands, facilitating detailed cytogenetic studies.
- o **Short generation time** (~10 days at 25°C), enabling rapid genetic crosses and data collection.
- High fecundity and low maintenance cost, permitting largescale experiments at minimal expense.

1.7 Drosophila life cycle

Drosophila melanogaster has a short life cycle, making it ideal for large-scale genetic, molecular, and biochemical studies. At 25 °C, development from fertilized egg to adult takes about 10 days, with a lifespan of 60–80 days depending on culture conditions. As a holometabolous insect, its life cycle includes four distinct stages: embryo, larva, pupa, and adult (post-eclosion) (Hales et al., 2015). After fertilization, embryogenesis takes 24 hours to complete and then hatches

into worm-like first instar larvae. This stage is characterized by active feeding. The first and second larval instars each span approximately one day, while the third instar lasts around two days. By the fifth day post-fertilization, larval development concludes, and the organism undergoes metamorphosis inside a rigid, chitinous pupal case (puparium) formed from the outer cuticle of the larva. Ecdysone, a key steroid hormone, orchestrates the transition from larval to adult stages in Drosophila by regulating gene expression patterns (Yamanaka et al., 2013). During the 4–5 days spent within the pupal case, most larval tissues are degraded, while adult structures form from 19 imaginal discs—clusters of progenitor cells established during earlier development. These discs later differentiate into adult features such as wings, legs, and eyes. The adult fly emerges from the pupal casing through a process known as eclosion and reaches sexual maturity within approximately 8–12 hours, enabling continuation of the life cycle (Hales et al., 2015).

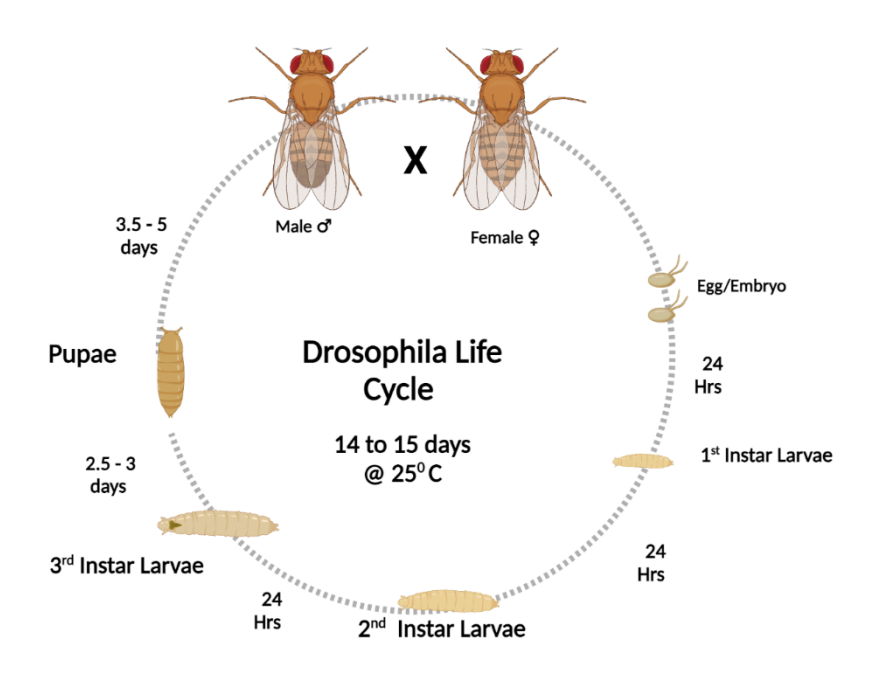


Figure 1.6: Schematic representation of the life cycle of *Drosophila* melanogaster.

1.8 Identification of male and female Drosophila melanogaster

Sexual dimorphism in *Drosophila melanogaster* is evident through distinct morphological characteristics. Females are generally larger in body size compared to males. The terminal segment of the abdomen is pointed in females, whereas in males, it is rounded. Additionally, the posterior abdominal segments (segments 5 and 6) exhibit a darker pigmentation in males relative to females.

Females possess seven visible abdominal segments, while males exhibit six, due to the fusion and internalization of the terminal segments in males during development. A distinguishing feature of males is the presence of sex combs—specialized rows of thickened bristles—on the third tarsal segment of the forelegs, which are absent in females. The female ovipositor is slender and pointed, adapted for egg-laying, whereas the male genitalia include a darkly pigmented, rounded structure known as the clasper, used during copulation.

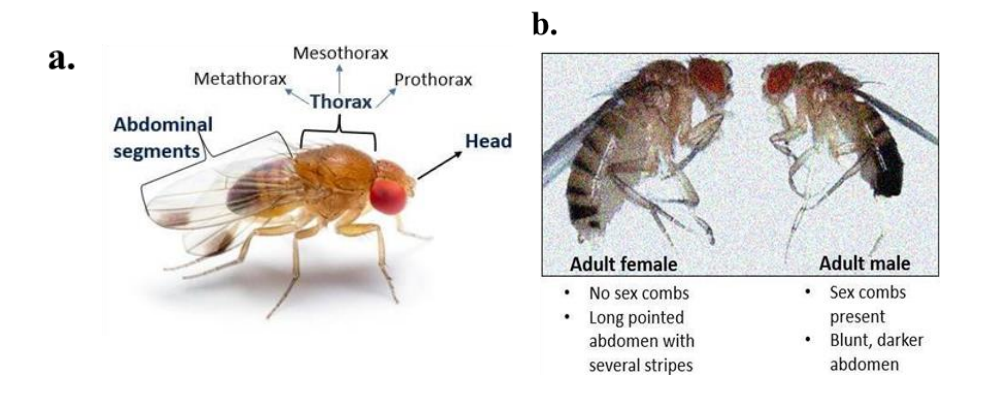


Figure 1.7: (a.) Adult *Drosophila* Fly. (b.) Male and female adult flies. (Adapted from T.H. Morgan 1910)

1.9 Organization of the thesis

Chapter 1 offers a succinct introduction to the thesis, providing a comprehensive overview of pathogenic repeat expansions and their underlying molecular mechanisms. The chapter delves into neurodegenerative disorders, repeat expansion disorders, detailing the resultant formation of PolyG proteins. Additionally, it addresses the development of therapeutic approaches targeting these repeat expansion disorders. The utility of *Drosophila melanogaster* as a model organism for studying CGG repeat expansion disorders, including FXTAS, is examined. Furthermore, an overview of the life cycle of *Drosophila melanogaster* is included to contextualize its relevance in research.

Chapter 2 discusses literature review about development of therapeutics against PolyG expressing repeat expansion disorders and formulates the research gap giving ample confidence for the research work outlined in the thesis.

Chapter 3 gives a concise overview of materials and methodologies followed in performing the present thesis work.

Chapter 4 discusses the results of the experiments performed. Elaborative biophysical experiments were performed to characterize the interactions between the lead small molecule and CGG repeat containing RNA. Thereafter, docking analysis and molecular dynamics simulations are discussed. Later, cell-based studies are discussed which describe the effects of small molecules on the aggregate formation. At last, *in-vivo* potency of the drug is validated using FXTAS *Drosophila* model.

Chapter 5 encompasses the concluding remarks and the future perspective of the thesis.

Chapter 2

Literature Review and Problem Formulation

Fragile X-associated tremor/ataxia syndrome (FXTAS) is a late-onset neurodegenerative disorder caused by CGG trinucleotide repeat expansions in the 5' untranslated region of the FMR1 gene. It is characterized by motor dysfunction, cognitive decline, and psychiatric symptoms, yet currently lacks any disease-modifying therapies. The CGG expansions lead to toxic RNA gain-of-function effects and the production of aberrant proteins via repeat-associated non-AUG (RAN) translation (Hagerman & Hagerman, 2016). The lifetime prevalence of FXTAS in the general population is estimated to be approximately 1 in 8,000, making it less common than other neurodegenerative diseases like essential tremor or Parkinson's disease in older adults. However, among male premutation carriers over age 50, about 40% develop FXTAS, compared to approximately 13% of female carriers. Given the growing prevalence of premutation carriers and the severe impact on quality of life, there is a pressing need for targeted therapeutic strategies (Jacquemont et al., 2004). The concern surrounding FXTAS stems from its progressive nature and the significant impact it has on the quality of life of affected individuals. Symptoms such as tremors, balance problems, and cognitive decline can lead to increased dependence and reduced autonomy. Early identification and management are crucial to mitigate these effects and provide appropriate support to patients and their families.

Approaches that can directly modulate pathogenic CGG RNA or its downstream effects—such as antisense oligonucleotides, RNA-targeting CRISPR, and small molecule modulators—are urgently required (Xu et al., 2021). Developing such interventions could not only improve outcomes for FXTAS patients but also provide insights into other repeat expansion disorders with similar mechanisms. Currently, there are no disease-modifying therapies for FXTAS, highlighting the

need for novel treatment strategies. Drug repurposing, which involves identifying new therapeutic uses for existing drugs, offers a promising approach to expedite the development of treatments for FXTAS.

CHANCE OF DEVELOPING CORE FXTAS SYMPTOMS BY AGE (MALE CARRIERS)

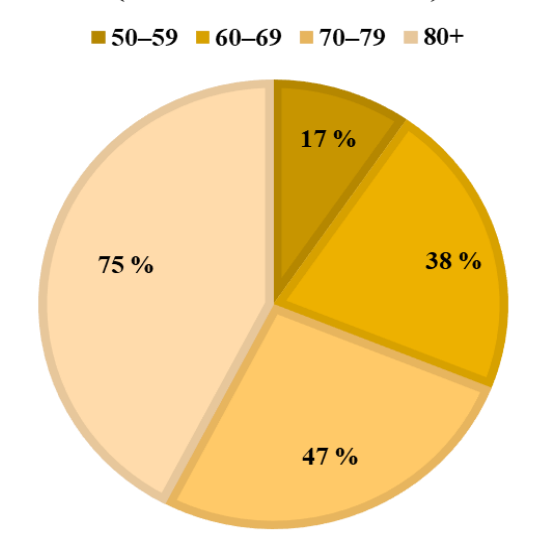


Figure 2.1: Pie chart representing the chance of developing FXTAS symptoms by age in case of male carriers. (Jacquemont et al., 2004)

The exploration of small molecules that target the pathogenic mechanisms of FXTAS underscores the potential of drug repurposing in developing effective treatments. By leveraging existing compounds with known safety profiles, this approach may accelerate the discovery of therapeutics that can alleviate or halt the progression of FXTAS. Small molecules offer distinct advantages as therapeutic agents, including oral bioavailability and superior permeability across the blood-brain barrier (Verma et al., 2022). Additionally, their pharmacokinetic properties and therapeutic potency can be more easily optimized, making them well-suited for treating neurological conditions such as FXTAS.

Previous studies have identified small molecules that can bind specifically to expanded CGG repeat RNAs, thereby mitigating their toxic effects (Disney et al., 2012). Memantine, an NMDA receptor

antagonist approved for Alzheimer's disease, was evaluated in a randomized, double-blind, placebo-controlled trial involving individuals with FXTAS. While memantine did not show significant benefits over placebo in primary outcome measures related to tremor severity and executive function, some improvements were noted in auditory processing and memory, indicating potential cognitive benefits in certain subgroups (Xu et al., 2021).

Neuropathological investigations in humans have demonstrated a strong correlation between CGG repeat length and the prevalence of intranuclear inclusions in both neurons and astrocytes. This suggests that CGG tract length serves as a robust predictor of both clinical severity such as earlier age of death—and neuropathological burden, as indicated by the number of inclusions (Greco et al., 2006). As the overexpression of mRNA is the root cause of the FXTAS, targeting the pathogenic secondary structures of repeat-expanded RNAs may offer a more precise and mechanism-specific strategy for therapeutic intervention and disease management rather than targeting the disease-associated downstream proteinopathy (Singh et al., 2025). Small molecules are capable of recognizing complex secondary and tertiary RNA structures (Disney et al., 2012) . Several small molecules, including natural compounds like myricetin and synthetic analogs, have demonstrated therapeutic potential by targeting r(CAG)_{exp} RNAs implicated in HD and spinocerebellar ataxias SCA.

Several investigational small molecules have shown promise in preclinical and early clinical studies such as Curcumin (Verma, Khan, Mishra, et al., 2020), Piperine (Verma et al., 2019), Citicoline (Hall et al., 2020) and Allopregnanolone (J. Y. Wang et al., 2017), but no FDA-approved small molecules have been tested for their treatment potential against FXTAS.

This thesis embarks on the exploration of FDA-approved small molecules that can selectively engage and modulate CGG repeat-containing RNA, opening new avenues for therapeutic innovation in

genetic disorders. By bridging the gap between existing pharmacology and novel treatment strategies, this work aims to pave the way for more precise, effective therapies for disorders like FXTAS.

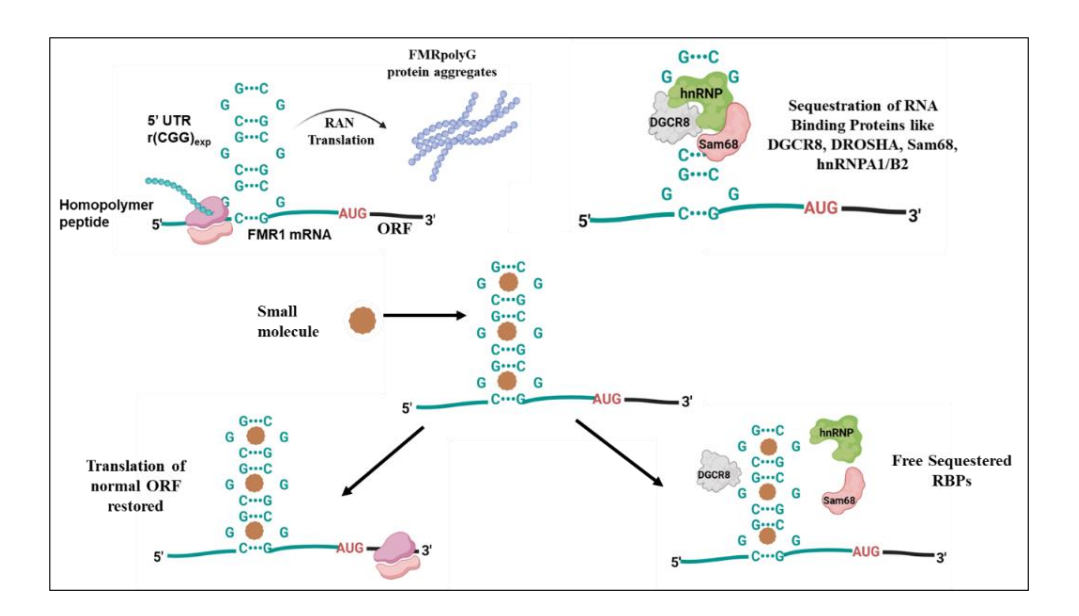


Figure 2.2: Schematic representation of the mode of action of small molecules in inhibition of RAN translation and reduction in sequestration of RNA binding proteins involved in splicing.

Chapter 3

Materials and Methods

3.1 Materials:

Cell culture reagents, chemicals like as NaCl, MgCl₂, KCl, K₂HPO₄, KH₂PO₄, NaH₂PO₄, Na₂HPO₄, NaOH, HCl, EDTA, Tris-base, DMSO, APS, TEMED, Acrylamide, bis-Acrylamide, ethanol, isopropanol, 2-butanol, methanol, urea, Triton-X 100 and others were sourced from Sigma-Aldrich Chemicals Ltd. based in St. Louis, Missouri, USA, and Sisco Research Laboratories Pvt. Ltd. in Mumbai, India. These were of molecular grade quality or HPLC purified. The dNTPs and rNTPs used for PCR amplification and *in vitro* transcription reactions were sourced from Sigma-Aldrich Chemicals Ltd. Additional supplies were obtained from Himedia Laboratories in India, including Luria broth, Luria agar, Agarose, Antibiotics such as ampicillin, chloramphenicol, kanamycin, Taq polymerase, and others. Glasswares were purchased from Borosil and standard plastic wares were procured from Tarsons Products Pvt. Ltd. from Kolkata, India.

Tissue culture supplies like plates and plasticwares were sourced from Thermo Fisher and Tarsons. Anti-PolyG and Anti-β-actin antibodies were obtained from Sigma-Aldrich and Santa Cruz Biotechnology. Lipofectamine 3000 was sourced from Invitro-Thermo Fisher. Calf thymus (CT-DNA) was purchased from Sigma Aldrich Chemicals Ltd.

3.2 Synthesis of RNA oligo synthesis using T7-RNA Polymerase (*In vitro* transcription):

3.2.1 Expression and Purification of T7- RNA Polymerase

A single colony of transformed bacterial cells was inoculated into LB broth supplemented with $50\,\mu\text{g/mL}$ ampicillin and $34\,\mu\text{g/mL}$ chloramphenicol and incubated overnight at $37\,^{\circ}\text{C}$. For large-scale expression, the overnight culture was diluted into fresh LB medium and

grown with agitation at 37 °C until reaching an optical density at 600 nm (OD600) of approximately 0.5. Protein expression was induced by the addition of 0.5 mM IPTG, followed by incubation for 4 hours at 37 °C. Post-induction, the cells were harvested by centrifugation at 9000 rpm, washed with lysis buffer, and lysed via sonication (55 % amplitude, 1-second pulse on/2 seconds off, total duration 1 minute). The lysate was cleared by centrifugation at 9500 rpm for 1.5 hours at 4 °C. The clarified supernatant was incubated with pre-cleaned, stripped, and recharged Ni-NTA resin at 4 °C for 3–4 hours under gentle agitation. The mixture was then applied to a Ni-affinity chromatography column and sequentially washed with lysis buffer (4–5 column volumes), low-salt buffer (3–4 column volumes), and high-salt buffer (1–2 column volumes). The bound protein was eluted using lysis buffer supplemented with 300 mM imidazole.

3.2.2 In-vitro Transcription

For all templates, 25 µL transcription reaction was prepared at room temperature sequentially adding: (i) 2.5 µL of 10× transcription buffer, (ii) 2 μ L of 10× rTNP mix, (iii) 12.75 μ L of template DNA, and (iv) 7.75 μL of T7 RNA Polymerase. This mixture was then incubated for 3-4 hours at 37 °C. The transcription reaction was analyzed using a 12 % denaturing urea-PAGE gel. Post- electrophoresis, RNA bands were identified by UV shadowing against a TLC plate. The bands corresponding to full-length transcripts were excised using a scalpel. These gel fragments were then placed into tubes with 300 mM NaCl and agitated overnight at 4 °C. Following this, the tubes were centrifuged, and the liquid phase was transferred to a new tube and subjected to two washes with equal volume of 1-butanol. The RNA was then precipitated by adding absolute chilled ethanol. RNA was allowed to incubate at 80 °C for 2-3 hours and centrifuged at 15600 rpm for 30 minutes at 4 °C. After the removal of excess alcohol through rota-evaporation the RNA precipitate was re-dissolved in MQ water. This was followed by the desalting of RNA using PD10 size exclusion column. The elutions collected were lyophilized to acquire high-purity RNA.

RNA sequences employed in biophysical studies and gel retardation assay were synthesized using *in vitro* transcription (run-off transcription) as described earlier (Khan et al., 2018). Briefly, T7 RNA polymerase was used to transcribe synthetic DNA templates amplified by PCR. Transcribed products were then purified through the PD-10 column and elutions were collected. These elutions were run on 3 % agarose prestained with ethidium bromide and imaged using ImageQuant LAS 4000 (GE Healthcare).

3.3 Fluorescence Titration Assay:

Using this experiment, we examined the changes in the fluorescence intensity of the small molecule upon the gradual addition of the RNA. RNA samples were prepared in 1X potassium phosphate buffer with 50 mM KCl. These were heated at about 95 °C for 10 minutes and allowed to reanneal at room temperature for about 30-45 minutes. 40 µM of RNA was serially diluted, and the last well was taken as blank and lacking RNA. Each sample was run in duplicate. The excitation and emission wavelengths for the molecules were predetermined. This assay was performed for extended r(CGG)_{exp} RNA repeats, 1 X 1 internal loop motif (5'CNG/3'GNC), and AU (5'CAG/3'GUC) duplex RNA control. DNA sequences of CT-DNA, c-myc, HRAS 1, and HRAS 2 served as control. The concentration of P2 was constant in each well to ensure consistency. Change in the emitted fluorescence of P2 was observed with the gradual titration of RNA. The assays were conducted on SynergyTM H1 multi-mode microplate reader using Corning half-area black 96 well microplate at 25 °C. The fluorescence data were analyzed using Sigma Plot 12.0 software (Systat Software, Chicago, USA). The binding equation used (Singh et al., 2025) -

$$f = \frac{Bmax^{1} \times abs(x)}{k_{d} \times abs(x)} + \frac{Bmax^{2} \times abs(x)}{k_{d} \times abs(x)}$$
(1)

Bmax and K_d represent maximum binding sites and equilibrium binding constant, respectively.

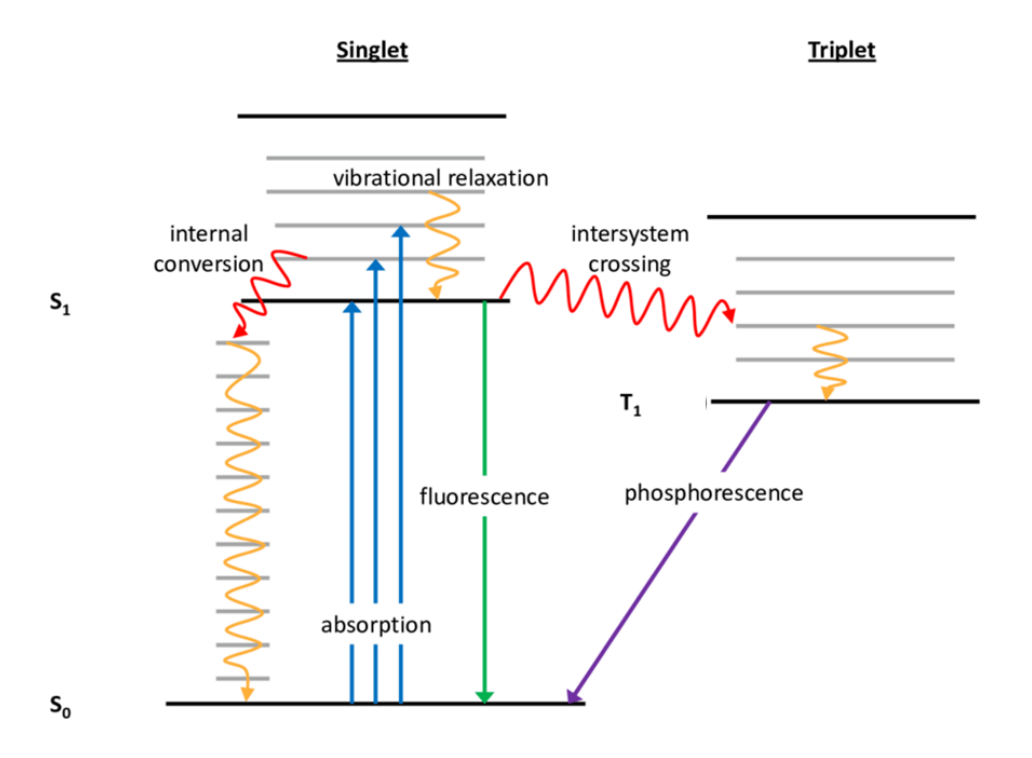


Figure 3.1: Jablonski diagram depicting fluorescence phenomenon where the molecule is excited to a higher energy state followed by the release of energy.

3.4 Circular Dichroism Spectroscopy:

These experiments were performed on a J-815 Spectropolarimeter (JASCO), and a Peltier junction temperature controller was used to maintain a constant temperature of 298 K throughout the experiment. A steady stream of dry nitrogen was directed into the cuvette-holding chamber to avoid the condensation of water droplets exterior of the cuvette. Spectra were recorded in a quartz cuvette of 1 mm path length at regular intervals of 0.1 nm and averaged over three scans. 10 µM RNA samples were titrated with increasing concentration of P2 in 50.0 mM KCl, 1X Potassium phosphate buffer at pH 7.2. As previously mentioned, in order to ensure accuracy, a blank spectrum of buffer (1X KPO₄, KCl, and milliQ water) was recorded before each measurement and deducted from the sample's CD spectrum. Analysis of data was performed using SigmaPlot 13.0 for a detailed interpretation of RNA-

ligand interactions and the stabilizing or destabilizing effects of ligand on loop structures.

3.5 Electrophoretic Mobility Shift Assay:

Gel Retardation assay was performed for P2 molecule against different r(CGG)_{exp} RNA. r(CGG)₂₀, r(CGG)₄₀, r(CGG)₆₀ and r(CGG)₉₉ RNA were prepared in 1X potassium phosphate buffer having 50 mM KCl. These samples were then subjected to heat at 95 °C and then allowed to cool down gradually at room temperature. This reaction mixture was incubated with an increasing concentration of P2 ranging from 0 to 1mM for 30 minutes at room temperature. Following this, the products obtained were separated using 3 % agarose prepared in 1X TBE and visualized through staining in ethidium bromide. The gel was pictured and analyzed using ImageQuant LAS 4000 (GE Healthcare).

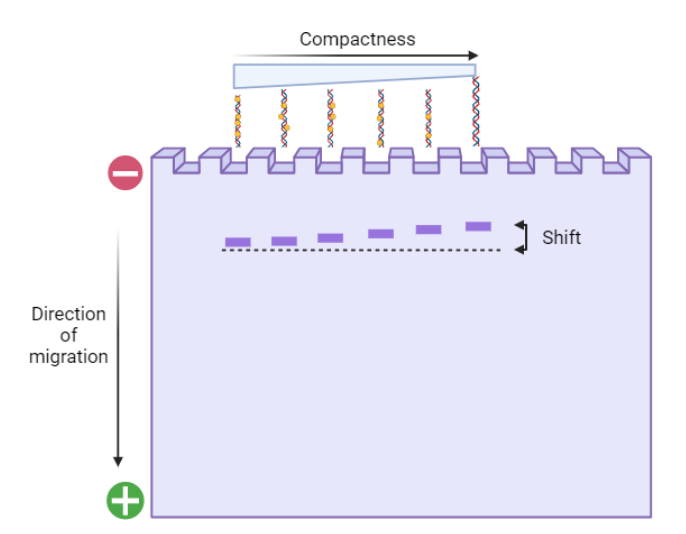


Figure 3.2: Schematic representation of Electrophoretic shift mobility.

3.6 PCR Stop Assay:

Template for GGx1 (5'- GGA GAG GGU UUA AUC GGU ACG AAA GUA CGG AUU GGA UCC GCA AGG - 3'), GGx6 (5'- GGA GAG

GGU UUA AUC GGC GGC GGC GGC GGU ACG AAA GUA CGG CGG CGG CGG CGG AUU GGA UCC GCA AGG - 3') and complementary sequence (5'- GGC CGG ATC CTA S5 ATA CGA CTC ACT ATA GGG AGA GGG TTT AAT - 3') were sourced from Integrated DNA Technologies pvt ltd. PCR master mix includes 1X PCR buffer, 4.25 mM MgCl₂, 10 pmol oligonucleotides, 0.33 mM dNTPs, 2.5 units Taq DNA polymerase (from Sigma Aldrich), and volume made up by milli Q water to 25 µL. For each concentration of P2, the reaction volume of the assay is 25 μL. Serial dilution of P2 ranging from 0.0 to 1.0 mM and proceeded with incubation in thermos cycler (Eppendorf) with conditions: 95 °C for 30 s, followed by 35 cycles of denaturation at 92 °C for 20 s, annealing at 56 °C for 35 s, and extension at 72 °C for 1 min, followed by final extension at 72 °C for 10 min and held finally at 4 °C for infinite time. The PCR products obtained were mixed with 6X loading dye, and resolved on 3 % agarose gel pre-stained with ethidium bromide. Gel mages were visualized using ImageQuant LAS 4000 (GE Healthcare) and analyzed using ImageJ.

3.7 RNA Thermal Denaturation Profile:

RNA thermal denaturation experiments were performed using a J-815 Spectropolarimeter (JASCO) equipped with a water Peltier system (PCB-1500) and a Peltier temperature programmer. For this, r(CGG)_{20/40/60/99} RNA and AU paired RNA were diluted in 1X KPO₄ buffer (50.0 mM KCl, 10.0 mM potassium phosphate) and heated at 90–92 °C for 5–10 minutes. Solutions were allowed to cool to room temperature for the next 30 minutes. To record melting curves of RNA, temperature was increased from 25 °C to 95 °C at a rate of 5 °C/min while titrating the drug P2 till the ratio of Drug/ Nucleic acid (D/N) reached to 1. The changes in normalized absorbance at 265 nm were plotted against temperature using SigmaPlot 12.0 software.

3.8 Molecular Docking of P2 with CGG RNA:

For docking, crystal structure of duplex CGG motif (PDB ID: 3JS2) was used. Autodock vina was employed to conduct the docking analysis.

Duplex RNA was treated as a rigid solid structure with RNA and P2 files were prepared in PDBQT format. The grid box was intended to cover the complete RNA structure, allowing P2 to explore the entire conformational space. The final image was prepared in Discovery Studio by processing the best possible docking result.

3.9 Nuclear Magnetic Resonance (NMR) Spectroscopy:

The RNA sequence r(CGG)₆ was subjected to NMR investigations utilizing high-resolution Avance III 400 and 500 MHz spectrometers (BioSpin International AG, Switzerland) fitted with z-field gradients and a broadband inverse probe. P2-RNA were prepared in a 1X potassium phosphate buffer (10 mM phosphate, pH 7.2, 0.1 M KCl, 50 mM EDTA) having 10% D₂O. For drug titration studies, RNA was added incrementally to the sample RNA. To lock the radio frequency, H₂O and D₂O were used in a ratio of 9:1. One-dimensional proton NMR spectra were recorded with 64000 data points, an 8-second relaxation delay, and 64 to 128 scans at 298K, achieving a resolution of 0.15 to 0.3 Hz/point. Baseline and phase corrections were applied to the obtained spectra during processing. To ensure uniformity across samples throughout the titration process, tuning, matching, and shimming were done. Using Topspin version 3.5 for data processing, integration, and analysis, DSS (4,4-dimethyl-4-silapentane-1-sulfonic acid) was used as the NMR reference standard.

3.10 Quantification of PolyG proteins by Western blot:

HEK273T cells were seeded in 6 well plate and allowed to grow to form a monolayer of cells. Cells were transfected with $r(CGG)_{99}$ -EGFP. After 4-5 hrs, the transfection mixture was replaced with fresh media containing the drug P2 having different concentrations, i.e., 25.0 μ M and 50 μ M. The cells were incubated for the next 24 hours. Cells were then lysed using RIPA buffer (approx. 150 μ l/well). Bradford assay was used to determine the concentration of protein. SDS-PAGE was performed for protein samples with equal concentration. The gel was then transferred to the PVDF membrane. After completion of the transfer,

blots were incubated with primary antibody antiFMR1PolyG from Merck Millipore. Following overnight (at 4 °C) primary antibody incubation, conjugated secondary antibody anti-IgG-horseradish peroxidase was used. A chemiluminescent signal was detected using Luminata Crescendo Western HRP substrate from Merck Millipore in ImageQuant LAS 4000 (GE Healthcare) and analyzed using ImageJ.

3.11 Reversal of pre-mRNA splicing defect in the cellular model:

FXTAS cellular model was used to determine if P2 can cause restoration of the pre-mRNA splicing defect. HEK293 cells were grown in 24 well plates as a monolayer in the growth medium containing 1X DMEM, 10 % fetal bovine serum, 1 % antibiotic, and antimycotic at 37 °C with 5 % CO₂. As confluency of 80-90 % is reached, cells are transfected with a plasmid having r(CGG)₉₉ repeat and targeted mini gene, i.e., *SMN2* and *Bcl-x*, as per the protocol. After 4-5 hrs, the transfection cocktail is replaced with P2-containing media. After 24 hours of incubation, cells were lysed in the plate, and whole RNA was recovered through an RNA isolation kit (Invitrogen), as per the manufacturer's guidelines.

All RNA samples obtained in different experimental conditions were subjected to (RT-PCR) employing a cDNA synthesis kit from Bio-Rad, as per the standard protocol. Out of 500 ng reverse transcribed mRNA, 100 ng were subjected to semi-quantitative PCR. PCR protocol was as follows: denaturation at 95 °C for 1 min, annealing at 55 °C for 1 min, extension at 72 °C for 2 min, followed by final extension at 72 °C for 10 min. This PCR protocol was run for 25-30 cycles. Analysis of PCR product was done on agarose gel electrophoresis, pre-stained with ethidium bromide. The image was recorded using ImageQuant LAS4000 (GE Healthcare), and quantification of splicing isoform intensity was done using ImageJ.

3.12 Drosophila stocks, dietary conditions, and drug treatment

Transgenic fly lines expressing EGFP (*UAS-EGFP/CyO*) and mutant lines with 90 CGG repeats (*UAS-(CGG)90-EGFP/CyO*) (Kazemi-

Esfarjani & Benzer, 2000) were generously provided by Prof. Abrar Qurashi from the University of Kashmir, India. The eye-specific driver line, GMR-Gal4 which drives expression to the adult eye and eye imaginal discs (Ray & Lakhotia, 2015), and the pan-neuronal driver line, Elav-Gal4, were generously provided by Dr. Anand K. Tiwari of the Institute of Advanced Research in Gandhinagar, Gujarat. Male transgenic strains were crossed with female GMR-Gal4 and Elav-Gal4 strains, respectively, to promote expression in the brain and ocular imaginal discs. The flies were cultured on a typical cornmeal-agar diet at a constant temperature of 25 ± 1 °C, with stable cycles of light and dark and humidity levels between 70% and 80%. P2 was incorporated in the food at concentrations 25.0 μ M and 50.0 μ M for experimental larvae and flies. Control flies were maintained on standard food lacking P2 at 25 ± 1 °C.

3.13 Assessment of rough eye phenotype, pigment loss, and FMR1PolyG inclusion bodies using Nikon SMZ745T Microscope and Fluorescence Confocal Microscopy:

Flies with 90 CGG repeats and those without CGG repeats under *GMR-GAL4* regulation were evaluated for their rough-eye phenotype. These flies were maintained at 25 °C on regular diet that was supplemented with P2 at concentrations of 25.0 and 50.0 μM. The Nikon SMZ745T microscope was used to investigate the exterior eye morphology. For each experimental condition, a total of 5 flies in 3 sets were analyzed.

FMRPolyG-EGFP protein inclusion in the rough eye and EGFP, respectively, was detected and recorded using confocal microscopy at 10× magnification in *GMR-Gal4* driven *UAS-(CGG)90-EGFP/CyO* and *UAS-EGFP/CyO* flies.

For pigmentation loss studies, 15-20 *GMR-Gal4* driven *UAS-(CGG)90-EGFP/CyO* fly heads were homogenized in PBS followed by recording absorbance at 480 nm.

Additionally, Flynotyper software was utilized to identify and measure the morphological changes in the treated and untreated fly eyes. To evaluate the degree of disorderliness in the organization of the ommatidia within the fly's eye, this software calculates a phenotypic score.

3.14 Scanning Electron Microscopy Analysis of *Drosophila* External Eye:

Sample for high magnification Scanning Electron Microscopy (SEM) was prepared using Critical Point Drying (CPD) method in accordance with the protocol outlined. First, whole flies were fixed for two hours in a solution of 1 % glutaraldehyde, 1 % formaldehyde, and 1 M sodium cacodylate (pH 7.2). 0.2 % Tween 20 (diluted in water) was added dropwise to the fixative to ensure total immersion. Following fixation, the flies were rinsed with water and then dehydrated using a series of graded ethanol: 50 %, 75 %, and 25 % ethanol for 12 hours each, and then two 12-hour washes in 100 % ethanol at room temperature. Post dehydration, the samples were sputter-coated for imaging and subjected to CPD.

3.15 Negative Geotaxis Assay (Drosophila Climbing Assay):

To assess the locomotor capabilities of the flies, the climbing assay was performed. Each experimental condition was tested with two groups of 20 flies, and a total of three trials were performed using a designated vertical column measuring 25 cm in length and 1.5 cm in diameter. The number of flies that climbed over the 10-cm threshold and those that stayed at the bottom were measured after the column was lightly tapped three times. The number of flies that approached or exceeded the 10 cm mark in a 15-second period was used to quantify the results.

3.16 Larval Crawling Assay:

The larvae's crawling potential was evaluated using a 100×10 mm Petri dish with a 3 % agar base. As previously mentioned, a track that was 2 mm wide, 30 mm long, and 5 mm deep was made inside the dish. The

third-instar larvae were positioned on the track after being given a minute to adapt. After 15 seconds of observation, the larvae's total distance traveled was calculated. Three trials were conducted with three larvae per condition.

3.17 Western blot analysis from *Drosophila*:

Western blot analysis was performed on adult *Drosophila* heads to evaluate protein expression across experimental groups. A total of 40 fly heads per group were dissected from diseased flies treated with varying concentrations of P2. Protein extraction was carried out following a previously established protocol. Protein concentrations were quantified using the Bradford assay, and 50.0 µg of total protein per sample was resolved by SDS–polyacrylamide gel electrophoresis (SDS–PAGE). Proteins were subsequently transferred onto polyvinylidene difluoride (PVDF) membranes. Membranes were incubated overnight at 4 °C with primary antibodies specific to FMR1PolyG and EGFP (Merck Millipore). After washing, membranes were incubated with horseradish peroxidase (HRP)-conjugated secondary anti-IgG antibodies. Protein bands were detected using the LuminataTM Crescendo Western HRP substrate (Merck Millipore) and imaged using the ImageQuant LAS 4000 system (GE Healthcare).

3.18 Assessment of ROS levels:

To evaluate the basal levels of reactive oxygen species (ROS), the fluorescent probe 2,7-dichlorofluorescein diacetate (DCF-DA) was employed. After a 14-day treatment period, twenty flies (14 days old) from each experimental group were collected and homogenized in 20 mM Tris buffer (pH 7.0). The homogenates were centrifuged at 1600 × g for 10 minutes at 4 °C, and the resulting supernatant was incubated with DCF-DA for one hour to facilitate its oxidation to the fluorescent product, 2,7-dichlorofluorescein (DCF). Fluorescence intensity was measured using a multimode plate reader with excitation and emission wavelengths set at 488 nm and 530 nm, respectively. An increase in DCF fluorescence is indicative of elevated ROS levels.

3.19 Histological Analysis of Larval Brain Tissue:

Larval brain tissue staining was performed following established protocols. Third-instar larval brains were dissected in 1× PBS and fixed in 4 % paraformaldehyde (PFA) in PBS at room temperature for 20 minutes. For propidium iodide (PI) staining, fixed tissues were incubated in 1 µg/mL PI solution (P4170; Sigma, St. Louis, MO, USA) for 15 minutes at room temperature. For mitochondrial superoxide detection, brains were incubated with 1 µM MitoSOX Red (Invitrogen, Thermo Fisher Scientific) for 30 minutes at room temperature. For mitochondrial membrane potential assessment, fixed brains were stained with 50.0 nM tetramethylrhodamine methyl ester (TMRM; Invitrogen, Thermo Fisher Scientific) for 30 minutes at room temperature. Post-staining, tissues were washed three times with PBST (PBS with 0.1 % Tween-20) for 10 minutes each. Samples were then mounted using FluorSaveTM mounting medium (Merck Millipore). Images were acquired at 10× magnification using an FV1200 MPE confocal microscope. Brightness and contrast adjustments were performed using FluoView FV1000 software.

3.20 Lifespan Analysis:

Virgin flies were collected within 24 hours post-eclosion from synchronously laid eggs. Diseased flies were sorted and distributed into separate vials, with 30 flies per vial containing either control or drug-supplemented food. P2 was incorporated into the experimental diet at final concentrations of 25.0 µM and 50.0 µM. Mortality was recorded at 3-day intervals, and flies were transferred to fresh food vials at the same frequency without the use of anesthesia. Lifespan assays were conducted in two independent biological replicates. Survival data were analyzed using GraphPad Prism statistical software.

3.21 Statistical Methods:

For statistical analysis and graphical representation, GraphPad Prism software (version 9.5) was utilized. Data were presented as mean \pm SD or S.E.M. Using the One-way ANOVA Test, the statistical significance of the comparisons between the various groups was examined. A two-way ANOVA was employed for the subgroup analysis analysis. When the P-value is less than 0.05, it is deemed statistically significant.

Chapter 4

Results and Discussion

4.1 P2 shows specific binding affinity and selectivity towards r(CGG)_{exp} RNA, elucidated by Fluorescence Titration Assay.

Expanded Repeat RNAs like r(CGG)_{exp} can be targeted for therapeutic interventions in different neurological, neurodegenerative, and neuromuscular disorders like HD, SCAs, and FXTAS. 14 FDA-approved drugs were subjected to fluorescence binding assay to assess their binding affinity towards r(CGG)₆. Through fluorescence titration assays, specificity in the interaction of P2 with possible combinations of 5'CNG/3'GNC RNA motifs was assessed. GC encloses these trinucleotide repeats that enable RNA to fold in a proper conformation. N can be any nucleotide- A, T, G, and C. As RNA is gradually added to the drug solution P2, there is a decrease in the fluorescence of the drug at an excitation wavelength of 260nm and emission wavelength of 375nm which were predetermined. Change in the fluorescence value with reference to blank was plotted against the concentration of RNA used. The graph provides the binding constant that denotes the binding affinity of P2 towards RNA (Figure 4.1).

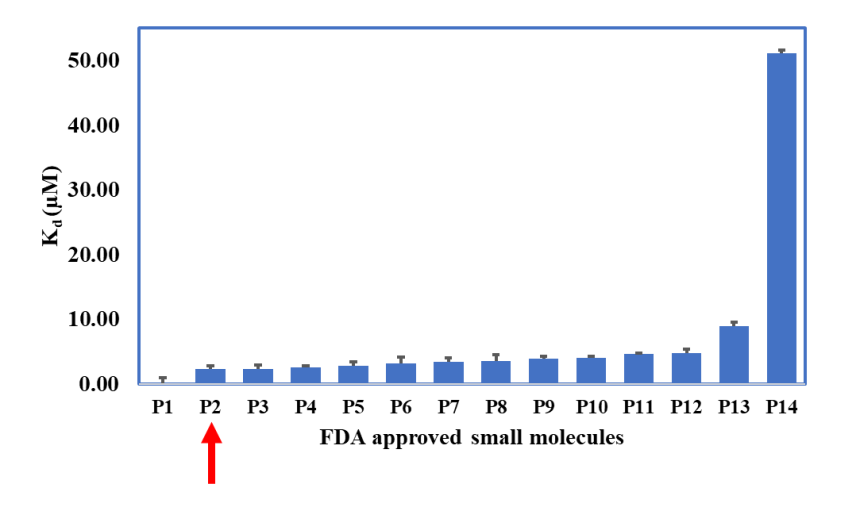


Figure 4.1: Primary screening showing binding affinities of 14 FDA-approved drugs towards r(CGG)₆ as screened by Fluorescence Binding Assay.

Table 4.1: Binding constants for 14 FDA-approved small molecules towards r(CGG)₆ as screened by Fluorescence Binding Assay.

FDA approved small molecules	K _d (μM)
P1	0.03
P2	2.36
P3	2.38
P4	2.55
P5	2.80
P6	3.12
P7	3.40
P8	3.59
P9	3.91
P10	4.07
P11	4.61
P12	4.72
P13	8.91
P14	51.16

From the results, the P2 molecule exhibited higher selectivity and binding affinity towards 5'CGG/3'GGC in comparison to other mismatched RNA motifs and AU-paired (5'CAG/3'GUC) RNA.

5'CAG/3'GUC RNA having normal base pairing can form a normal duplex structure. Looking at the higher selectivity of P2 towards 5'CGG/3'GGC, other repeats of CGG like r(CGG)₁, r(CGG)₂, r(CGG)₃, r(CGG)₆, r(CGG)₂₀, r(CGG)₄₀, r(CGG)₆₀ and r(CGG)₉₉ were assessed for binding affinities. Higher binding affinity was observed with large CGG repeats. Other repeats r(CCG)₆, r(CAG)₆, and r(CUG)₆ form CC, AA, and UU 1x1 hairpin structure, respectively. P2 binds specifically and selectively to CGG repeats as inferred by the binding assays. P2 was specific for CGG over other DNA controls like Bcl2, c-myc (genes forming G-quadruplex), HRAS 1, HRAS 2, and duplex CT-DNA (Figure 4.3).

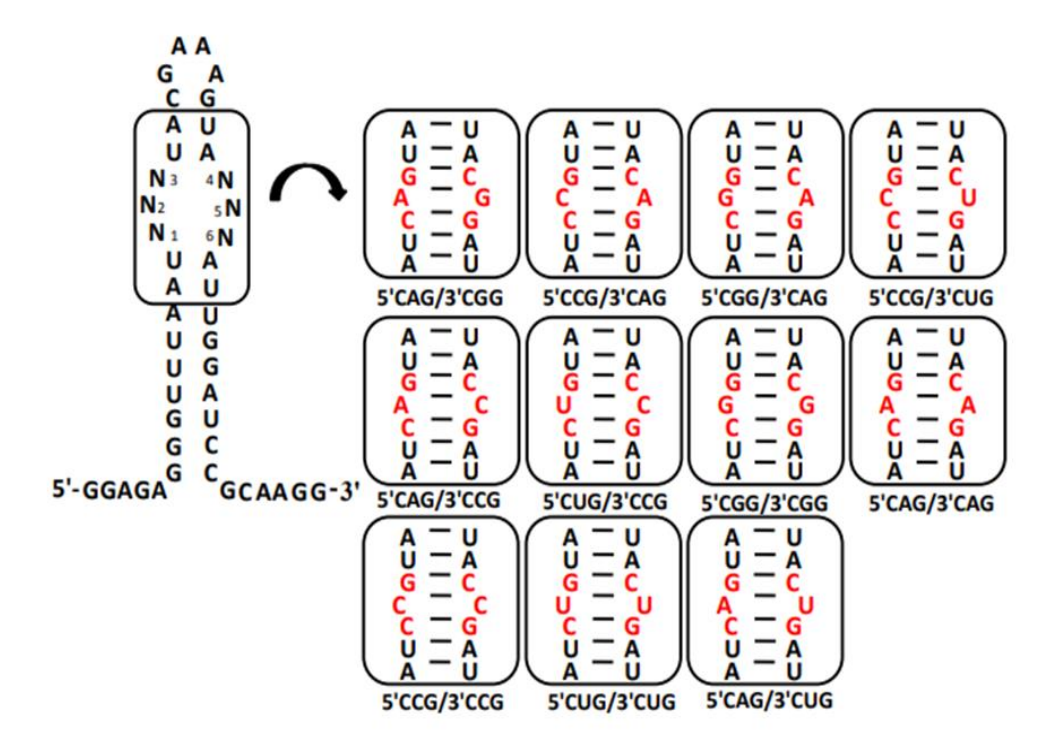
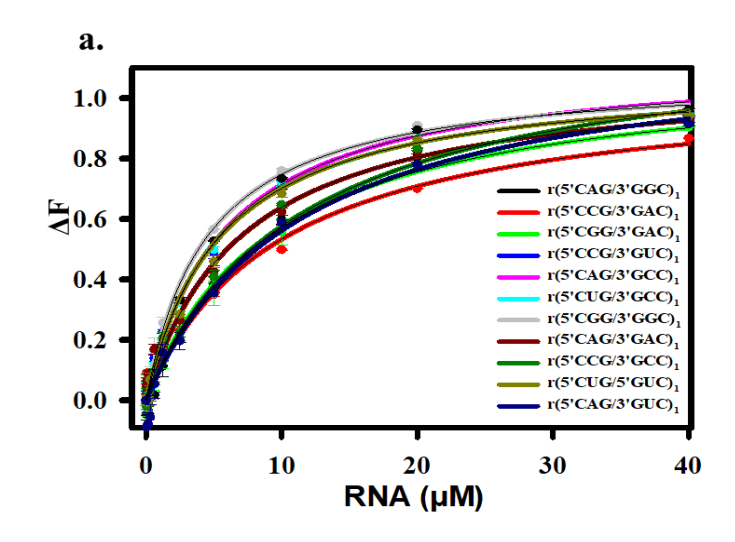
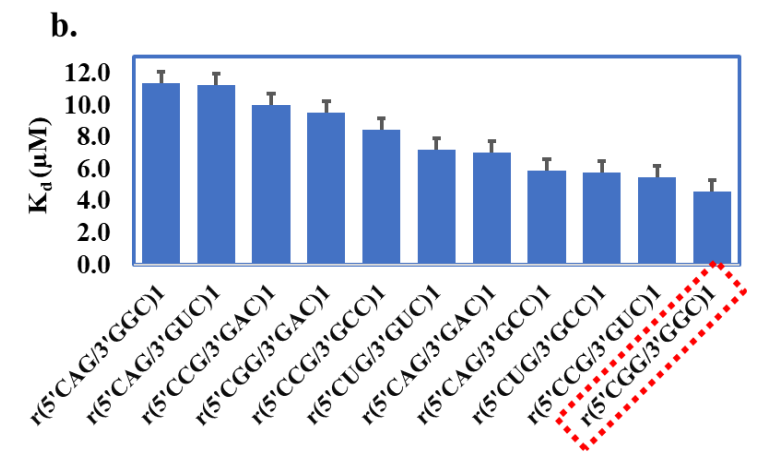
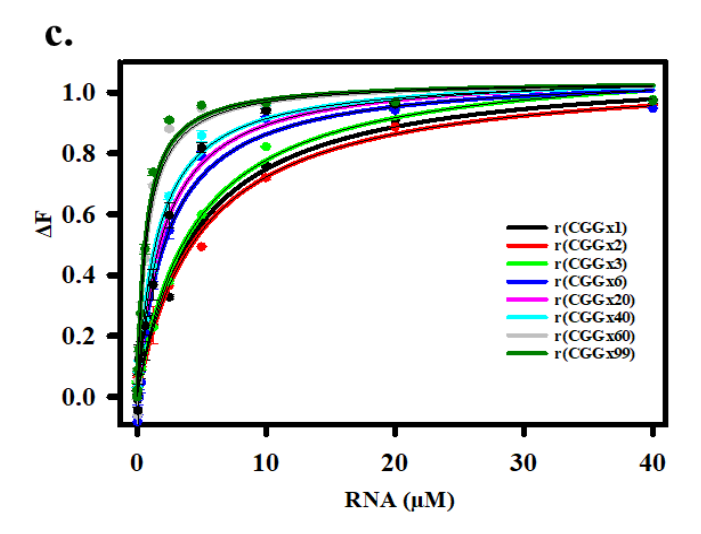
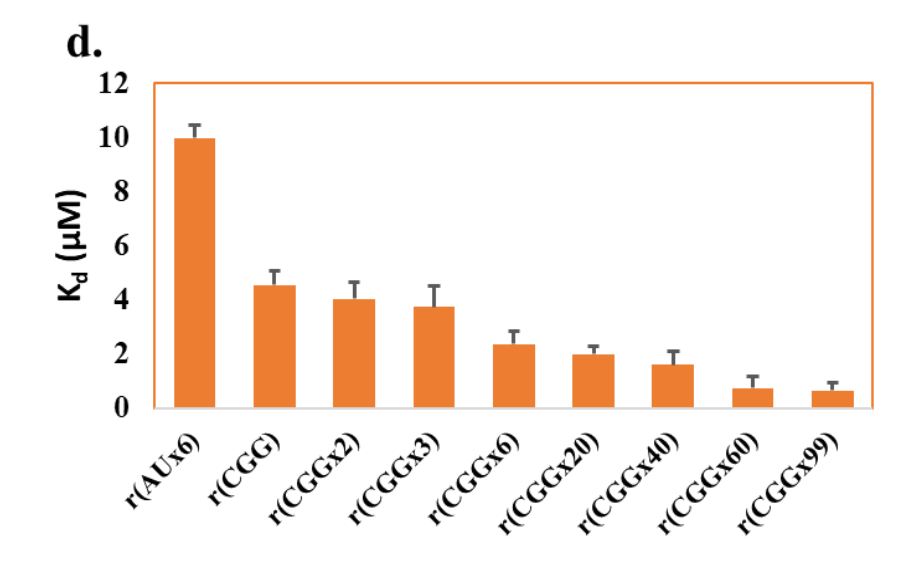


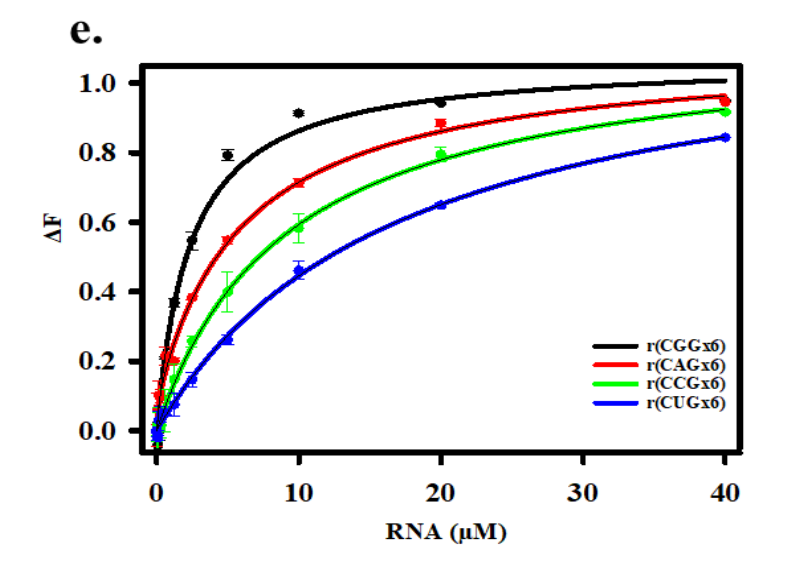
Figure 4.2: Secondary structures of different RNA sequences with internal loops comprise one nucleotide each. DNA molecule binding is studied using the secondary structure of RNA sequences. Below their secondary structure is their nomenclature (Khan et al. 2018).

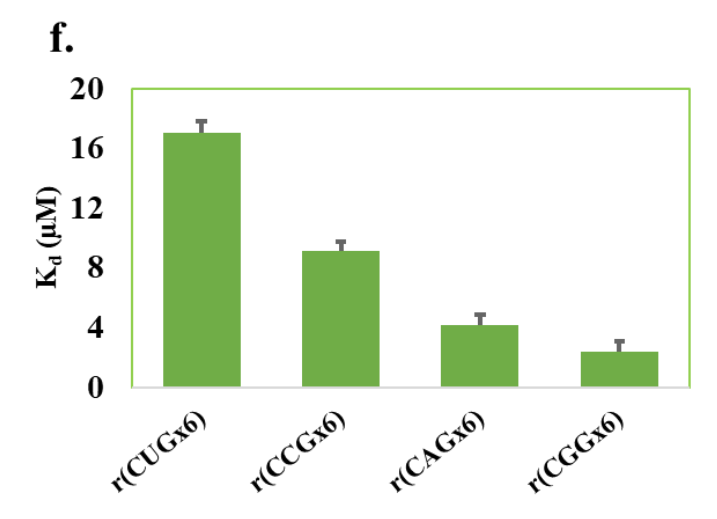












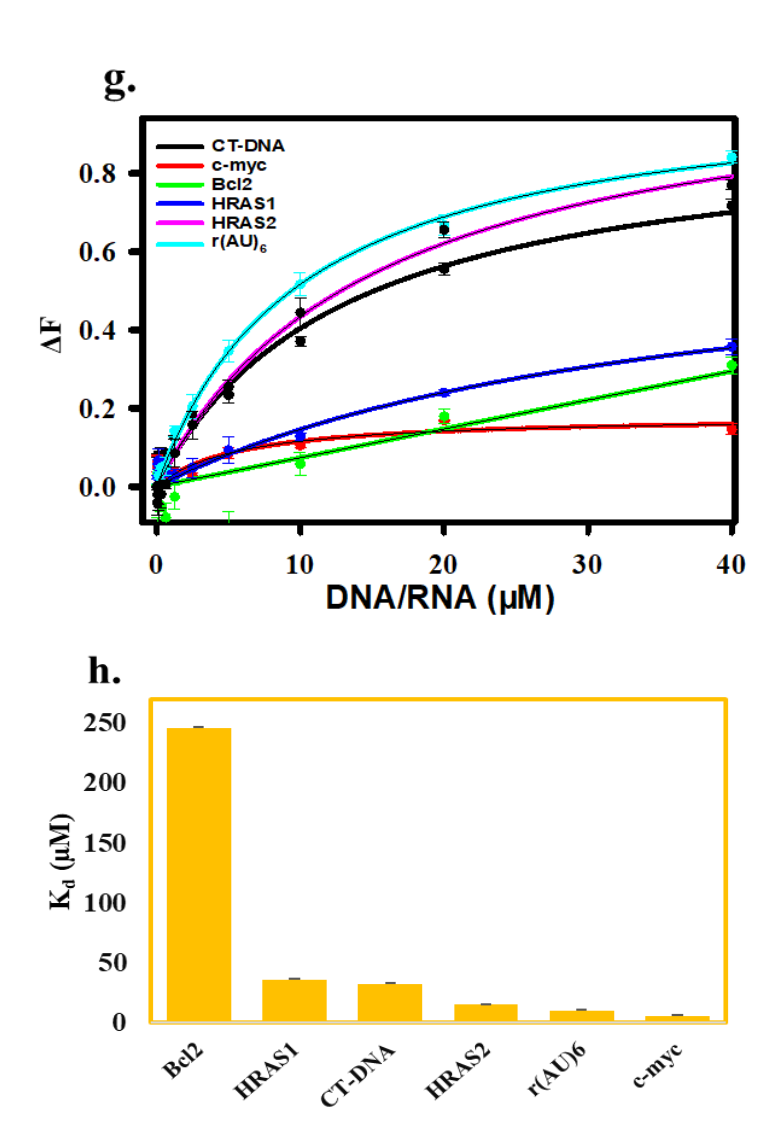


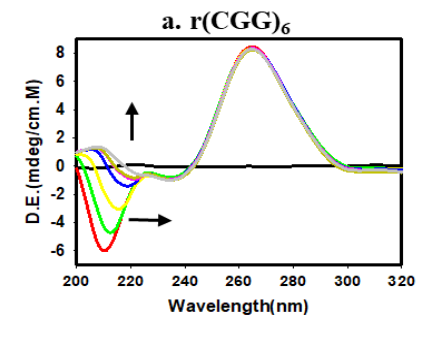
Figure 4.3: P2 shows specific binding affinity and selectivity towards r(CGG)_{exp} RNAs as demonstrated by Fluorescence Titration Assays.

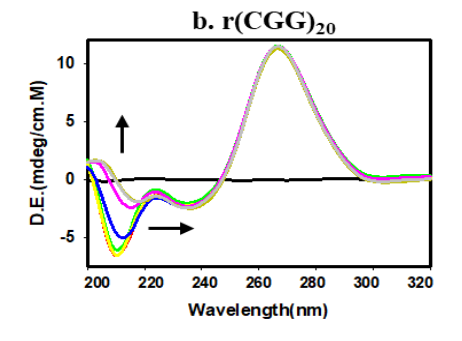
(a.) Plot showing the change in fluorescence for (5'CNG/3'GNC) RNA internal loops. (b.) Bar graph depicting binding affinities of (5'CNG/3'GNC) RNA motifs towards P2. (c.) Plot showing the change in fluorescence for different r(CGG)_{exp} repeats. (d.) Bar graph showing binding affinities of expanded r(CGG)_{exp} repeats towards P2. (e.) Plot showing the change in fluorescence for different r(CGG)_{exp} repeats and control repeats (r(CUG)₆, r(CCG)₆, r(CAG)₆). (f.) Bar graph showing binding affinities of control repeats (r(CUG)₆, r(CCG)₆, r(CAG)₆) towards P2. (g.) Plot showing a change in fluorescence for different control DNA and RNA. (h.) Bar graph depicting binding affinities of different control DNA and RNA towards P2.

4.2 Confirmation of specific topological effects of P2 binding to target RNA by Circular Dichroism Spectroscopy and Thermal Profile.

CD Spectroscopy examined RNA sequences with GG mismatches. RNA with normal A-U base pairing was compared to the GG mismatched pairs to evaluate the P2 molecule's selectivity and specificity. CD spectra of r(CGG)_{exp} RNAs depict a distinct positive peak at 265-270nm and a negative peak at 215-220 nm, characteristic of double-stranded A-type RNA conformation (Verma et al., 2022).

The gradual addition of P2 to $r(CGG)_{exp}$ RNA solution causes a decrease in hypochromic shift (ellipticity) and bathochromic (red) shift in negative peaks in a concentration-dependent manner (Figure 4.4 (a-e.)). But, the overall RNA structure was found to be unaltered. Along with that, a hypochromic and bathochromic shift is observed in the positive peak of RNAs comprising higher CGG repeats i.e., $r(CGG)_{99}$, thereby indicating the higher binding affinity of the drug towards higher pathogenic CGG repeats. A simultaneous reduction in both the positive and negative peaks in CD spectra typically indicates weak van der Waals interactions, often arising from π – π stacking between the small molecules and their target RNA structures (Verma et al., 2022). Conversely, no modifications were observed in the case of paired AU-RNA (Figure 4.3 (i)). Hence, this change in conformation is exclusive in GG mismatch containing RNA.





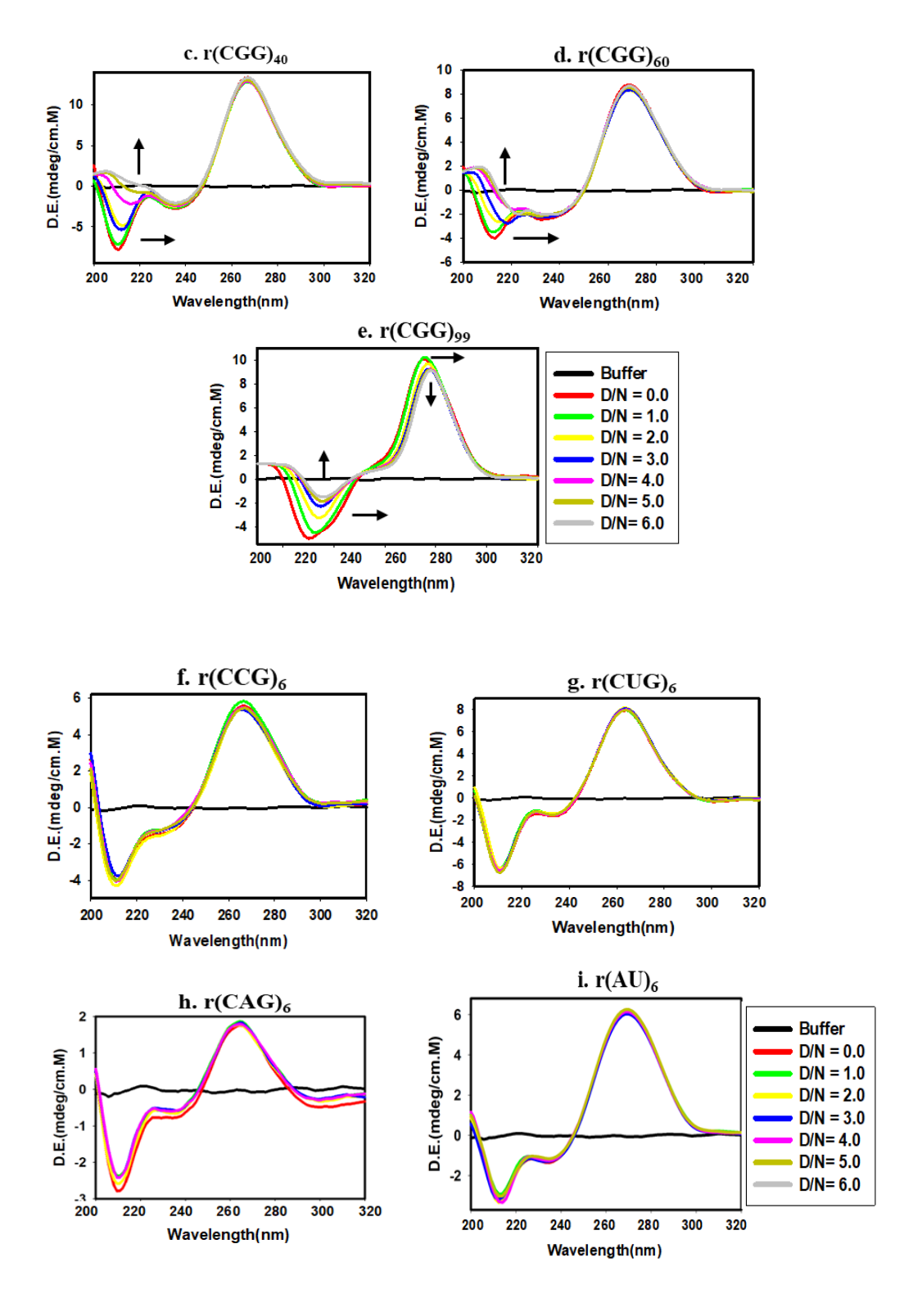


Figure 4.4. CD spectroscopy titration of P2 with r(CGG)_{exp} and r(AU)₆ duplex RNA. CD spectroscopy of P2 with (a.) r(CGG)₆, (b.) r(CGG)₂₀, (c.) r(CGG)₄₀, (d.) r(CGG)₆₀, (e.) r(CGG)₉₉, (f.) r(CCG)₆, (g.) r(CUG)₆, (h.) r(CAG)₆, (i.) r(AUx6) duplex control RNA.

4.3 Validation of thermal stabilization of CGG repeat RNAs by small molecule P2.

To evaluate the effect of the small molecule P2 on the structural stability of CGG repeat-containing RNAs, we analyzed their thermal denaturation profiles using a UV-based melting assay. This method is widely utilized to investigate the interactions between bioactive compounds and nucleic acids. The extent of change in melting temperature (ΔT_m) reflects both the binding affinity and stoichiometry of ligand-RNA interactions. UV absorbance at 265 nm was monitored as a function of temperature, with the D/N (Drug-to-Nucleic acid) molar ratio varied up to 1.0. The results demonstrated a concentrationdependent increase in the thermal stability of CGG repeat RNAs upon treatment with P2. Notably, the melting temperature of RNAs with varying repeat lengths for r(CGG)₆, r(CGG)₂₀, r(CGG)₄₀, r(CGG)₆₀ and r(CGG)₉₉ increased progressively in the presence of P2, with the highest stabilization observed for r(CGG)99 (Figure 4.5). This effect likely arises from the greater number of accessible binding sites and structural variations in the longer hairpin loops (Khan et al., 2019).

In contrast, no significant alteration in T_m was detected for $r(AU)_6$ -paired RNA. These findings indicate that the increase in T_m upon P2 binding correlates with enhanced stability of the target RNA. The observed thermal stabilization can be attributed to the planar aromatic structure of P2, which facilitates π – π stacking interactions with guanine bases in the hairpin loop. Importantly, such thermal stabilization of GG-rich RNA motifs may inhibit aberrant Repeat-Associated Non-AUG (RAN) translation and prevent the sequestration of key splicing regulators. Previous studies have shown that both natural and synthetic small molecules capable of stabilizing expanded repeat RNAs can mitigate pathological phenotypes associated with disorders like FXTAS and HD (Singh et al., 2025). Therefore, P2 holds potential as a neuroprotective therapeutic candidate for FXTAS by targeting and stabilizing expanded CGG repeat RNAs.

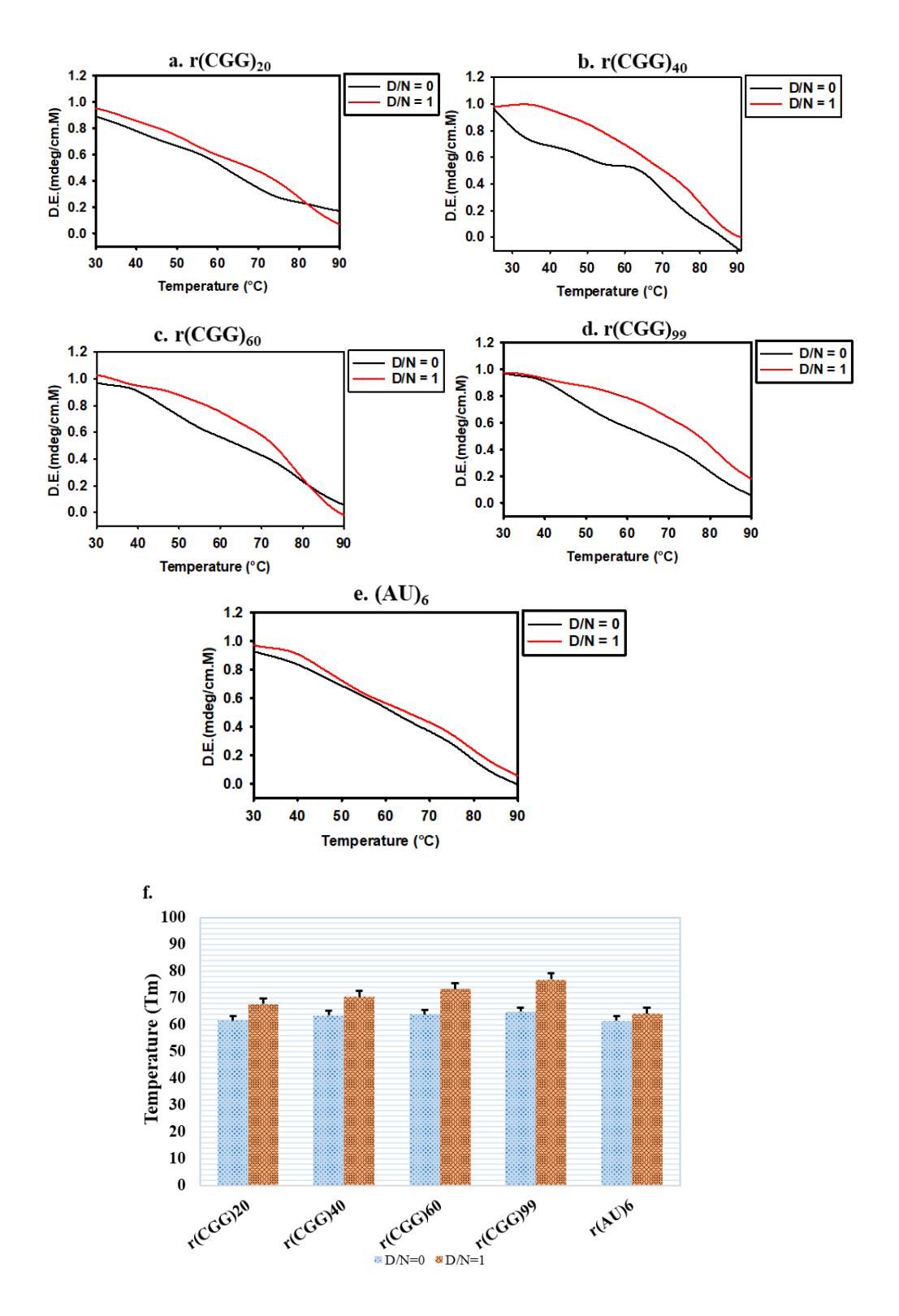


Figure 4.5: Thermal Denaturation Profile. Normalized CD melting plots of (a.) $r(CGG)_{20}$, (b.) $r(CGG)_{40}$, (c.) $r(CGG)_{60}$, (d.) $r(CGG)_{99}$, (e.) $r(AU)_{6}$, with increasing D/N ratio. (f.) Bar graph representing a change in melting temperature (T_m) in ${}^{\circ}C$ with respect to drug and nucleic acid ratio (D/N) ratios for different repeats.

Table 4.2. Table showing the changes in the melting temperature upon titration with P2 to D/N 1.

RNA	Change in T _m (°C)
$r(CGG)_{20}$	6.11
r(CGG) ₄₀	7.02
r(CGG) ₆₀	9.12
r(CGG) ₉₉	9.4
r(AU) ₆	2.78

4.4 Changes in band patterns in Electrophoretic Mobility Shift Assay and Polymerase Chain Reaction Stop Assay upon the interaction of P2 and r(CGG)_{exp}.

Electrophoretic mobility shift assay (EMSA) and Polymerase Chain Reaction (PCR) Inhibition assay were performed to validate the interaction between P2 and r(CGG) RNA. Significant retardation in the mobility of all r(CGG) RNA bands was observed upon adding an increasing concentration of P2 molecule (Figure 4.6). In contrast, no appreciable shift in mobility was detected for the AU-paired control RNA (r(AU)₆), indicating selective binding. The observed gel retardation is consistent with the formation of a stable RNA–compound complex, which is influenced by both the sequence context and the secondary structure of the RNA.

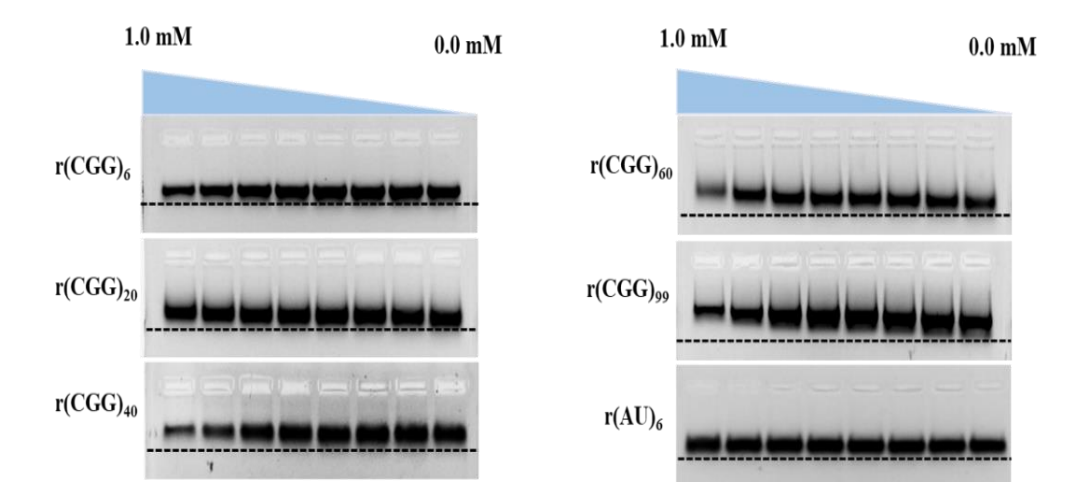


Figure 4.6: Gel retardation images show that with an increasing concentration of P2, the mobility of CGG repeat RNAs significantly increases over AU duplex RNA.

Alongside, PCR stop assay was conducted to assess the ability of the P2 to bind to DNA templates containing (CGG)₁ and (CGG)₆. The underlying principle is that the drug's binding to the template will impede the progression of Taq polymerase, thereby, reducing the PCR product yield. Supporting the hypothesis, treatment with P2 resulted in a concentration-dependent decrease in the band intensity of PCR products derived from CGG-containing templates. In contrast, PCR amplification of AU-rich duplex control templates remained largely unaffected, highlighting the selective binding affinity of the compounds toward CGG repeat sequences (Figure 4.7).

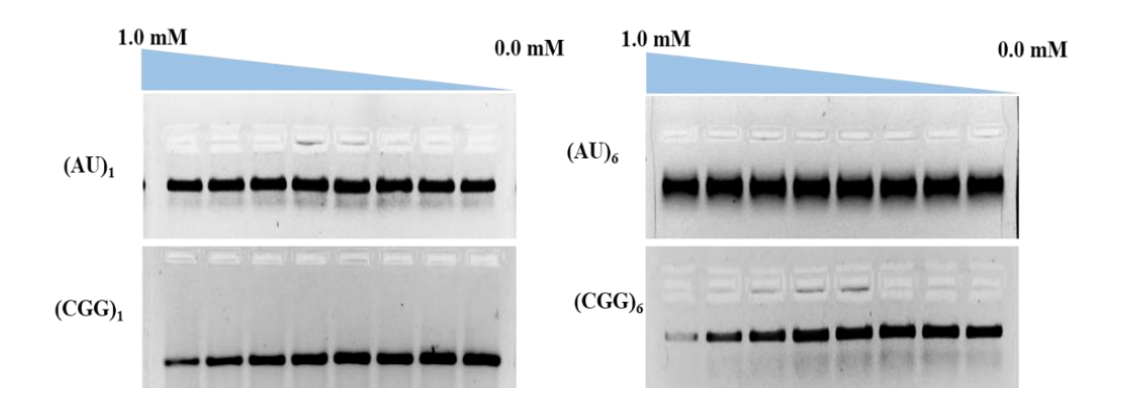


Figure 4.7: Gel images show the decreased intensity of the PCR product with increasing concentration of P2 compared with the AU-paired template.

These gel-based assays demonstrate the selective binding of the lead compounds to GG-mismatch-containing nucleic acid motifs, emphasizing their potential application in targeting CGG repeat expansions associated with disease.

4.5 Structural evaluation of the r(CGG)₆ repeat RNA-drug complex using NMR Spectroscopy and Molecular Docking.

To assess the details of atomic-level interactions, Molecular docking was conducted to understand real time interactions between CGG RNA and P2 molecule. The grid utilized the entire RNA structure (CGG RNA, PDB ID: 3SJ2) to optimally match molecules into the strongest binding sites. P2 can intercalate at the C4G5G6 triad of the RNA, exhibiting a binding energy of -8.0 kcal/mol. Nucleotides G8 and G11 form hydrogen bonding with P2. G11 can also form π - π T-shaped interaction. Nucleotide C13 can form π -an alkyl bond and carbon-hydrogen bond with an aromatic chain of P2. Other C and G nucleotides participate in van der Waals interactions with P2 (**Figure 4.8**). Docking, along with

other biophysical analyses, has validated the specificity of P2 towards GG-mismatched pair RNA in the C4G5G6 triad.

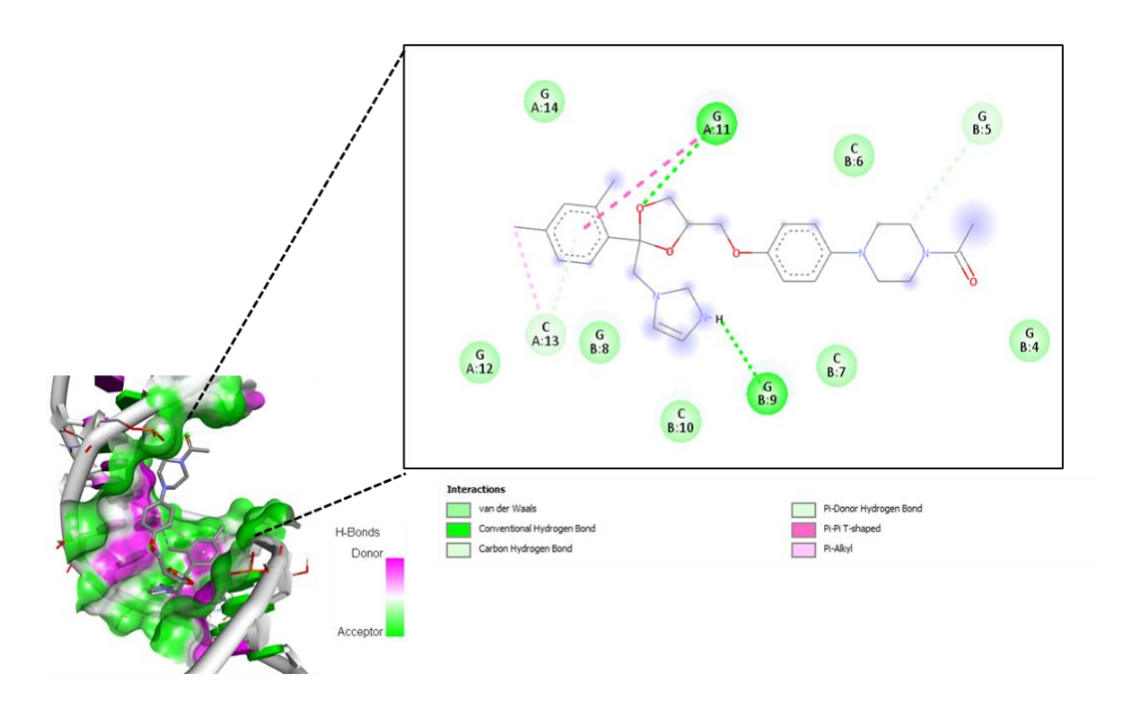
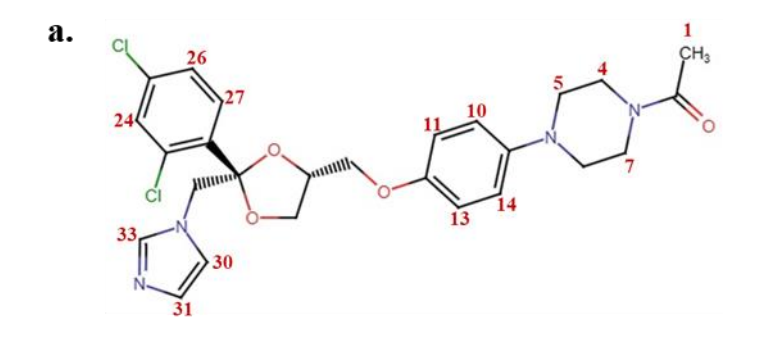


Figure 4.8: Molecular Docking study for molecular interactions between CGG repeat RNA and molecule P2. P2 can intercalate at the C4G5G6 triad of the RNA, exhibiting a binding energy of –8.0 kcal/mol.

NMR titration of r(CGG)₆ with P2 was performed to unravel the atomic level intricacies. Changes in chemical shifts (both upfield and downfield) and peak broadening upon nucleic acid binding provide essential information regarding the involvement of specific ligand protons in these interactions. The variations in the resonance peak intensity, broadening, and chemical shift of protons were observed consistently at each stage of the titration procedure, with special emphasis paid to the corresponding changes in the P2 attributes. The addition of r(CGG)₆ RNA to the P2 solution resulted in diminished resonance peaks of P2 protons. Incremental titration of r(CGG)₆ RNA into the P2-containing solution resulted in noticeable peak broadening accompanied by both downfield and upfield chemical shifts of ligand

protons, observed over a molar ratio range of 100:1 to 100:8. The exchangeable protons of P2 interacting with GG mismatch pair RNA resonated in the aromatic region within 6.5-8.0 ppm, indicating π - π stacking interactions. Additionally, other protons of the drug were also involved in the interaction, like aliphatic protons (1.0–2.5 ppm) and piperazine protons (3.6-3.8 ppm) (Figure 4.9). Thus, binding interactions of the drug with GG mismatch pair RNA reveal the involvement of specific protons and confirm the participation of the aromatic ring and backbone in π - π and conventional hydrogen bonds.



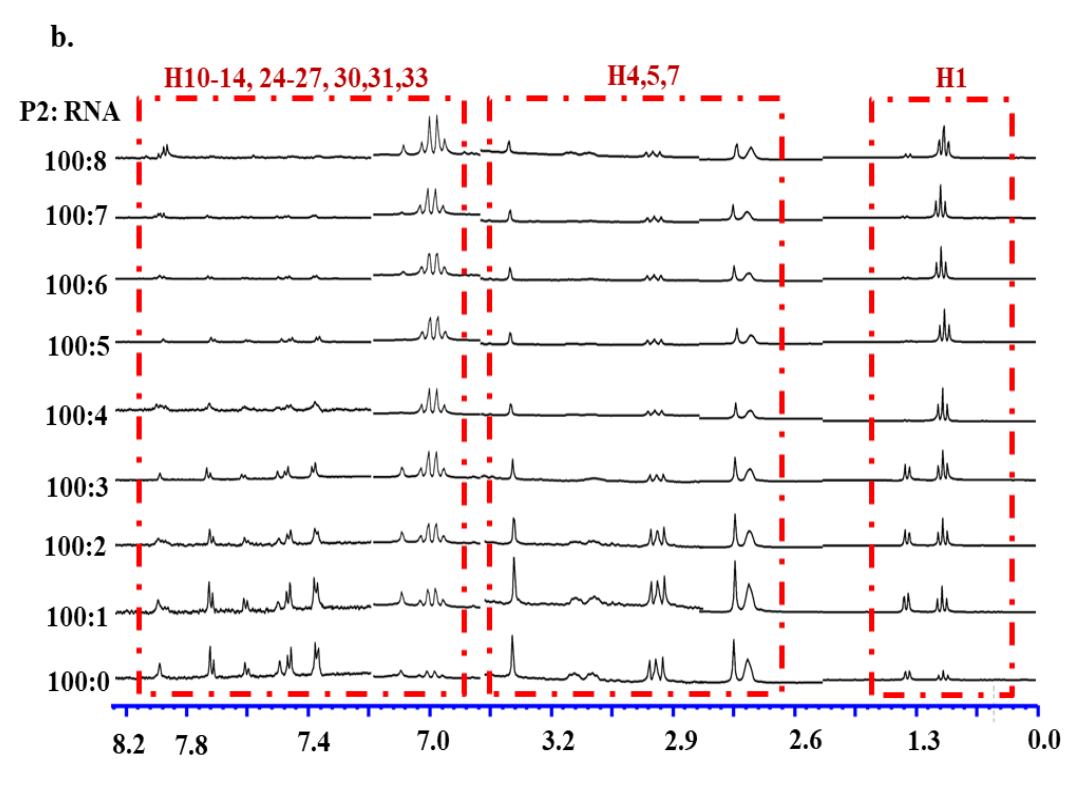
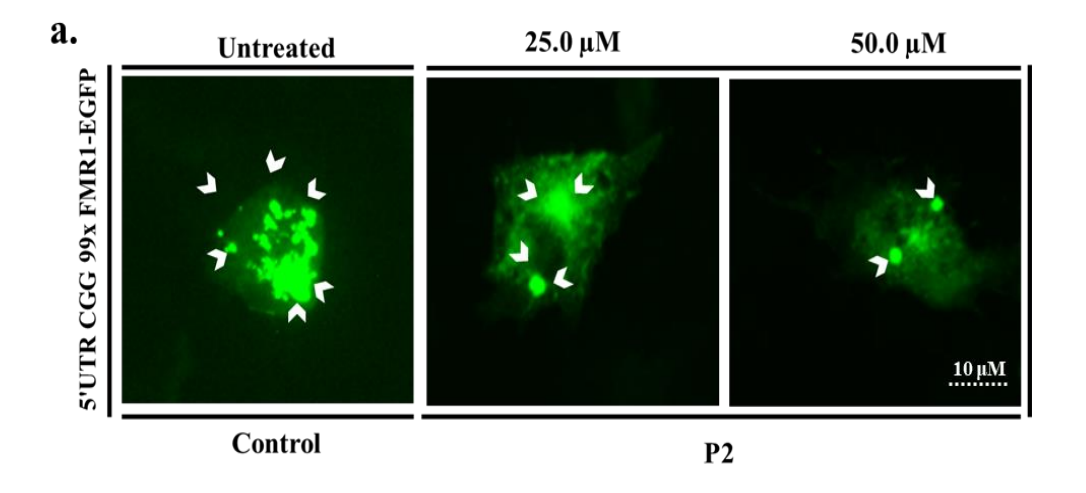


Figure 4.9: Proton spectrum 1D-1H NMR. (a.) Structure of P2 with labelled protons. **(b.)** 1D-1H NMR peak broadening of P2 with (CGGx6) RNA.

4.6 Evaluation of functional inhibition of RAN Translation by P2 in cellular FXTAS models.

To assess the therapeutic potential of P2 in mitigating aggregate-induced toxicity in FXTAS, a cellular model was established using COS-7 cells, a fibroblast-like cell line with a relatively large morphology suitable for visualizing intracellular aggregates. Cells were transfected with a plasmid encoding 99 CGG repeats inserted into the 5' UTR of the EGFP gene, enabling the expression and detection of FMR1-derived PolyG aggregates. Treatment with P2 resulted in a concentration-dependent reduction in FMRPolyG aggregation. Approximately, a 45% decrease in aggregate formation was observed at 25.0 μ M, with up to 90% reduction at 50.0 μ M, as indicated by the intracellular foci marked by arrowheads in the figure (Figure 4.10). Notably, EGFP translation remained unaltered at these concentrations, indicating the selective inhibitory effect of P2 on RAN translation without impacting canonical translation.



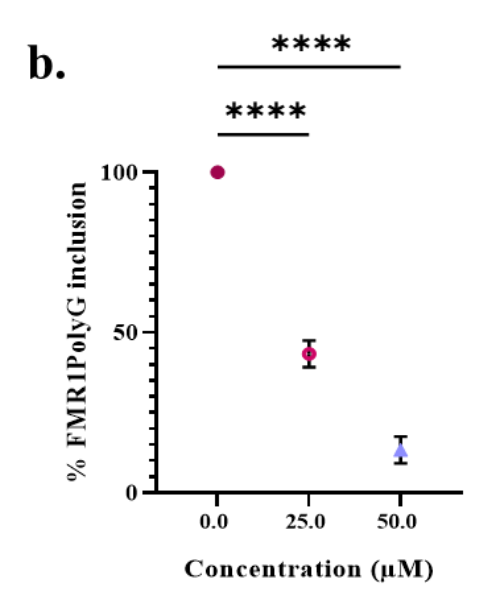


Figure 4.10: Validation of P2's efficiency to reduce the intracellular FMR1PolyG aggregation. (a.) Treatment with P2 reduced the FMR1PolyG-EGFP aggregation in COS7 cells in a concentration-specific manner. (b.) Graph depicting the percentage reduction in the FMR1PolyG-EGFP inclusions at different concentrations of P2 (25.0 μ M and 50.0 μ M). Statistical significance was determined using one-way ANOVA; ****P \leq 0.00001, n=3.

For western blot analysis, HEK-293 cells were transiently transfected with the above-mentioned plasmid. After transfection, cells were treated with varying concentrations of P2. Total cell lysates were extracted and then used for immunoblotting. PolyG Expression patterns were observed using anti-PolyG and anti-β actin antibodies. Notably, the treatment resulted in a dose-dependent decrease in FMR1PolyG protein expression levels by 55% and 85% at 25.0 μM and 50.0 μM, respectively. No significant inhibition of EGFP canonical protein translation was observed upon treatment with P2 (Figure 4.11). Analysis of the blot images was done using ImageJ, followed by plotting a graph, and a decrease in PolyG expression was assessed. P2 can hinder the non-canonical RAN translation by interfering with the ribosome machinery, hence resulting in reduced PolyG aggregation.

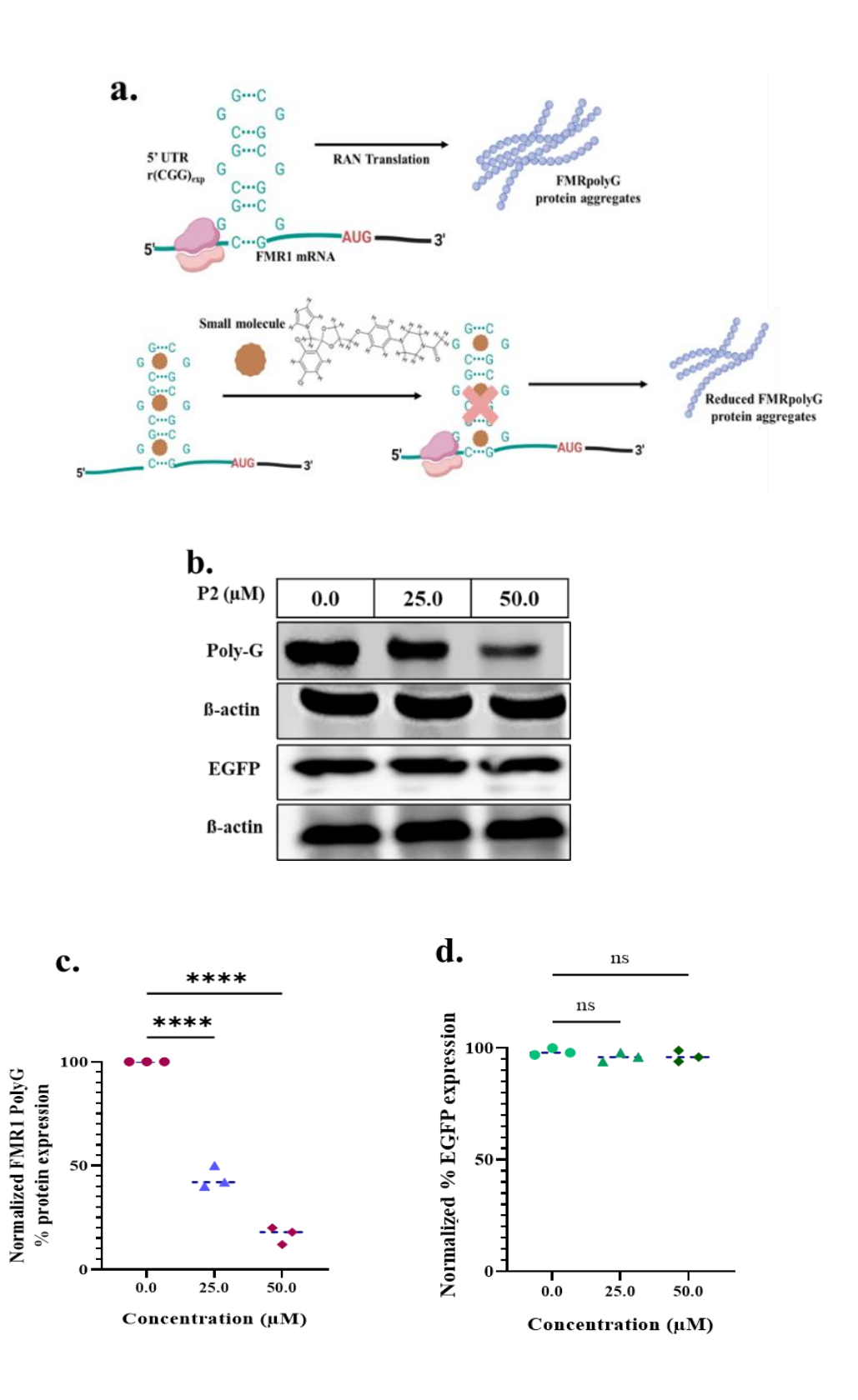


Figure 4.11: Assessment of P2's potency to inhibit RAN translation. (a.) Schematic representation of the impact of P2 on the accumulation of FMRPolyG protein produced by CGG repeats in cellular models. (b.)

FMRPolyG protein was observed to be inhibited after 24 hrs following

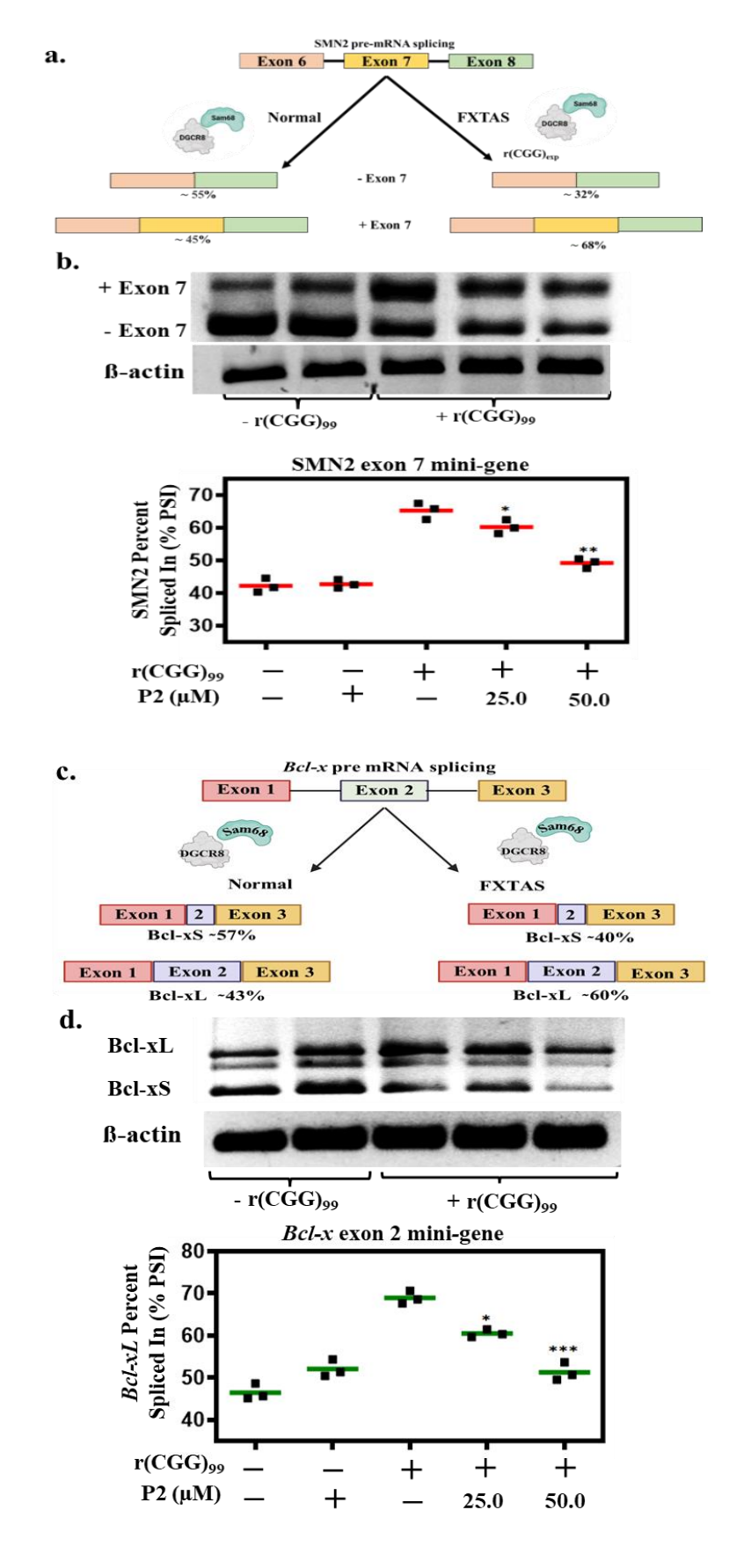
treatment with P2 as inferred from the blot images. At the same dose, P2 has no apparent impact on EGFP's canonical translation. (c-d.) Quantification of the FMR1PolyG expression and EGFP expression. Statistical significance was determined using one-way ANOVA; ****P<0.00001.

4.7 Improvement in pre-mRNA alternative splicing defects in FXTAS cell line models.

Consequently, the FXTAS cellular model was used to evaluate the ability of P2 to improve the splicing defects. In normal cells, the RNA binding proteins Sam 68 and DGCR8 modulate the splicing machinery of *SMN2* (survival motor neuron 2) pre-mRNAs. In the presence of enlarged CGG repeat RNA, splicing anomalies arise. Cells expressing CGG repeat expansions exhibited defective splicing patterns, including a marked increase in exon 7 inclusion in *SMN2* mRNA (~68%) compared to healthy controls (~45%), indicating the impact of expanded r(CGG) repeats on pre-mRNA splicing regulation.

HEK-293 cells were co-transfected with plasmids containing r(CGG)₉₉ and SMN2 mini gene. Following this, the media was supplemented with an increasing concentration of P2 for the next 24 hours. P2 enhanced normal splicing in a dose-dependent fashion, with 25.0 μM correcting approximately 30% of the SMN2 splicing defect and 50.0 μM achieving near-complete restoration to wild-type levels (~80%). P2 can restore the pre-mRNA alternative splicing defects almost near to the wild type that lacks r(CGG)₉₉ at higher concentration (Figure 4.12 (a,b)). Similarly, Bcl-x mRNA exists in two isoforms: Bcl-xL and Bcl-xS. In healthy cells, approximately 40% of the minigene is expressed as the Bcl-xL isoform. However, in a cell model containing expanded r(CGG)₉₉, this proportion increases to around 60%. P2 has been shown to correct the pre-mRNA splicing defect of Bcl-x in a dose-dependent manner. Notably, treating cells with 25.0 μM P2 led to a ~40% improvement in Bcl-x mis-splicing, with further enhancement of ~80% observed at 50.0 μM. Contrary to

this, P2 has no influence on the alternative splicing pattern in the absence of r(CGG)₉₉ (Figure 4.12 (c,d)).



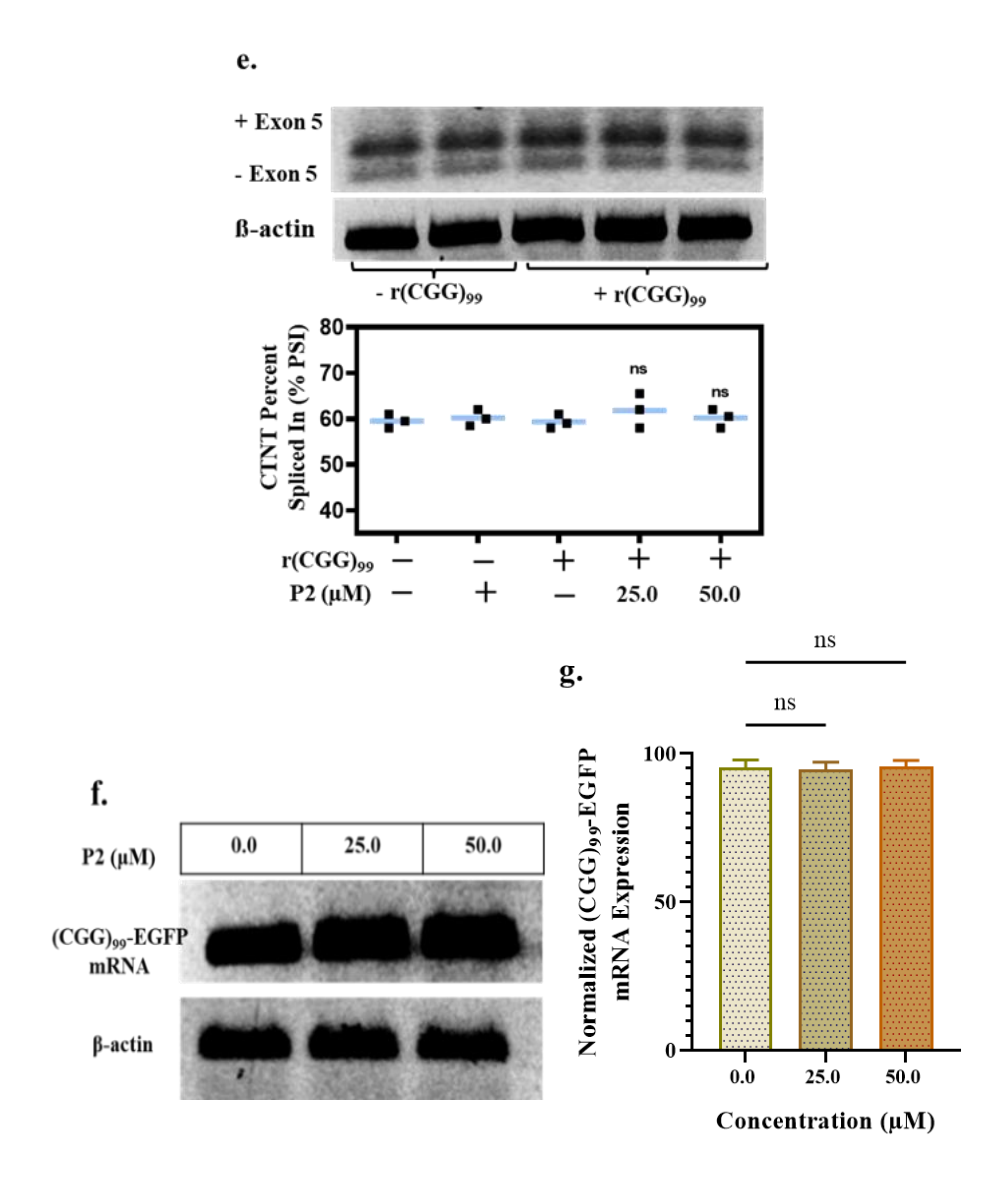


Figure 4.12: Evaluation of *in-vitro* potency of P2 to improve the splicing defects in developed FXTAS cellular models. (a.) Schematic representing splicing defects associated with SMN2 in the FXTAS model. (b.) Gel image and graph illustrate that P2 corrects the SMN2 splicing defects in relation to their concentration. c. Schematic representing splicing defects associated with Bcl-x in the FXTAS model. (d.) Gel image and graph illustrate that the drug corrects the Bcl-x splicing defects in relation to their concentration. (e.) Gel image and graph illustrate that the drug has no impact on the splicing of control CTNT gene. (f.) Blot showing that P2 has no effect on EGFP expression. (g.) Quantitative analysis of normalized EGFP expression. Statistical significance was determined using one-way ANOVA; ***P \leq 0.0001; *P \leq 0.001.

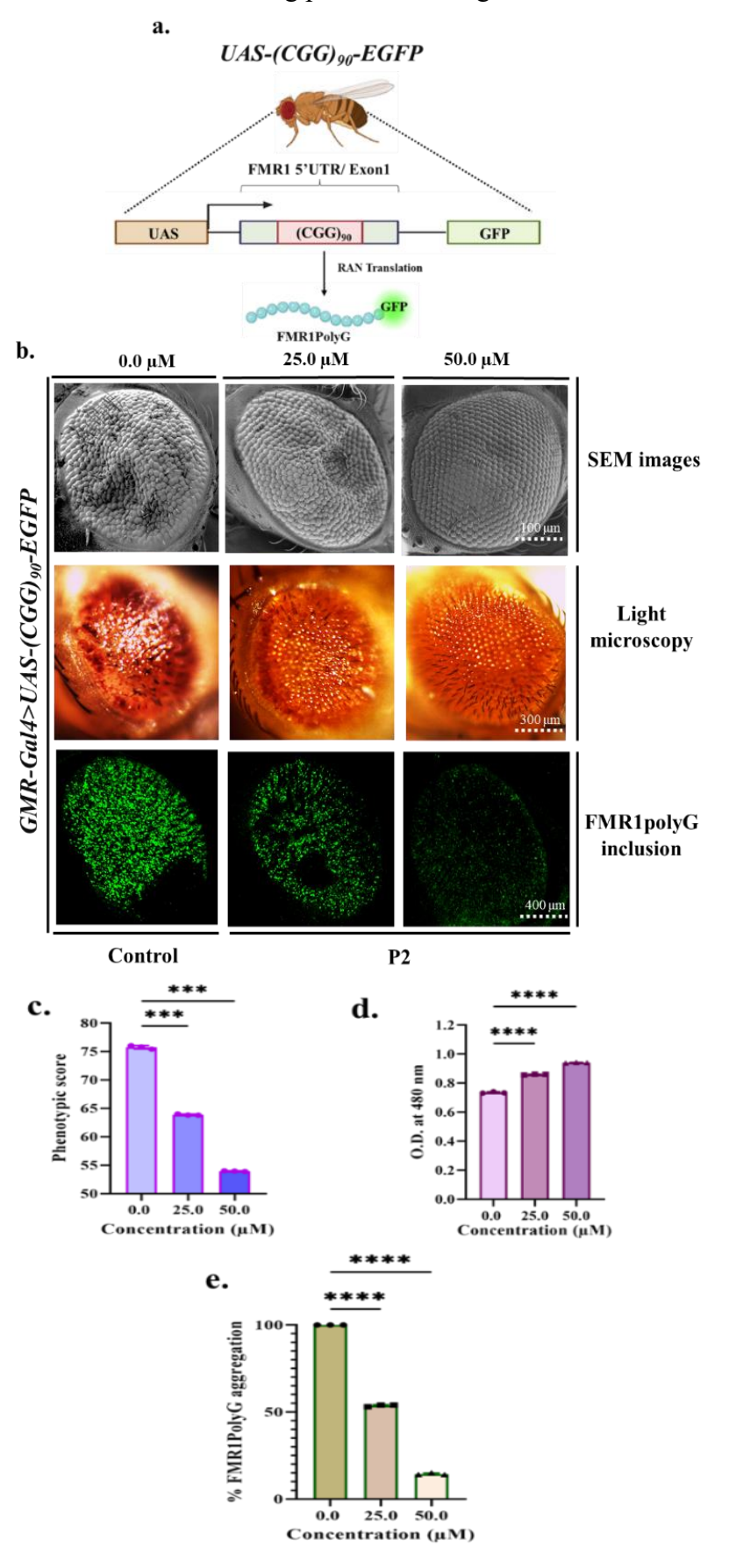
P2 binds selectively to r(CGG)_{exp} repeats, displacing splicing factors sequestered within their abnormal secondary structures. This interaction restores normal RNA processing and corrects CGG-associated splicing defects. The specificity of P2 is further evidenced by its lack of effect on unrelated splicing events, such as those involving the CTNT minigene, which is not influenced by r(CGG)_{exp}-mediated sequestration (Figure 4.12 (e)).

4.8 P2 reduces neurodegeneration, alleviates rough eye phenotype, and prevents pigment loss in fly model of FXTAS induced by PolyG toxicity.

A previously established FXTAS *Drosophila* model was utilized to evaluate the drug's effectiveness. The pan-retinal *GMR-GAL4/+* driver line was used to induce the expression of *UAS-(CGG)90-EGFP* and *UAS-EGFP* transgenes, specifically in the compound eyes of flies. P2 was administered through the diet at variable concentrations. Increasing P2 levels led to a significant reduction in external morphological abnormalities in (CGG)90 flies, including necrotic lesions, rough eye phenotype, and pigment loss. In contrast, the control group expressing only EGFP showed no notable changes (**Figure 4.13**). The improvements in the rough eye phenotype and pigment preservation suggest that P2 counteracts the progressive degeneration of pigmented cells. Notably, dietary supplementation with P2 alleviated eye impairments at 7 days post-eclosion, demonstrating a prolonged therapeutic effect.

Flynotyper software (http://flynotyper.sourceforge.net) was used to further assess rough eye morphology by quantifying the ommatidia disorderliness index to generate a phenotypic score. As expected, untreated samples displayed significantly higher phenotypic scores than

those treated with the drug, reinforcing the observed improvements in eye structure and corroborating previous findings.



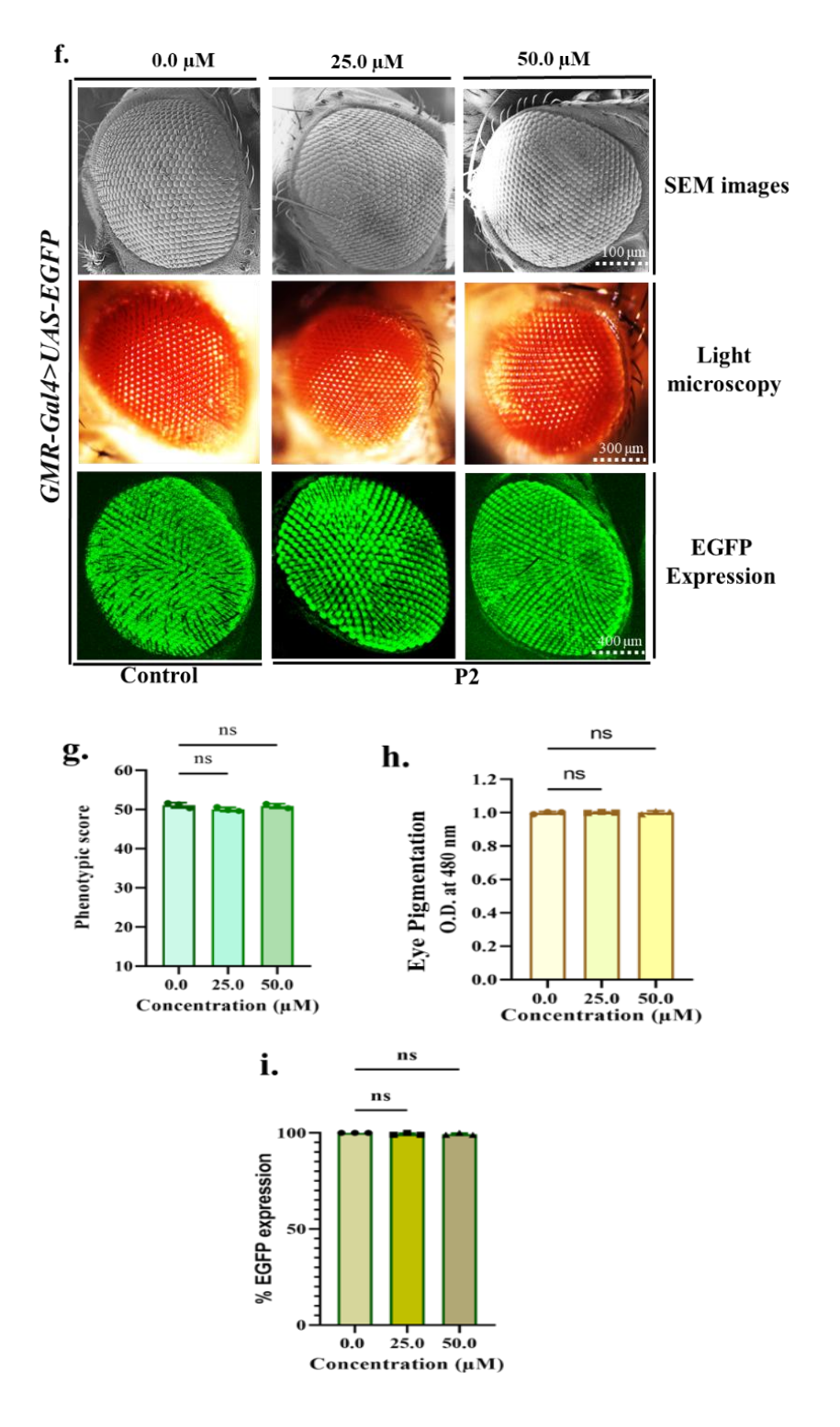


Figure 4.13: P2 reduces rough eye phenotype and pigment loss induced by PolyG toxicity in the *Drosophila* model of FXTAS. (a.) Schematic representation of the $UAS-(CGG)g_0-EGFP$ construct used for the FXTAS fly model. (b.) SEM, Light microscopic and confocal images of eyes of $GMR-Gal4>UAS-(CGG)g_0-EGFP$ flies treated with different concentrations of the drug. (c.) Graph representing quantitative analysis

of Phenotypic score. (d.) Graph representing quantitative analysis of Eye pigmentation. (e.) Graph representing quantitative analysis of FRM1 PolyG inclusion in percentage. (f.) SEM, Light microscopic and confocal images of eyes of *GMR-Gal4>UAS-EGFP* flies treated with different concentrations of P2. (g.) Graph representing quantitative analysis of Phenotypic score. (h.) Graph representing quantitative analysis of Eye pigmentation. (i.) Graph representing quantitative analysis of FRM1 PolyG inclusion in percentage. Data are presented as mean \pm standard error of the mean (SEM), with statistical significance indicated as appropriate. Statistical significance was determined using one-way ANOVA; *P < 0.05, **P < 0.01, and ***P < 0.001, n=3.

4.9 P2 rescues eye morphology disrupted by FMR1PolyG repeats, demonstrating dose-dependent effectiveness in a *Drosophila* FXTAS model.

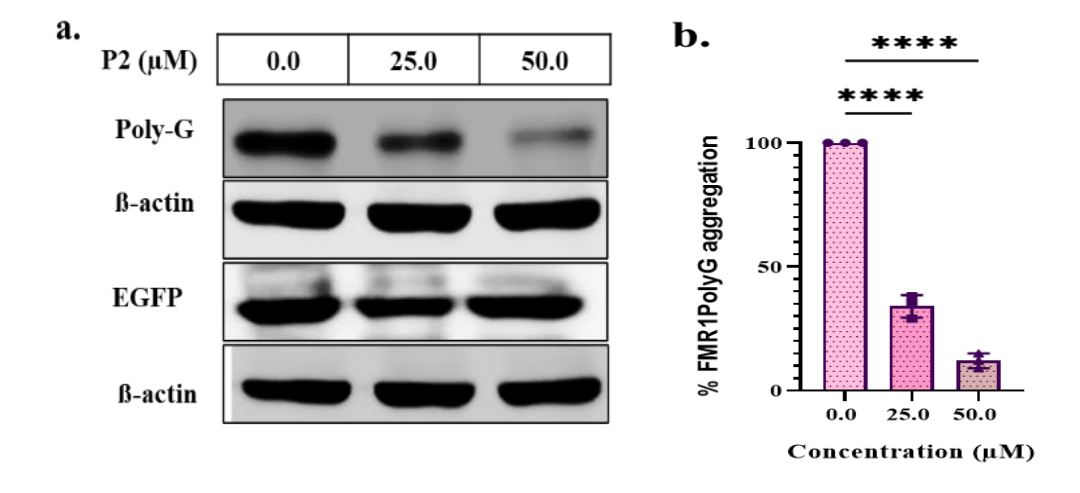
Scanning Electron Microscopy (SEM) analysis provided further validation of the significant improvements in eye morphology in flies treated with P2, revealing a dose-dependent effect. Under normal conditions, the *Drosophila* compound eye consists of approximately 800 ommatidia arranged in a precise hexagonal pattern with distinct interommatidial bristles. However, in disease conditions or upon expression of disease-associated proteins, this organization becomes disrupted, leading to a rough eye phenotype. P2 treatment alleviated these structural abnormalities, restoring the typical ommatidial arrangement and spacing. The SEM images clearly demonstrated that P2 effectively improved the rough eye phenotype, reinforcing its therapeutic potential (Figure 4.13).

Confocal microscopy analysis revealed prominent PolyG inclusions in the eyes of the disease model, visualized using an EGFP tag fused to CGG repeats (*GMR-GAL4>UAS-(CGG)90-EGFP*). These inclusions were strongly associated with degeneration linked to expanded CGG repeats. In contrast, control models expressing only EGFP showed no

such inclusions, confirming that their presence is specifically related to pathological CGG repeat expansions. Notably, treatment with the tested drugs significantly reduced the fluorescence intensity of PolyG inclusions, indicating effective drug-mediated suppression of PolyG accumulation. This reduction likely results from direct interactions between the drugs and CGG repeat expansions. Quantitative analysis further demonstrated a statistically significant decline in PolyG inclusions across all treatment conditions, highlighting the therapeutic potential of these compounds in counteracting CGG-associated toxicity (Figure 4.13).

4.10 P2 effectively reduces PolyG protein levels in FXTAS model flies.

Western blot analysis was conducted on whole-body protein extracts from the FXTAS *Drosophila* model treated with different concentrations of the drug. Anti-PolyG antibodies were used to measure PolyG protein levels in treated flies and compare them with experimental controls. The results showed a significant reduction in PolyG protein levels across all treatment groups, highlighting the drug's effectiveness in reducing PolyG accumulation. Importantly, β-actin levels remained unchanged, indicating that P2 specifically targeted PolyG. Additionally, flies expressing solely EGFP exhibited no changes in the intensity of EGFP or β-actin bands, confirming that the drug's effects were specific to PolyG expression (Figure 4.14). These results indicate the in vivo efficacy of P2 in disrupting aberrant RAN translation, leading to a significant reduction in the accumulation of RAN translation-derived proteins.



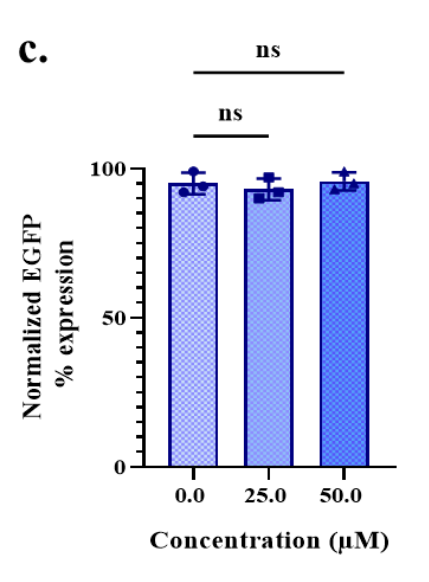


Figure 4.14: P2 helps to mitigate the PolyG aggregates in the FXTAS *Drosophila* model. (a.) Blot showing reduced PolyG expression in proteins isolated from diseased flies $(CGG)_{90}$ treated with various P2 concentrations. (b.) The graph illustrates the normalized percentage expression of PolyG. Data are presented as mean \pm SEM from at least three independent experiments. Statistical significance was determined using one-way ANOVA; ****P \leq 0.00001.

4.11 P2 improves locomotor defects induced by PolyG accumulation in the *Drosophila* FXTAS model.

To evaluate the drug's effect on motor function, we used the neuron-specific *Elav-Gal4^{C155}* driver line to express *UAS-EGFP* and *UAS-(CGG)₉₀-EGFP* in flies. Larvae from both the *Elav-GAL4>UAS-(CGG)₉₀-EGFP* and *Elav-GAL4>UAS-EGFP* groups were treated with varying drug concentrations. After treatment, third-instar larvae underwent a crawling assay to assess locomotor performance. Results indicated that drug administration significantly improved the crawling ability of larvae carrying 90 CGG repeats, with the extent of enhancement showing a dose-dependent trend (**Figure 4.15**).

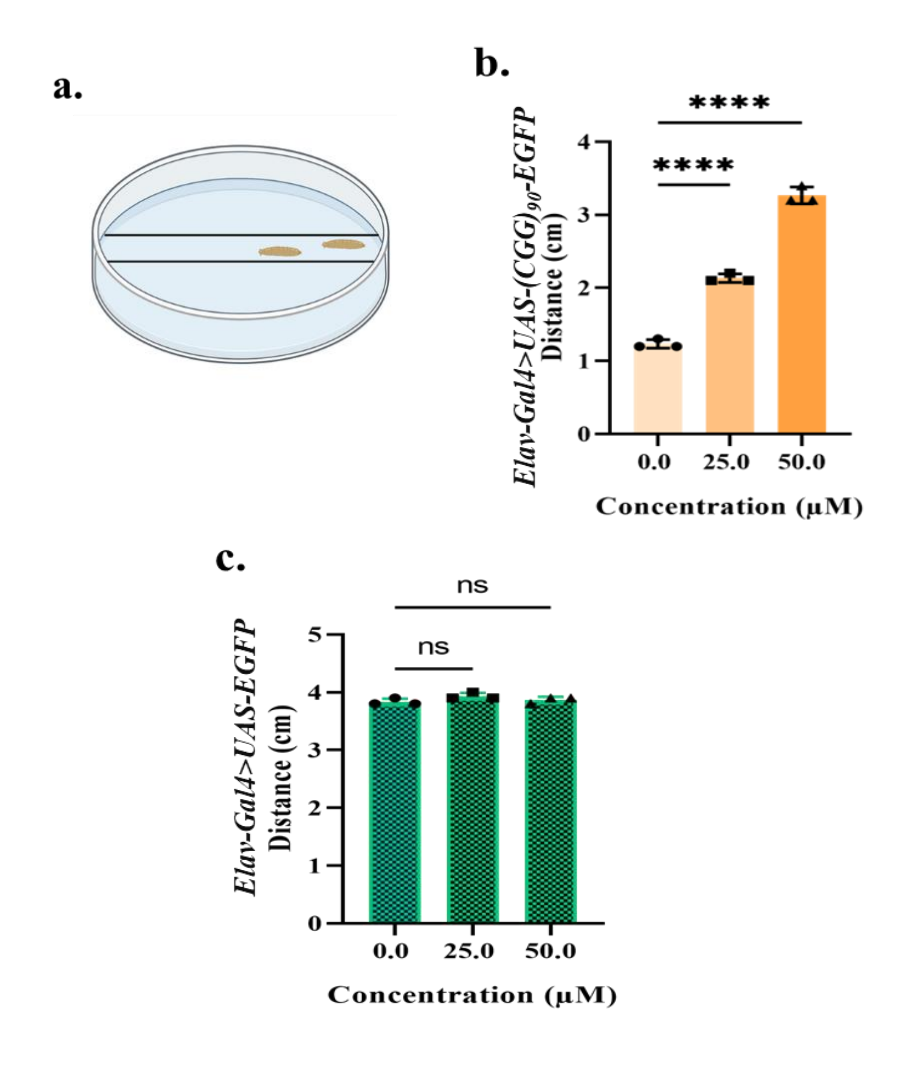
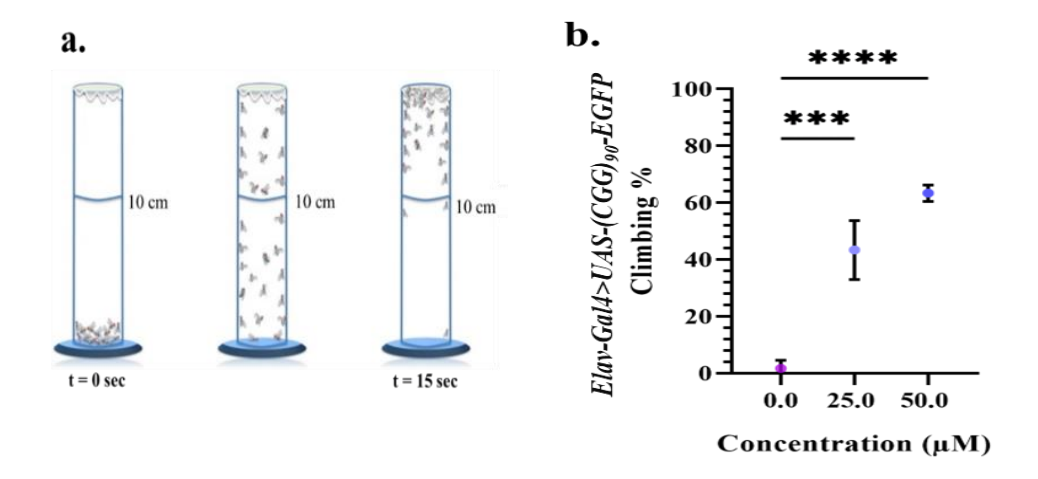


Figure 4.15: P2 improves locomotor dysfunctions (Larval crawling assay). (a.) Schematic representation of the plate used for larval

crawling assay. **(b.)** Crawling assay results for third-instar larvae (*Elav-GAL4>UAS-(CGG)90-EGFP*) treated with P2, assessing motor coordination and function. **(c.)** Schematic for the climbing assay. Data are presented as mean \pm SEM from at least three independent experiments. Statistical significance was determined using one-way ANOVA, ****P \leq 0.00001.

To further evaluate motor function in adult flies, we assessed the climbing and flight ability of 14-day-old male flies treated with varying doses of P2. The results indicated that P2 treatment had no significant effect on the locomotion of control flies expressing only EGFP. However, in flies carrying (CGG) $_{90}$ repeats, climbing ability significantly improved with increasing P2 concentrations. Notably, at a 50.0 μ M dose, approximately 60% of the flies successfully crossed the 10 cm mark (Figure 4.16).



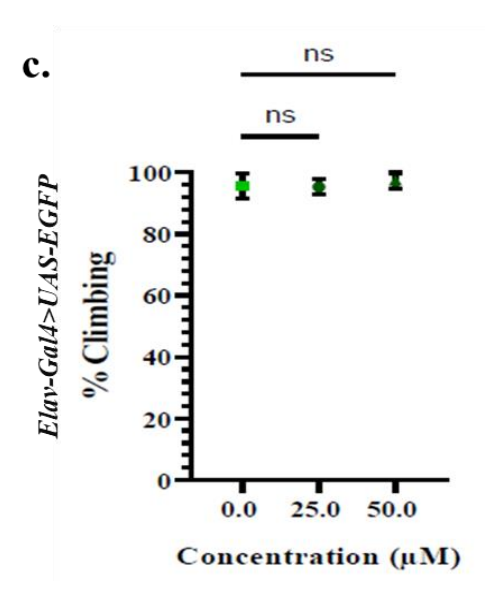


Figure 4.16: P2 improves locomotor dysfunctions (Climbing assay).

(a.) Schematic representation of Negative geotaxis assay (Climbing assay). (b.) Graph showing the % climbing of Elav-Gal4 > UAS- $(CGG)_{90}$ -EGFP flies fed on varying concentrations of P2. (c.) Graph showing the % climbing of Elav-Gal4 > UAS-EGFP flies fed on varying concentrations of P2. Statistical significance was determined using one-way ANOVA; ***P < 0.001, and ****P \leq 0.00001, n=3.

In addition to enhanced climbing performance, a significant increase in flight capability was observed in (CGG)₉₀-expressing flies with increasing concentrations of P2, as evidenced by representative screen captures and a quantitative bar graph illustrating the average landing height (**Figure 4.17**). These findings suggest that P2 treatment enhances locomotor performance in both larval and adult stages. In conclusion, this P2 molecule may interact with trinucleotide repeat-containing sequences, offering the potential for preventing and treating FXTAS.

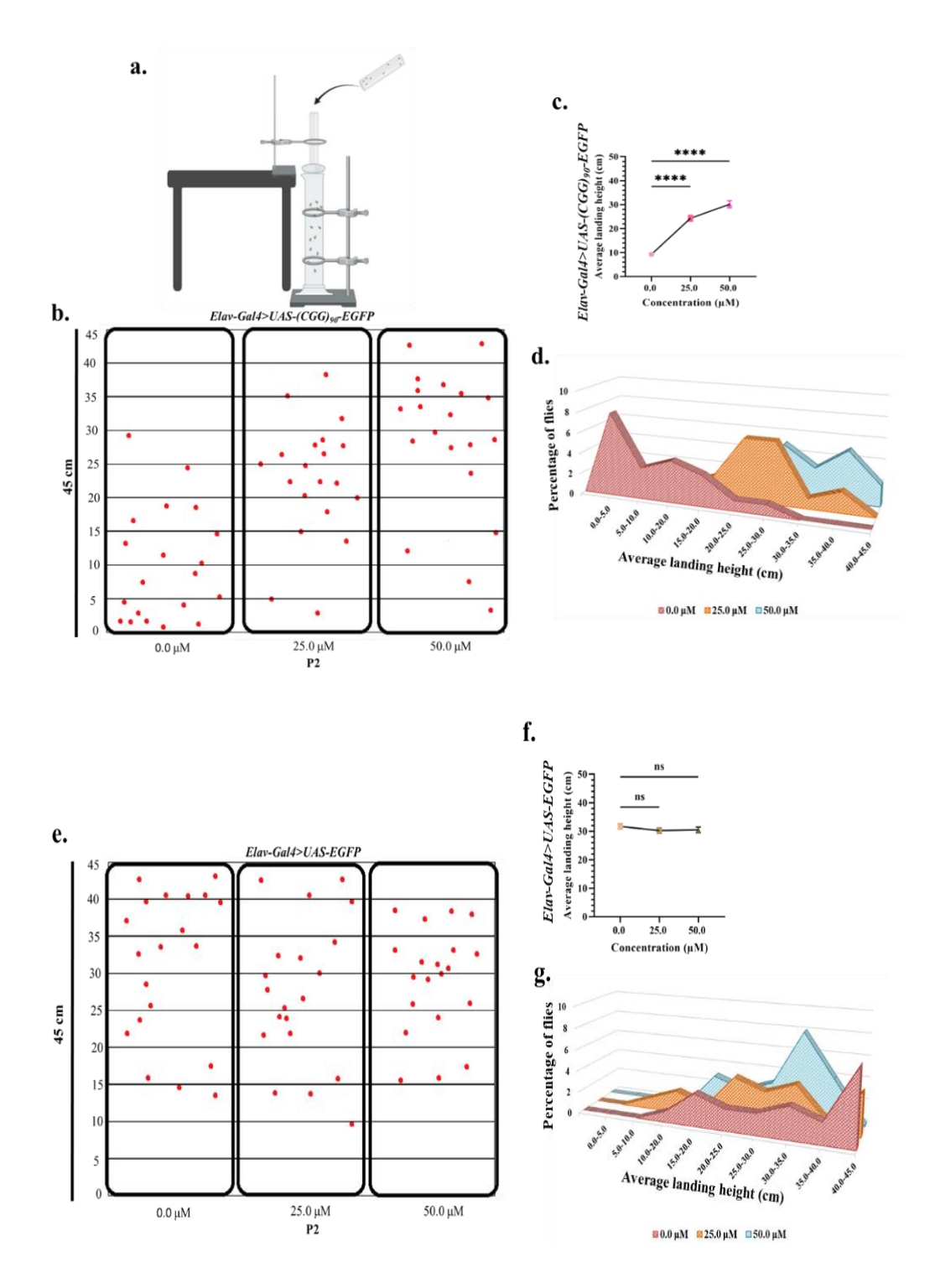


Figure 4.17: P2 improves locomotor dysfunctions (Flight assay). (a.)

Schematic representation of apparatus used for flight assay. **(b.)** Screen captures for *Elav-GAL4>UAS-(CGG)90-EGFP* flies displaying the landing heights of individual flies. Each red dot represents the location of an individual fly. These landing heights are used to calculate the average landing height. **(c.)** Graph representing the average landing

height (cm) (d.) as well as the overall distribution of the flies in the sheet. (e.) Screen captures for Elav-GAL4>UAS-EGFP flies displaying the landing heights of individual flies. Each red dot represents the location of an individual fly. These landing heights are used to calculate the average landing height. (f.) Graph representing the average landing height (cm) (g.) as well as the overall distribution of the flies in the sheet. Data are presented as mean \pm SEM from at least three independent experiments. Statistical significance was determined using one-way ANOVA, ****P \leq 0.00001.

4.12 Quantitative analysis of ROS generation.

Previous research has demonstrated that the accumulation of toxic FMR1PolyG interferes with several cellular pathways, including oxidative stress and mitochondrial dysfunction, thereby leading to an elevation in reactive oxygen species (ROS) production. To evaluate basal ROS levels in both treated and control flies, a DCF-DA assay was conducted. ROS levels were significantly elevated in diseased flies, whereas higher concentrations of P2 led to a notable decrease in ROS production. In contrast, no significant changes in ROS levels were observed in control flies lacking CGG repeats (Figure 4.18). Further investigations are necessary to better understand the molecular mechanisms through which P2 exerts its protective role and to explore whether these effects extend to other forms of cellular dysfunction linked to FMR1PolyG toxicity.

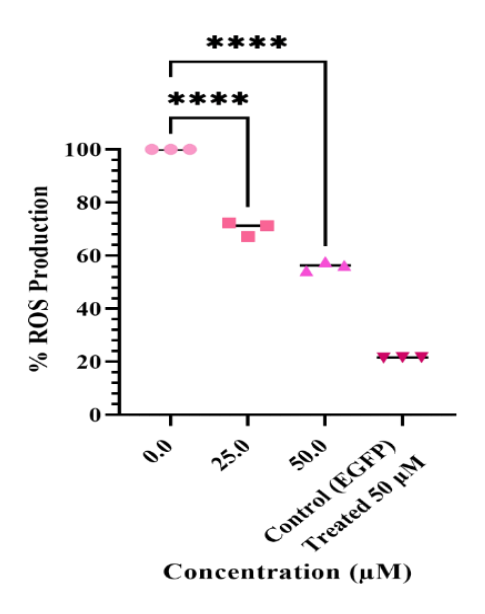


Figure 4.18: Assessment of ROS levels. Bar graph representing % ROS production in *Elav-GAL4>UAS-(CGG)*₉₀-*EGFP* fed with different concentrations (25.0 μ M, and 50.0 μ M) of P2 and *Elav-GAL4>UAS-EGFP* fed with 50.0 μ M of P2. Statistical significance was determined using one-way ANOVA; ****P \leq 0.00001, n=3.

4.13 Assessment of P2's impact on mitochondrial oxidative stress and membrane potential.

Mitochondrial dysfunction is a major contributor to neurodegenerative diseases, often leading to elevated production of reactive oxygen species (ROS), which play a critical role in disease pathogenesis and neuronal cell death. To assess the mitochondrial ROS (mtROS) levels in both diseased and P2-treated Drosophila models, MitoSOX staining was performed. Consistent with DCFDA-based findings, increasing concentrations of P2 resulted in a marked reduction in MitoSOX fluorescence, indicating that P2 effectively attenuates mtROS production and alleviates mitochondrial dysfunction (Figure 4.19).

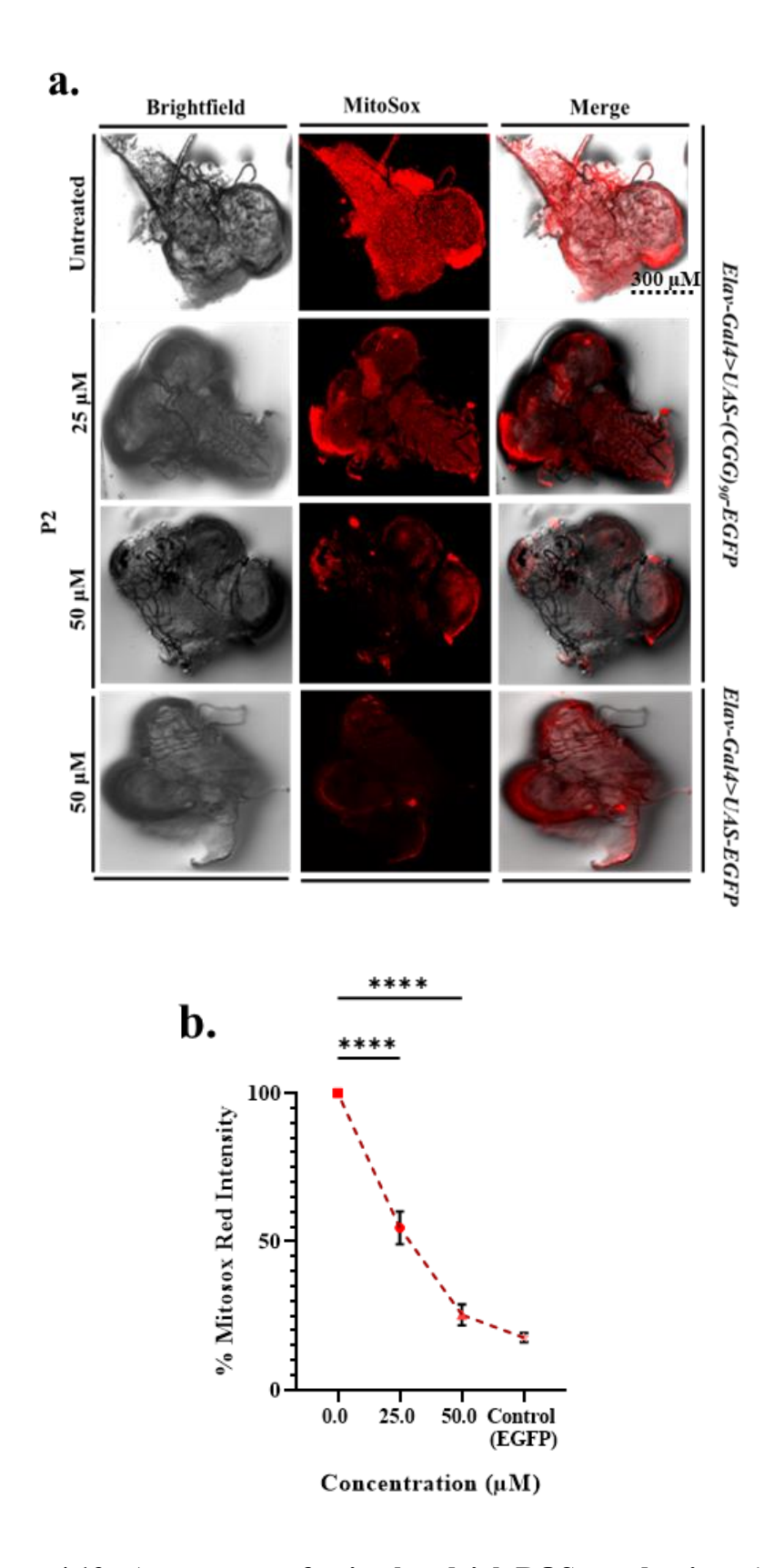


Figure 4.19: Assessment of mitochondrial ROS production. (a.) Mitosox staining of Elav-GAL4>UAS-(CGG)90-EGFP flies fed with different concentrations (25.0 μ M, and 50.0 μ M) of P2 and Elav-

GAL4>UAS-EGFP flies fed with 50.0 μM of P2. **(b.)** Bar graph representing % Mitosox red intensity. Statistical significance was determined using one-way ANOVA; **** $P \le 0.00001$, n=3.

To further evaluate the protective effect of P2 on mitochondrial integrity, mitochondrial membrane potential was assessed using the tetramethylrhodamine methyl ester (TMRM) assay. TMRM is a voltagesensitive, cell-permeable dye that accumulates within polarized mitochondria, emitting red fluorescence proportional to membrane potential. In the *Drosophila* FXTAS model, a dose-dependent increase in TMRM fluorescence was observed following P2 treatment, suggesting enhanced mitochondrial membrane polarization and improved mitochondrial function. In contrast, EGFP-expressing control flies exhibited no significant change in TMRM intensity, indicating stable mitochondrial health irrespective of treatment (Figure 4.20). Collectively, these findings indicate that P2 mitigates FMR1PolyGinduced compromised mitochondrial activity by restoring mitochondrial membrane potential, and potentially enhancing ATP production and mitochondrial DNA integrity.

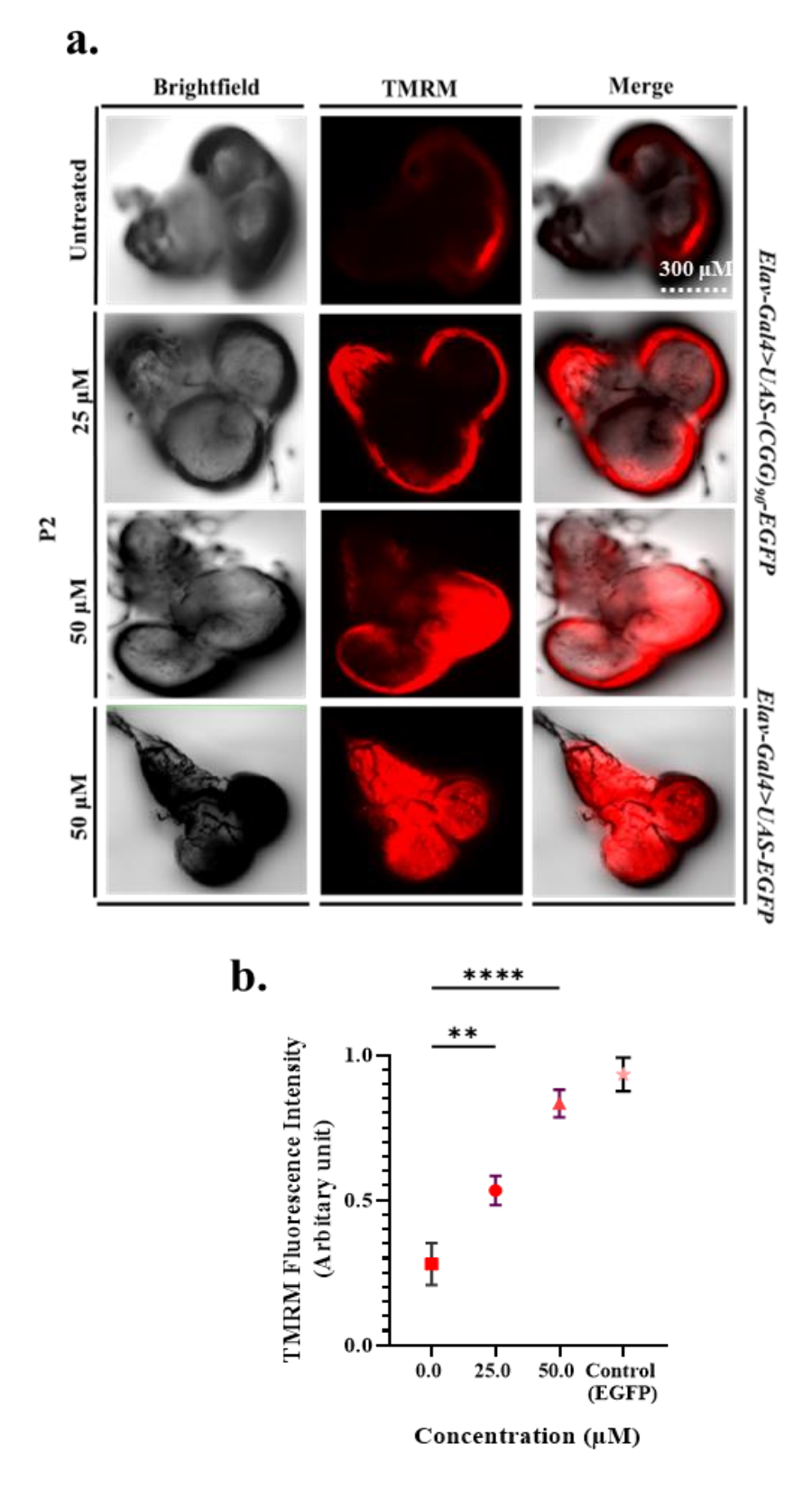


Figure 4.20: Assessment of the membrane potential upon treatment with P2. (a.) TMRM staining of Elav-GAL4>UAS- $(CGG)_{90}$ -EGFP flies fed with different concentrations (25.0 μ M, and 50.0 μ M) of P2 and Elav-GAL4>UAS-EGFP flies fed with 50.0 μ M of P2. (b.) Bar graph

representing TMRM fluorescence intensity. Statistical significance was determined using one-way ANOVA; **P < 0.01, and ****P < 0.00001, n=3.

4.14 Detection of neuronal cell death via Propidium iodide (PI) staining.

Emerging evidence multiple interconnected suggests that neuroinflammation, oxidative mechanisms—including stress, mitochondrial dysfunction, and impaired autophagy—collectively contribute to the cellular damage underlying neurodegenerative diseases. These pathological cascades ultimately culminate in neuronal cell death, a hallmark of disease progression in repeat-associated disorders such as FXTAS. To assess neuronal cell death in our Drosophila FXTAS model, Propidium Iodide (PI) staining was employed. PI is a membrane-impermeable, nucleic acid-binding dye that selectively stains cells with compromised membrane integrity, emitting red fluorescence upon intercalation with nucleic acids—thereby serving as a reliable indicator of cell death.

Third-instar larval brains expressing *Elav-GAL4>UAS-(CGG)90-EGFP* were treated with increasing concentrations of the lead compound P2 and compared to control *Elav-GAL4>UAS-EGFP* brains. Brains from untreated (CGG)90-expressing larvae exhibited markedly higher red fluorescence intensity, indicating increased neuronal cell death. In contrast, P2 treatment resulted in a concentration-dependent reduction in red fluorescence, with the highest dose (50.0 μM) significantly attenuating cell death. Quantitative analysis of PI fluorescence further corroborated these observations, demonstrating a substantial decrease in PI signal intensity in P2-treated brains (**Figure 4.21**). These findings support the neuroprotective potential of P2 in mitigating CGG repeatinduced neuronal cell death.

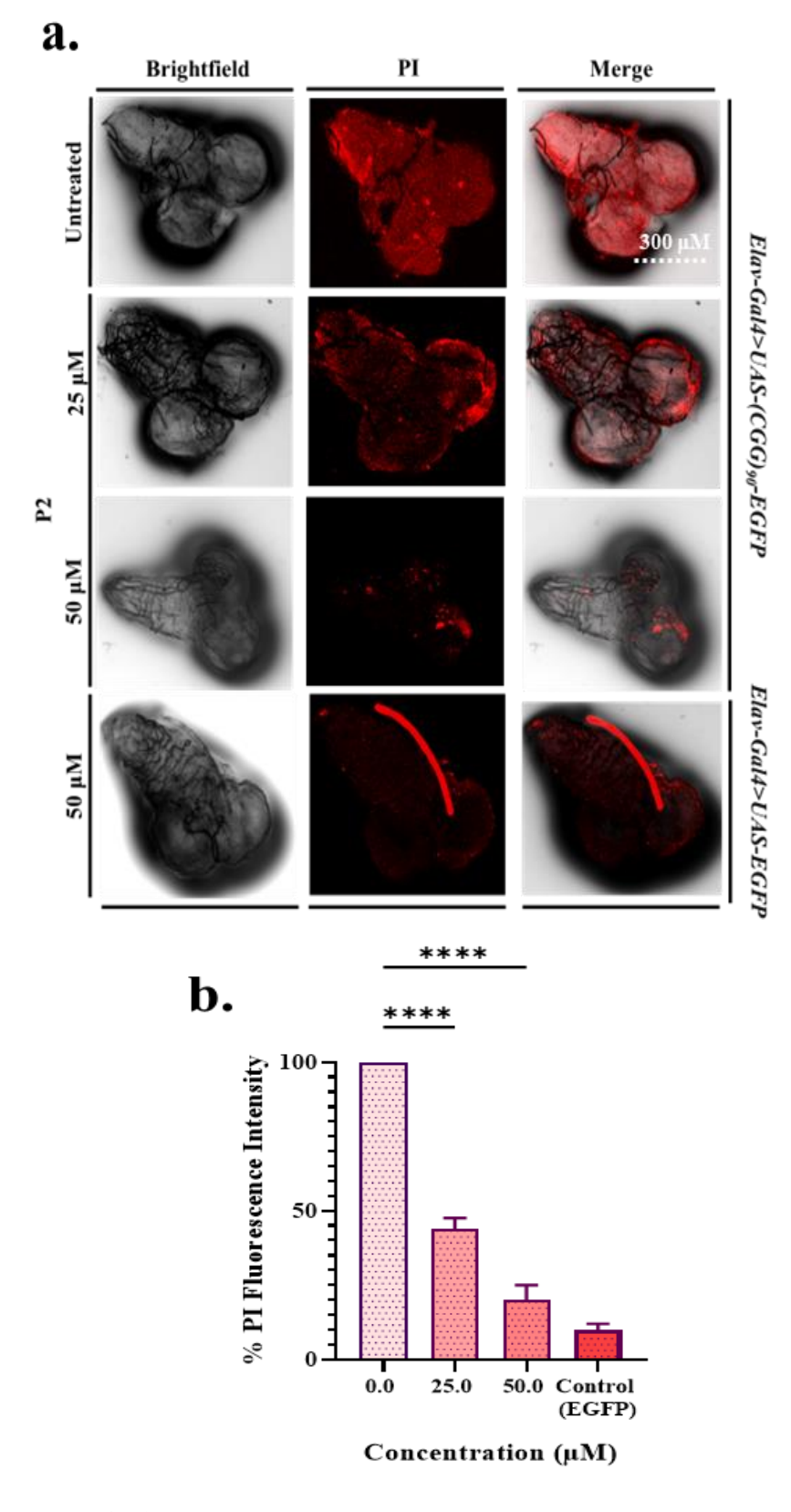


Figure 4.21: P2 treatment reduces cell death in the FXTAS *Drosophila* model. Confocal microscopy of larval brains. (a.) *Elav-GAL4>UAS-(CGG)*90-EGFP fed with different concentrations (25.0 μ M, and 50.0 μ M) of P2 and *Elav-GAL4>UAS-EGFP* flies fed with

50.0 μ M of P2. **(b.)** Bar graph representing fluorescence intensity (Arbitrary Units) of PI. Statistical significance was determined using one-way ANOVA; **** $P \le 0.00001$, n=3.

4.15 Dosage-dependent lifespan profiling of P2.

Neurodegenerative diseases, including FXTAS, are often associated with reduced lifespan. To investigate whether P2 administration could mitigate this phenotype, a lifespan analysis was conducted in Drosophila expressing (CGG)₉₀ repeats. P2 was administered at different time points to assess the effects of early and delayed treatment. Continuous exposure to 25.0 μM and 50.0 μM P2 from eclosion significantly enhanced survival in (CGG)₉₀-expressing flies. Notably, post-eclosion treatment initiated on day 7 with 50.0 μM P2 also conferred a measurable improvement in longevity. In contrast, P2 treatment had no effect on the survival of control flies expressing only EGFP, suggesting the observed benefits are specific to the CGG repeat pathology (**Figure 4.22**). These findings indicate that P2 extends lifespan in the FXTAS model, potentially through mechanisms that reduce cellular damage accumulation or enhance endogenous repair processes.

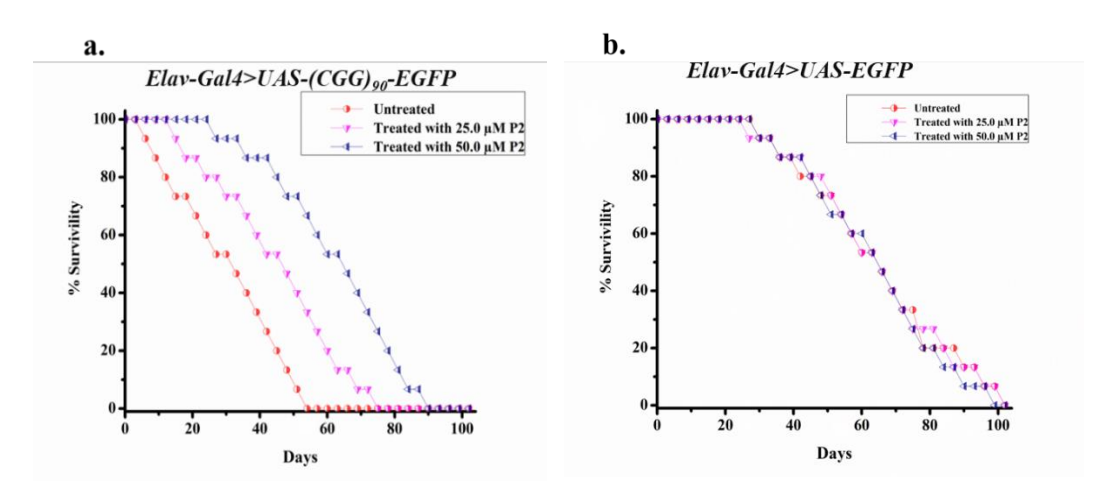


Figure 4.22: *In-vivo* efficacy of P2 in enhancing lifespan in FXTAS *Drosophila* model. (a.) Survival curves of *Elav-GAL4>UAS-(CGG)90-EGFP* flies fed with different concentrations (25.0 μ M, and 50.0 μ M) of

P2 from Day 7 (post eclosion). **(b.)** Survival curves of *Elav-GAL4>UAS-EGFP* flies fed with different concentrations (25.0 μ M, and 50.0 μ M) of P2 from Day 7 (post eclosion).

4.16 Expression analysis of neuroinflammatory, neuroprotective, and autophagy-related genes via RT-qPCR.

Autophagy plays a vital role in cellular quality control by facilitating the removal of damaged organelles, such as mitochondria, and misfolded proteins, thereby protecting cells from inflammation and oxidative stress. Impairments in autophagic pathways are a hallmark of several neurodegenerative disorders and are implicated in the accelerated progression of neuronal damage. Previous studies have suggested that the small molecule P2 can modulate autophagic activity. To investigate this in the context of FXTAS, we assessed the transcript levels of key autophagy-related genes in a Drosophila model expressing expanded CGG repeats. Specifically, we examined the expression of Atg1, Atg4b, Atg5, Atg7, and Atg8a (Figure 4.23).

Atg1 is a key regulator of autophagosome formation through recruitment of downstream Atg proteins; Atg4b encodes a protease involved in autophagy-related processing; Atg5 contributes to autophagosome expansion; Atg7 functions as an E1-like activating enzyme critical for autophagosome membrane elongation; and Atg8a is essential for nervous system integrity and autophagosome biogenesis. In the FXTAS model, significant downregulation of Atg1, Atg4b, Atg5 and Atg7 was observed, whereas Atg8a expression remained unchanged. Treatment with 50.0 μM P2 restored the expression of these downregulated autophagy genes, excluding Atg8a, indicating that P2 selectively enhances autophagy pathways impaired in the disease state. This restoration likely contributes to the clearance of dysfunctional mitochondria and other cytotoxic cellular debris, thereby promoting cellular homeostasis.

Given our previous findings that mitochondrial dysfunction is a central feature of the disease phenotype and is attenuated by P2, these results support the hypothesis that P2 exerts its neuroprotective effects, at least in part, via enhancement of autophagic clearance mechanisms.

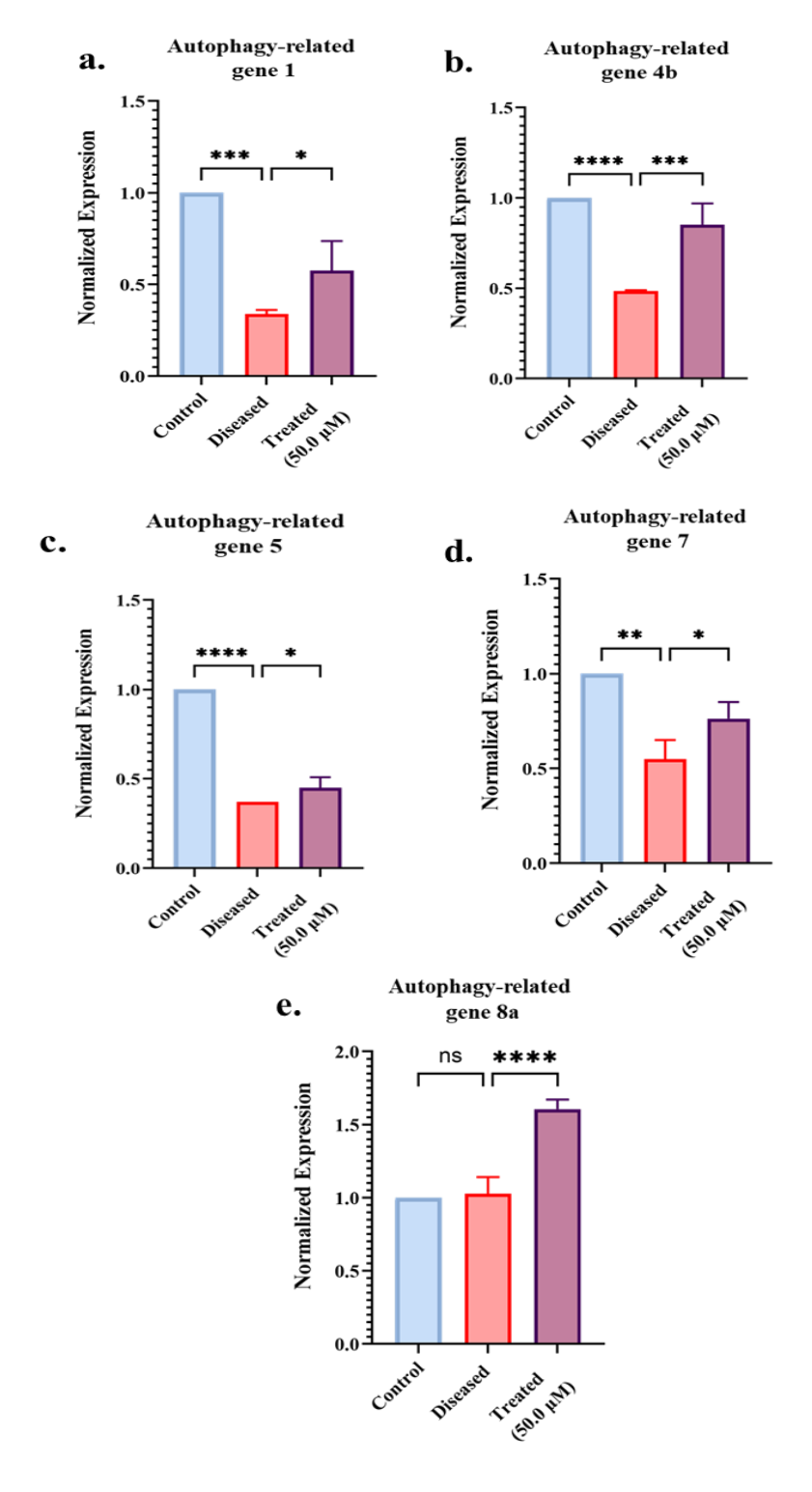
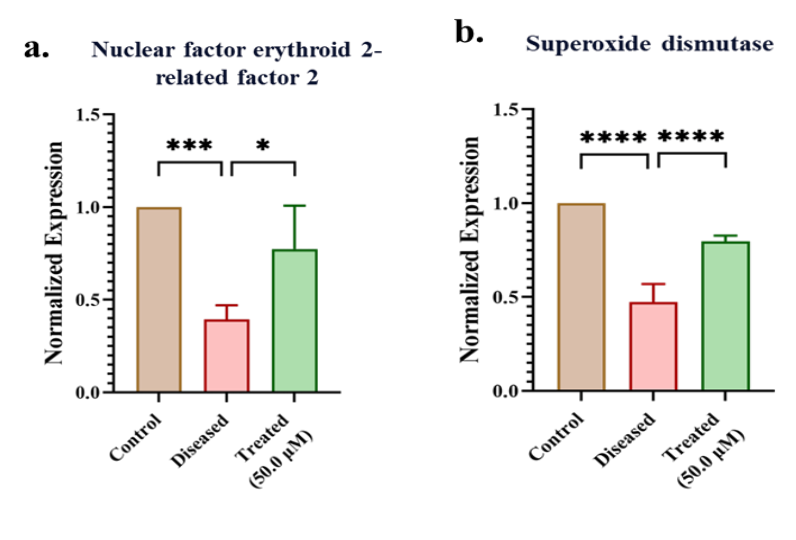


Figure 4.23: Effect of P2 on the expression levels of Autophagy genes in FXTAS *Drosophila* using RT-qPCR. The graphs represent the fold

change of genes treated with P2 (50.0 μ M), diseased control (UT) as well as normal control (Without CGG90 expression). GAPDH was used as an internal control for data normalization. All data are representative of three independent experiments and are presented as the mean \pm SD. Statistical significance was determined using one-way ANOVA; *P < 0.05, **P < 0.01, ***P < 0.001, and ****P < 0.00001, n=3.

To further explore the neuroprotective capacity of P2, we also investigated its effects on genes known to be modulated by P2 and associated with antioxidant defense mechanisms. Expression of superoxide dismutase (SOD), nuclear factor erythroid 2–related factor 2 (Nrf2), and glutathione S-transferases (GSTs), was evaluated in CGG₉₀-expressing flies. In the disease model, SOD, Nrf2, and GST were significantly downregulated (**Figure 4.24**). Treatment with 50.0 μM P2 resulted in upregulation of SOD, Nrf2, and GSTs, indicating an enhancement of the cellular antioxidant response and attenuation of oxidative stress. The significant elevation of Nrf2 also implies the potential activation of its downstream targets involved in neuroprotection.

Collectively, these findings underscore the therapeutic potential of P2 in FXTAS, highlighting its dual role in restoring autophagic function and activating antioxidant defense pathways to mitigate neuronal toxicity.



C. Glutathione S-transferase

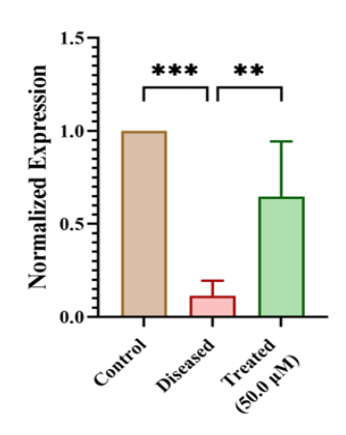


Figure 4.24: Effect of P2 on the expression levels of neuroprotective and neuroinflammatory genes in FXTAS *Drosophila* using RT-qPCR. The graphs represent the fold change of genes treated with P2 (50.0 μ M), diseased control (UT) as well as normal control (Without CGG90 expression). GAPDH was used as an internal control for data normalization. All data are representative of three independent experiments and are presented as the mean \pm SD. Statistical significance was determined using one-way ANOVA; *P < 0.05, **P < 0.01, ***P < 0.001, and ****P < 0.00001, n=3.

Chapter 5

Conclusion and Future Perspectives

Repeat expansion disorders, such as Fragile X-associated Tremor/Ataxia Syndrome (FXTAS), are driven by diverse pathogenic mechanisms including RNA toxicity, aberrant protein translation via Repeat-Associated Non-AUG (RAN) mechanisms, and protein gain-of-function effects. Historically, therapeutic strategies primarily targeted the downstream toxic proteins. However, recent advances have redirected attention to pathogenic RNA as a central therapeutic target. Among the emerging strategies, small molecule-based interventions have shown particular promise due to their favorable pharmacokinetic properties, including efficient penetration of the blood-brain barrier.

In FXTAS, expanded CGG repeats in the 5' untranslated region of the FMR1 gene result in the production of toxic RNA structures and the generation of polyglycine-containing peptides (FMRPolyG) via RAN translation. These pathogenic features contribute to neuronal dysfunction and degeneration. The use of small molecules capable of directly binding to expanded CGG repeat-containing RNAs offers a novel approach to disrupt toxic RNA-protein interactions and prevent aberrant translation processes.

In the present study, we systematically screened FDA-approved small molecules for their ability to bind CGG repeat RNA structures implicated in FXTAS. Through comprehensive biophysical assays, compound P2 emerged as a selective and high-affinity binder to CGG repeat RNA motifs. Subsequent in vitro analyses demonstrated that P2 effectively reduced intracellular accumulation of FMRPolyG proteins and alleviated RNA-mediated cellular toxicity. Moreover, administration of P2 in *in vivo* models led to dose-dependent improvements in neurobehavioral outcomes and a reduction in neuronal cell death.

This work underscores the therapeutic promise of repurposing clinically approved small molecules for the treatment of FXTAS and potentially other CGG repeat-associated disorders. By targeting upstream RNAbased mechanisms, such compounds offer a disease-modifying approach that complements and extends beyond current symptomatic treatments. Future investigations will aim to optimize lead compounds, such as P2, to achieve greater specificity, improved bioavailability, and enhanced metabolic stability. In parallel, mechanistic studies will be conducted to elucidate the molecular basis of their interaction with CGG repeat-containing RNAs and their impact on downstream pathogenic processes. To establish long-term therapeutic potential, extended in vivo studies using advanced FXTAS models will be essential to evaluate the durability of treatment effects, neuroprotective efficacy, and safety profile under chronic dosing conditions. This strategy holds the potential to accelerate the translation of RNA-targeting small molecules into clinically viable therapies for FXTAS and related repeat expansion neurodegenerative diseases.

APPENDIX

Table 1. Sequences of PCR primers used for the assay of alternative splicing defects.

S.	Gene	Forwards primer	Reverse primer
No		_	_
•			
1.	SMN		
	2	5'GGTGTCCACTCCCA	5'GCCTCACCACCGTG
	mini	GTTCAA	CTGG
	-		
	gene		
2.	cTN		
	T	5'GTTCACAACCATCT	5'GTTGCATGGCTGGT
	mini	AAAGCAAGATG	GCAGG
	-		
	gene		
3.	β-	~ ,	5.
	Acti	5'	5'
	n	CCTGGCACCCAGC	GGGCCGGACTCGT
		ACAAT	CATAC
4.	(CG		
	G)99-	5'GCACGACTTCTTCA	5'GCGGATCTTGAAGT
	EGF	AGTCCGCCATGCC	TCACCTTGATGCC
	P		

Table 2. Sequences of PCR primers used for the assay of expression levels of autophagy genes, neuroprotective and neuroinflammatory genes.

S.N o.	Gene	Forwards primer	Reverse primer
1.	Atg1	5'GGATTTTGGGTTTGC GCGAT	5'CAGAGATCCGCCT TGGAGTC
2.	Atg4b	5'GACCATTGTAGAGG GTAGCCG	5'CGATGAATCGTCT GTATGGGG
3.	Atg5	5'ATATGCTTCCAGGCG GATCG	5' AACCACACAGCTCC ATCCTG
4.	Atg7	5'GATGTTACGGCCCCT GGAAA	5' GCCAGCTCCTTACG AGGATG
5.	Atg8 a	5'TCTAGCCACAGCAG TTAGCG	5' TTGTGTAGAGTGAC CGTGCG
6.	Nrf2	5' AGCTTCTGTCGCATG GTTGA	5' AGCCGTTGCTAACA TGTCCA
7.	GSTs	5' CAGACCGTCAAGGA CAACGA	5' TCGCGCTTGACCAT GTAGTT 3'
8.	SOD	5' ACCGACTCCAAGATT ACGCTCT	5' GTTGCCCGTTGACT TGCTC
9.	GAP DH	5'TAAATTCGACTCGA CTCACGGT	5'CTCCACCACATAC TCGGCTC

REFERENCES

- Aubé, J. (2012). Drug Repurposing and the Medicinal Chemist.
 ACS Medicinal Chemistry Letters, 3(6), 442–444.
 https://doi.org/10.1021/ml300114c
- 2. Belzil, V. V., Gendron, T. F., & Petrucelli, L. (2013). RNA-mediated toxicity in neurodegenerative disease. Molecular and Cellular Neuroscience, 56, 406–419. https://doi.org/10.1016/j.mcn.2012.12.006
- Bilen, J., & Bonini, N. M. (2005). Drosophila as a Model for Human Neurodegenerative Disease. Annual Review of Genetics, 39(Volume 39, 2005), 153–171. https://doi.org/10.1146/annurev.genet.39.110304.095804
- 4. Brand, A. H., & Perrimon, N. (1993). Targeted gene expression as a means of altering cell fates and generating dominant phenotypes. Development, 118(2), 401–415. https://doi.org/10.1242/dev.118.2.401
- Brunberg, J. A., Jacquemont, S., Hagerman, R. J., Berry-Kravis, E. M., Grigsby, J., Leehey, M. A., Tassone, F., Brown, W. T., Greco, C. M., & Hagerman, P. J. (2002). Fragile X premutation carriers: Characteristic MR imaging findings of adult male patients with progressive cerebellar and cognitive dysfunction. AJNR. American Journal of Neuroradiology, 23(10), 1757– 1766.
- Castanotto, D., & Rossi, J. J. (2009). The promises and pitfalls of RNA-interference-based therapeutics. Nature, 457(7228), 426–433. https://doi.org/10.1038/nature07758
- Chen, Z., Morris, H. R., Polke, J., Wood, N. W., Gandhi, S., Ryten, M., Houlden, H., & Tucci, A. (2024). Repeat expansion disorders. Practical Neurology. https://doi.org/10.1136/pn-2023-003938
- 8. Disney, M. D., Liu, B., Yang, W.-Y., Sellier, C., Tran, T., Charlet-Berguerand, N., & Childs-Disney, J. L. (2012). A Small

- Molecule That Targets r(CGG)exp and Improves Defects in Fragile X-Associated Tremor Ataxia Syndrome. ACS Chemical Biology, 7(10), 1711–1718. https://doi.org/10.1021/cb300135h
- 9. Ellerby, L. M. (2019). Repeat Expansion Disorders: Mechanisms and Therapeutics. Neurotherapeutics, 16(4), 924–927. https://doi.org/10.1007/s13311-019-00823-3
- 10. Erkkinen, M. G., Kim, M.-O., & Geschwind, M. D. (2018). Clinical Neurology and Epidemiology of the Major Neurodegenerative Diseases. Cold Spring Harbor Perspectives in Biology, 10(4), a033118. https://doi.org/10.1101/cshperspect.a033118
- Glineburg, M. R., Todd, P. K., Charlet-Berguerand, N., & Sellier,
 C. (2018). Repeat-associated non-AUG (RAN) translation and other molecular mechanisms in Fragile X Tremor Ataxia Syndrome. Brain Research, 1693, 43–54. https://doi.org/10.1016/j.brainres.2018.02.006
- 12. Gohel, D., Berguerand, N. C., Tassone, F., & Singh, R. (2020).
 The emerging molecular mechanisms for mitochondrial dysfunctions in FXTAS. Biochimica et Biophysica Acta (BBA)
 Molecular Basis of Disease, 1866(12), 165918.
 https://doi.org/10.1016/j.bbadis.2020.165918
- 13. Greco, C. M., Berman, R. F., Martin, R. M., Tassone, F., Schwartz, P. H., Chang, A., Trapp, B. D., Iwahashi, C., Brunberg, J., Grigsby, J., Hessl, D., Becker, E. J., Papazian, J., Leehey, M. A., Hagerman, R. J., & Hagerman, P. J. (2006). Neuropathology of fragile X-associated tremor/ataxia syndrome (FXTAS). Brain, 129(1), 243–255. https://doi.org/10.1093/brain/awh683
- 14. Hagerman, R. J., & Hagerman, P. (2016). Fragile X-associated tremor/ataxia syndrome—Features, mechanisms and management. Nature Reviews Neurology, 12(7), 403–412. https://doi.org/10.1038/nrneurol.2016.82
- 15. Hales, K. G., Korey, C. A., Larracuente, A. M., & Roberts, D. M. (2015). Genetics on the Fly: A Primer on the Drosophila Model

- System. Genetics, 201(3), 815–842. https://doi.org/10.1534/genetics.115.183392
- Hall, D. A., Robertson, E. E., Leehey, M., McAsey, A., Ouyang, B., Berry-Kravis, E., & O'Keefe, J. A. (2020). Open-label pilot clinical trial of citicoline for fragile X-associated tremor/ataxia syndrome (FXTAS). PLOS ONE, 15(2), e0225191. https://doi.org/10.1371/journal.pone.0225191
- 17. Jacquemont, S., Hagerman, R. J., Leehey, M. A., Hall, D. A., Levine, R. A., Brunberg, J. A., Zhang, L., Jardini, T., Gane, L. W., Harris, S. W., Herman, K., Grigsby, J., Greco, C. M., Berry-Kravis, E., Tassone, F., & Hagerman, P. J. (2004). Penetrance of the Fragile X–Associated Tremor/Ataxia Syndrome in a Premutation Carrier Population. JAMA, 291(4), 460–469. https://doi.org/10.1001/jama.291.4.460
- Jacquemont, S., Hagerman, R. J., Leehey, M., Grigsby, J., Zhang, L., Brunberg, J. A., Greco, C., Des Portes, V., Jardini, T., Levine, R., Berry-Kravis, E., Brown, W. T., Schaeffer, S., Kissel, J., Tassone, F., & Hagerman, P. J. (2003). Fragile X Premutation Tremor/Ataxia Syndrome: Molecular, Clinical, and Neuroimaging Correlates. The American Journal of Human Genetics, 72(4), 869–878. https://doi.org/10.1086/374321
- Kakoti, B. B., Bezbaruah, R., & Ahmed, N. (2022). Therapeutic drug repositioning with special emphasis on neurodegenerative diseases: Threats and issues. Frontiers in Pharmacology, 13. https://doi.org/10.3389/fphar.2022.1007315
- 20. Kazemi-Esfarjani, P., & Benzer, S. (2000). Genetic Suppression of Polyglutamine Toxicity in Drosophila. Science, 287(5459), 1837–1840. https://doi.org/10.1126/science.287.5459.1837
- 21. Khan, E., Biswas, S., Mishra, S. K., Mishra, R., Samanta, S., Mishra, A., Tawani, A., & Kumar, A. (2019). Rationally designed small molecules targeting toxic CAG repeat RNA that causes Huntington's disease (HD) and spinocerebellar ataxia (SCAs). Biochimie, 163, 21–32. https://doi.org/10.1016/j.biochi.2019.05.001

- 22. Khan, E., Tawani, A., Mishra, S. K., Verma, A. K., Upadhyay, A., Kumar, M., Sandhir, R., Mishra, A., & Kumar, A. (2018). Myricetin Reduces Toxic Level of CAG Repeats RNA in Huntington's Disease (HD) and Spino Cerebellar Ataxia (SCAs). ACS Chemical Biology, 13(1), 180–188. https://doi.org/10.1021/acschembio.7b00699
- 23. Leehey, M. A. (2009). Fragile X-Associated Tremor/Ataxia Syndrome: Clinical Phenotype, Diagnosis, and Treatment. Journal of Investigative Medicine, 57(8), 830–836. https://doi.org/10.2310/JIM.0b013e3181af59c4
- 24. Liguori, F., Pandey, U. B., & Digilio, F. A. (2023). Editorial:

 Drosophila as a model to study neurodegenerative diseases.

 Frontiers in Neuroscience, 17.

 https://doi.org/10.3389/fnins.2023.1275253
- 25. Liu, W., Wang, G., Wang, Z., Wang, G., Huang, J., & Liu, B. (2022). Repurposing small-molecule drugs for modulating toxic protein aggregates in neurodegenerative diseases. Drug Discovery Today, 27(7), 1994–2007. https://doi.org/10.1016/j.drudis.2022.04.003
- 26. Lu, B., & Vogel, H. (2009). Drosophila Models of Neurodegenerative Diseases. Annual Review of Pathology: Mechanisms of Disease, 4(Volume 4, 2009), 315–342. https://doi.org/10.1146/annurev.pathol.3.121806.151529
- 27. Malik, I., Kelley, C. P., Wang, E. T., & Todd, P. K. (2021). Molecular mechanisms underlying nucleotide repeat expansion disorders. Nature Reviews Molecular Cell Biology, 22(9), 589–607. https://doi.org/10.1038/s41580-021-00382-6
- 28. McCampbell, A., Cole, T., Wegener, A. J., Tomassy, G. S., Setnicka, A., Farley, B. J., Schoch, K. M., Hoye, M. L., Shabsovich, M., Sun, L., Luo, Y., Zhang, M., Comfort, N., Wang, B., Amacker, J., Thankamony, S., Salzman, D. W., Cudkowicz, M., Graham, D. L., ... Miller, T. M. (2018). Antisense oligonucleotides extend survival and reverse decrement in muscle response in ALS models. The Journal of Clinical

- Investigation, 128(8), 3558–3567. https://doi.org/10.1172/JCI99081
- 29. Oostra, B. A., & Willemsen, R. (2009). FMR1: A gene with three faces. Biochimica et Biophysica Acta (BBA) General Subjects, 1790(6), 467–477. https://doi.org/10.1016/j.bbagen.2009.02.007
- 30. Oprea, T. I., & Mestres, J. (2012). Drug Repurposing: Far Beyond New Targets for Old Drugs. The AAPS Journal, 14(4), 759–763. https://doi.org/10.1208/s12248-012-9390-1
- 31. Parvathaneni, V., Kulkarni, N. S., Muth, A., & Gupta, V. (2019). Drug repurposing: A promising tool to accelerate the drug discovery process. Drug Discovery Today, 24(10), 2076–2085. https://doi.org/10.1016/j.drudis.2019.06.014
- 32. Paulson, H. (2018). Chapter 9—Repeat expansion diseases. In D. H. Geschwind, H. L. Paulson, & C. Klein (Eds.), Handbook of Clinical Neurology (Vol. 147, pp. 105–123). Elsevier. https://doi.org/10.1016/B978-0-444-63233-3.00009-9
- 33. Perkins, L. A., Holderbaum, L., Tao, R., Hu, Y., Sopko, R., McCall, K., Yang-Zhou, D., Flockhart, I., Binari, R., Shim, H.-S., Miller, A., Housden, A., Foos, M., Randkelv, S., Kelley, C., Namgyal, P., Villalta, C., Liu, L.-P., Jiang, X., ... Perrimon, N. (2015). The Transgenic RNAi Project at Harvard Medical School: Resources and Validation. Genetics, 201(3), 843–852. https://doi.org/10.1534/genetics.115.180208
- 34. Port, F., Chen, H.-M., Lee, T., & Bullock, S. L. (2014). Optimized CRISPR/Cas tools for efficient germline and somatic genome engineering in Drosophila. Proceedings of the National Academy of Sciences, 111(29), E2967–E2976. https://doi.org/10.1073/pnas.1405500111
- 35. Quilez, J., Guilmatre, A., Garg, P., Highnam, G., Gymrek, M., Erlich, Y., Joshi, R. S., Mittelman, D., & Sharp, A. J. (2016). Polymorphic tandem repeats within gene promoters act as modifiers of gene expression and DNA methylation in humans.

- Nucleic Acids Research, 44(8), 3750–3762. https://doi.org/10.1093/nar/gkw219
- 36. RAY, M., & LAKHOTIA, S. C. (2015). The commonly used eye-specific sev-GAL4 and GMR-GAL4 drivers in Drosophila melanogaster are expressed in tissues other than eyes also. Journal of Genetics, 94(3), 407–416. https://doi.org/10.1007/s12041-015-0535-8
- 37. Reiter, L. T., Potocki, L., Chien, S., Gribskov, M., & Bier, E. (2001). A Systematic Analysis of Human Disease-Associated Gene Sequences In Drosophila melanogaster. Genome Research, 11(6), 1114–1125. https://doi.org/10.1101/gr.169101
- 38. Sareen, D., O'Rourke, J. G., Meera, P., Muhammad, A. K. M. G., Grant, S., Simpkinson, M., Bell, S., Carmona, S., Ornelas, L., Sahabian, A., Gendron, T., Petrucelli, L., Baughn, M., Ravits, J., Harms, M. B., Rigo, F., Bennett, C. F., Otis, T. S., Svendsen, C. N., & Baloh, R. H. (2013). Targeting RNA Foci in iPSC-Derived Motor Neurons from ALS Patients with a C9ORF72 Repeat Expansion. Science Translational Medicine, 5(208), 208ra149-208ra149.
 - https://doi.org/10.1126/scitranslmed.3007529
- Sellier, C., Freyermuth, F., Tabet, R., Tran, T., He, F., Ruffenach, F., Alunni, V., Moine, H., Thibault, C., Page, A., Tassone, F., Willemsen, R., Disney, M. D., Hagerman, P. J., Todd, P. K., & Charlet-Berguerand, N. (2013). Sequestration of DROSHA and DGCR8 by Expanded CGG RNA Repeats Alters MicroRNA Processing in Fragile X-Associated Tremor/Ataxia Syndrome. Cell Reports, 3(3), 869–880. https://doi.org/10.1016/j.celrep.2013.02.004
- 40. Singh, K., Shukla, S., Ghosh, T., Das, A. K., & Kumar, A. (2025). Tyrosine Peptides Alleviates Multifaceted Toxicity Linked to Expanded CGG Repeats in Fragile X-Associated Tremor/Ataxia Syndrome. ACS Pharmacology & Translational Science. https://doi.org/10.1021/acsptsci.4c00647

- 41. Smith, C. I. E., & Zain, R. (2019). Therapeutic Oligonucleotides: State of the Art. Annual Review of Pharmacology and Toxicology, 59(Volume 59, 2019), 605–630. https://doi.org/10.1146/annurev-pharmtox-010818-021050
- 42. Tassone, F., Hagerman, R. j., Taylor, A. k., Mills, J. b., Harris, S. w., Gane, L. w., & Hagerman, P. j. (2000). Clinical involvement and protein expression in individuals with the FMR1 premutation. American Journal of Medical Genetics, 91(2), 144–152. https://doi.org/10.1002/(SICI)1096-8628(20000313)91:2<144::AID-AJMG14>3.0.CO;2-V
- 43. Tassone, F., Iwahashi ,Christine, & and Hagerman, P. J. (2004). FMR1 RNA within the Intranuclear Inclusions of Fragile X-Associated Tremor/Ataxia Syndrome (FXTAS). RNA Biology, 1(2), 103–105. https://doi.org/10.4161/rna.1.2.1035
- 44. Todd, P. K., Oh, S. Y., Krans, A., He, F., Sellier, C., Frazer, M., Renoux, A. J., Chen, K., Scaglione, K. M., Basrur, V., Elenitoba-Johnson, K., Vonsattel, J. P., Louis, E. D., Sutton, M. A., Taylor, J. P., Mills, R. E., Charlet-Berguerand, N., & Paulson, H. L. (2013). CGG Repeat-Associated Translation Mediates Neurodegeneration in Fragile X Tremor Ataxia Syndrome. Neuron, 78(3), 440–455. https://doi.org/10.1016/j.neuron.2013.03.026
- 45. Todd, P. K., & Paulson, H. L. (2010). RNA-mediated neurodegeneration in repeat expansion disorders. Annals of Neurology, 67(3), 291–300. https://doi.org/10.1002/ana.21948
- 46. Verheyen, E. M. (2022). The power of Drosophila in modeling human disease mechanisms. Disease Models & Mechanisms, 15(3), dmm049549. https://doi.org/10.1242/dmm.049549
- 47. Verma, A. K., Khan, E., Bhagwat, S. R., & Kumar, A. (2020). Exploring the Potential of Small Molecule-Based Therapeutic Approaches for Targeting Trinucleotide Repeat Disorders. Molecular Neurobiology, 57(1), 566–584. https://doi.org/10.1007/s12035-019-01724-4

- 48. Verma, A. K., Khan, E., Mishra, S. K., Jain, N., & Kumar, A. (2019). Piperine Modulates Protein Mediated Toxicity in Fragile X-Associated Tremor/Ataxia Syndrome through Interacting Expanded CGG Repeat (r(CGG)exp) RNA. ACS Chemical Neuroscience, 10(8), 3778–3788. https://doi.org/10.1021/acschemneuro.9b00282
- 49. Verma, A. K., Khan, E., Mishra, S. K., & Kumar, A. (2022). Small Molecule Screening Discovers Compounds that Reduce FMRpolyG Protein Aggregates and Splicing Defect Toxicity in Fragile X-Associated Tremor/Ataxia Syndrome. Molecular Neurobiology, 59(3), 1992–2007. https://doi.org/10.1007/s12035-021-02697-z
- 50. Verma, A. K., Khan, E., Mishra, S. K., Mishra, A., Charlet-Berguerand, N., & Kumar, A. (2020). Curcumin Regulates the r(CGG)exp RNA Hairpin Structure and Ameliorate Defects in Fragile X-Associated Tremor Ataxia Syndrome. Frontiers in Neuroscience, 14. https://doi.org/10.3389/fnins.2020.00295
- 51. Wang, J. Y., Trivedi, A. M., Carrillo, N. R., Yang, J., Schneider, A., Giulivi, C., Adams, P., Tassone, F., Kim, K., Rivera, S. M., Lubarr, N., Wu, C.-Y., Irwin, R. W., Brinton, R. D., Olichney, J. M., Rogawski, M. A., & Hagerman, R. J. (2017). Open-Label Allopregnanolone Treatment of Men with Fragile X-Associated Tremor/Ataxia Syndrome. Neurotherapeutics, 14(4), 1073–1083. https://doi.org/10.1007/s13311-017-0555-6
- 52. Wang, Y., Aldahdooh, J., Hu, Y., Yang, H., Vähä-Koskela, M., Tang, J., & Tanoli, Z. (2022). DrugRepo: A novel approach to repurposing drugs based on chemical and genomic features. Scientific Reports, 12(1), 21116. https://doi.org/10.1038/s41598-022-24980-2
- 53. Willemsen, R., Levenga, J., & Oostra, B. (2011). CGG repeat in the FMR1 gene: Size matters. Clinical Genetics, 80(3), 214–225. https://doi.org/10.1111/j.1399-0004.2011.01723.x
- 54. Wilson, D. M., Cookson, M. R., Van Den Bosch, L., Zetterberg, H., Holtzman, D. M., & Dewachter, I. (2023). Hallmarks of

- neurodegenerative diseases. Cell, 186(4), 693–714. https://doi.org/10.1016/j.cell.2022.12.032
- 55. Xu, K., Li, Y., Allen, E. G., & Jin, P. (2021). Therapeutic Development for CGG Repeat Expansion-Associated Neurodegeneration. Frontiers in Cellular Neuroscience, 15. https://doi.org/10.3389/fncel.2021.655568
- 56. Yamanaka, N., Rewitz, K. F., & O'Connor, M. B. (2013).
 Ecdysone Control of Developmental Transitions: Lessons from Drosophila Research. Annual Review of Entomology,
 58(Volume 58, 2013), 497–516.
 https://doi.org/10.1146/annurev-ento-120811-153608
- 57. Zhang, Y., Liu, X., Li, Z., Li, H., Miao, Z., wan, B., & Xu, X. (2024). Advances on the Mechanisms and Therapeutic Strategies in Non-coding CGG Repeat Expansion Diseases. Molecular Neurobiology, 61(12), 10722–10735. https://doi.org/10.1007/s12035-024-04239-9